

See discussions, stats, and author profiles for this publication at: <https://www.researchgate.net/publication/349476746>

INFRAME – design and construction of a sequentially erected elastic timber gridshell

Thesis · January 2020

CITATIONS

0

READS

51

1 author:



Judyta Cichocka

Wroclaw University of Science and Technology

13 PUBLICATIONS 43 CITATIONS

SEE PROFILE

Some of the authors of this publication are also working on these related projects:



Optimization algorithms [View project](#)



Walkability optimization [View project](#)

INFRAME

-

design and construction of a sequentially erected elastic timber gridshell

by

Judyta M. Cichocka

BEng.Arch (2012) MSc.Eng.Arch (2013) Dr Eng.Arch (2018)
Wroclaw University of Technology and Science

Submitted to the Department of Civil and Environmental Engineering in Partial Fulfillment of the
Requirements for the Degree of

MASTER OF ENGINEERING

at the

MASSACHUSETTS INSTITUTE OF TECHNOLOGY

February 2020

© 2020 Judyta M. Cichocka. All rights reserved.

The author hereby grants to MIT permission to reproduce and to distribute publicly paper and electronic
copies of this thesis document in whole or in part in any medium now known or hereafter created.

Signature of Author:

Department of Civil and Environmental Engineering
January 17, 2019

Certified by:

Caitlin T. Mueller
Associate Professor of Department of Architecture and Civil and Environmental Engineering
Thesis Supervisor

Accepted by:

Colette L. Heald
Professor of Civil and Environmental Engineering
Chair Graduate Program Commit

INFRAME

-

design and construction of a sequentially erected elastic timber gridshell

by

Judyta M. Cichocka

Submitted to the Department of Civil and Environmental Engineering on 17th January 2020 in Partial
Fulfillment of the Requirements for the Degree of Master of Engineering

Abstract

This thesis presents a design-oriented methodology for the design, optimization and construction of sequentially erected elastic timber gridshells. A multi-objective approach toward simultaneous optimization of the overall size and grid configurations is implemented to achieve maximum structural performance and minimize cost. The proposed methodology is applied to a 1:1 design of an open-air outdoor stage within the MIT campus. The design was certified compliant with the building regulations in the jurisdiction where it was constructed. The construction of the INFRAME pavilion brings a few insights towards the potential adaptation of bending-active systems to the building codes and presents a new application of temporary elastic timber gridshell structures for outdoor events.

Elastic timber gridshell, sequentially erected gridshell, bending-active structure, design methodology, temporary deployable pavilion

Thesis supervisor: Caitlin T. Mueller

Title: Professor of Department of Architecture and Civil and Environmental Engineering

Acknowledgements

First, I would like to thank my advisor, Prof. Caitlin Mueller, for guiding my research and for being an amazing mentor. I strongly value her endless assistance, input and support. I am particularly grateful to her for allowing me to explore and develop my own ideas and her constructive feedback.

Secondly, I thank Josephine Carstensen for her enthusiasm and never-ending will to support, develop, and push boundaries of topology optimization. The Topology Optimization course taught by her gave me the baseline skills and inspiration for the application of the elastic timber gridshell design. Generously inputting the frame topology optimization in Matlab, the further extensions have been possible, and the research on topology optimization of elastic structural systems has been initiated.

I would like to thank a few people in particular who have had an important part in making this dissertation possible. First of all, I am very grateful to my friend Agnieszka Wierzbicka, who encouraged me to apply for the Fulbright Graduate Award. It is because of her open-mindedness and support that I would have started my education at MIT. I would also like to express my gratitude to Dr Michal Pelczarski, who introduced me during my last year of architectural studies to the work of Prof. Waław Zalewski. The innovativeness, expressiveness and structural art of his projects was a great inspiration ever since. I would like to give thanks to all the members of the Digital Structures group for their insightful comments, guidance and technical help. I would also like to thank Riccardo La Magna for his feedback and help in setting up the analysis in SOFiSTiK. Thank you to Samuel Dickinson for his help in proofreading this document.

I am thankful to BuroHappold Engineering, whose professional philosophy oriented on innovation and delivery of creative designs made the INFRAME project possible. I am especially indebted to Paul Richardson, who guided the project from an early design stage to the construction and to Craig Schwitter, who generously agreed to stamp the construction documentation.

I am extremely grateful to Gabriela Bila Advincula and other people engaged in the construction of the pavilion: the MIT Media Lab City Science group, the CEE MEng 2020 group, with special thanks to Michael Ramirez and Daniel Camp Seats.

The components of the INFRAME pavilion were partially fabricated thanks to the MIT Hobby Shop. Thank you to the Office of Environment, Health & Safety (EHS), and the Department of Facilities for their trust and enthusiasm, without Katie Blass and Camille Mekdeci the INFRAME project would have never become to realization.

I would like to thank Fulbright Poland for their financial support. The construction of the pavilion was possible thanks to the financial support from the CAMIT Grant – Arts at MIT and the CEE Department.

Lastly, I thank my parents for their continuing support behind the scenes.

Table of contents

Key terms	9
1. Introduction.....	13
1.1 Motivation and goals	14
1.2 Definition and classification.....	15
1.3 Research question.....	16
2. Literature review	17
2.1 Review of research works on elastic timber gridshells	17
2.2 Form-finding methods	19
2.3 Structural analysis of bending-active systems	21
2.4 Review of built elastic timber gridshells	23
2.5 Research gap.....	28
3. Conceptual design methodology	29
3.1 Project overview	29
3.2 Initial concepts	29
3.3 Design workflow	31
3.4 Design concepts.....	33
3.5 Multi-objective optimization	36
4. Engineering calculations and codes.....	39
4.1 Conceptual overview	39
4.2 Material properties	41
4.3 Bending stress and radius of curvature.....	42
4.4 Load cases	45
4.5 Structural model	46
4.6 Analysis of the final structural configuration	49
4.6.1 Nodal displacements.....	50
4.6.2 Bending and axial stresses.....	51
4.6.3 Reaction forces	58
4.6.4 Vertical forces - uplift	59
4.7 Final structural notes	60
5. Fabrication and construction	63
5.1 Base design.....	65
5.2 Details.....	67
5.3 Photos	70
5.4 Relocation, disassembly and transport	74
6. Conclusion	77
6.1 Summary of contributions	77
6.2 Potential impact.....	77
6.3 Future work	78
6.4 Concluding remarks.....	78
References	79
Appendix A – material testing results.....	83
Appendix B – construction approval procedures, project budget	87
Appendix C – custom discretization of curves - Python source code.....	93

Key terms

Term	Explanation
ACTIVE-BENDING	“systemized elastic deformation” (Lienhard <i>et al.</i> , 2013:p.187)
BENDING-ACTIVE CURVED BEAMS OR SURFACES	beams or surfaces which derive their shape from elastic deformation (bending) of initially straight or planar elements (Lienhard <i>et al.</i> , 2013)
BENDING-ACTIVE STRUCTURES	spatial structures undergoing large displacements (Rombouts <i>et al.</i> , 2017); “on a structural level, they are curved structures that are influenced by residual stress in their load bearing capacity and behavior” (Lienhard <i>et al.</i> , 2013:p.187)
BRACING MEMBERS	“profiles or cables, which diagonalise or triangulate the grid (...) to provide the structure with in-plane shear strength” (Lafuente Hernandez, 2015:p.6)
BUCKLING LOAD FACTOR (BLF)	a factor, which “expresses how much the applied load can be scaled before buckling occurs” (Brandt-Olsen, 2016:p.56)
DEVELOPABLE (REGULAR, SITE-SPRUNG) GRIDSHELL	“the grid is usually bent as a whole from a flat position (...) distortion and scissoring of the grid is possible by using hinged joints at the grid nodes.” (Lafuente Hernandez, 2015:p.6)
GEODESIC CURVE	“curve of zero geodesic curvature” (Struik, 1950), it follows the shortest path on the surface and becomes straight when unrolled onto a plane (Struik, 1988), “A geodesic line on a surface is defined as a curve, where the normal vector of both curve and surface are parallel or antiparallel at each point. The shortest distance between two points on a surface is always a geodesic line.” (Pirazzi & Weinand, 2006), “geodesics – being minimizers of distance – are the equilibrium shapes of elastic curve constrained to the surface” (Pottmann <i>et al.</i> , 2010:p.43:1)
GEODESIC GRIDSHELL	a gridshell “in which network of curves are intentionally following geodesic curves [on a surface]” (Soriano, 2017:p.30)
GRIDSHELL (RETRICULATED SHELL, LATTICE SHELL)	” ‘reticulated’, ‘lattice’ and ‘grid’ shell are largely interchangeable [...] a grid shell is essentially a shell with its structure concentrated into individual linear elements in a relatively thin grid compared to the overall dimensions of the grid shell” (Richardson <i>et al.</i> , 2013:p.230)
ELASTIC GRIDSHELL	“bending active frames” (Cuvilliers <i>et al.</i> , 2018:p.1), “shell structures composed of a single- or multi-layer grid of continuous profiles, which are initially straight and will be progressively bent until achieving an architecturally and structurally satisfactory geometry” (Lafuente Hernandez, 2015:p.IV), gridshells with “the mounting sequence [...] based on the

	elastic bending deformation of the members [...] in opposition to <i>rigid grid shells</i> , which are built from individual rigid members” (Mesnil, Ochsendorf & Douthe, 2015:p.27), a gridshell “that consist of flexible members” (Kuijkenhoven & Hoogenboom, 2012:p.31), “an ensemble of constrained elastica and a continuum of inextensible rods” (Baek <i>et al.</i> , 2018:p.75)
ELASTICA	“is defined as the shape of buckled beam-column with large deflection” (Sakai & Ohsaki, 2017:p.1), “an initially straight member that is bent into a spatial continuous curve” (Adriaenssens <i>et al.</i> , 2014:p.89), “can be seen as the post-buckling curve of a beam between two pinned supports with an applied normal force” (Brütting <i>et al.</i> , 2017:p.3)
FORM-ACTIVE STRUCTURE	“structures that react to external loads and constraints with large deformations” (Cuvilliers <i>et al.</i> , 2018:p.73)
FORM-FINDING	“Finding an (optimal) shape of a [form-active structure] that is in (or approximates) a state of static equilibrium.” (Veenendaal & Block, 2012:p.3742), “finding an appropriate architectural and structural shape”(Coenders & Bosia, 2006)
MOLDLESS CONSTRUCTION PROCESS	a process that does not require scaffolding or formwork (Brütting <i>et al.</i> , 2017)
NUMBER OF LAYERS	“refers only to one grid direction (...) single- and a double-layer grids are composed, respectively, of two and four superposed profiles in total” (Lafuente Hernandez, 2015:p.6)
NEAR-GEODESIC	a curve on the surface which deviates from a true geodesic curve, often is the result of the optimization problems e.g. finding a pattern of equidistance geodesics on a free form surface (Pottmann <i>et al.</i> , 2010)
PLANK /PLANK LINE	(a geodesic with width) - “a line with an given width (like a plank of wood) that passes over a surface and does not curve in the tangential plane, and whose width is always tangential to the surface” (Leung, 2018)
RELEASED GEOMETRY OF THE GRID	“the geometry that it [grid] acquires once it has been bent and fixed at its edges, and the shaping forces have been removed” (Lafuente Hernandez, 2015:p.6)
RIBBED TIMBER SHELL STRUCTURE	a shell structure built from “wooden planks to form the ribs” (Kensek, Leuppi & Noble, 2000:p.261)
SEGMENTED SHELL	“Initially planar plate elements are bent only by support displacements and then connected to form shell structures.” (Brütting <i>et al.</i> , 2017:p.1)
SEQUENTIALLY ERECTED TIMBER GRIDSHELL	a gridshell with all laths bent and installed sequentially on-site
SITE-SPRUNG GRIDSHELL	an elastic gridshell which is bent from an initially flat grid on site

STRESS STIFFENING (GEOMETRIC STIFFENING, INITIAL STRESS STIFFENING)	“stiffening effect of tension normal forces or stresses on the geometric stiffness matrix [...] inclusion of such effects in structural analysis is only provided in fully non-linear analysis and is still subject of today’s research” (Lienhard, 2014:p.21)
STIFFENING	“addition of diagonal ties with a cross-sectional area less than the laths” (Adriaenssens <i>et al.</i> , 2014:p.90)
STRUCTURAL SPLINE	a lath (Adriaenssens <i>et al.</i> , 2014:p.89)
STRAINED GRIDSHELL (ACTIVE-BENDING GRIDSHELL)	a gridshell formed in a way that “the initial bending active action strains the shell” (Adriaenssens <i>et al.</i> , 2014:p.90), an elastic gridshell for which “form-giving bending process induces important residual stresses on the grid profiles” (Lafuente Hernandez, 2015:p.6)
UNSTRAINED GRIDSHELL	“is a curved system that in its initial state is stress-free (apart from stresses due to self-weight)” (Adriaenssens <i>et al.</i> , 2014:p.90)
ZOLLINGER/ LAMELLA CONSTRUCTION	a construction process where “rigidity is achieved through the alternating connection of midpoint to endpoint” (Schulitz, 2017:p.1)

1. Introduction

How can structures positively respond to the humanization of the cities' densities? Referring to Prof. Werner Sobek (Sobek, 2017) structures that are loved, are also naturally sustainable, as people care about them and therefore keep them alive. Such emotional relationships can be created and nurtured by means of an active and close involvement of citizens within the structure's design, construction or renovation processes. Once structures are loved, they will never die too early and will actively support the sustainable development of cities they are located in. One of the most relevant ways in which structures are able to sustain their social importance is by dint of their adaptive nature. Providing necessary amenities on demand can maintain their functional relevance. Additionally, it is hypothesized that temporary structures, which can be built without sophisticated means are capable of creating a social value both through their ability to adapt and the social engagement of their construction.

Gridshells are highly efficient, lightweight and sustainable structures (Vassallo & Malek, 2017) and active-bending systems are a promising approach to bring novelty into the field of traditional unstrained gridshell design (Lienhard & Gengnagel, 2018). Current research on elastic gridshells is mostly focused on the structural systems constructed with the site-sprung methods, while the sequentially erected prestressed gridshells have been left underdeveloped. Site-sprung elastic timber gridshells can span long distances and at small material cost, but their erection method is costly and complex. Moreover, resulting geometries are limited and their topologies are fixed (Block, 2009). In addition to said shortcomings, they frequently require post-stiffening after erection (Cuvilliers et al., 2017). Conversely, sequentially erected gridshells can achieve a wider variety of geometries and are not fixed in their topology. Therefore, they are capable of forming stiff systems through irregular grid configurations. The design and construction of sequentially erected timber gridshells have recently become more elaborate, mostly based on prototypes (Harding et al., 2014, 2017; Secretan et al., 2011; Adiels et al., 2018; Schultz, 2017). However, none of the built prototypes was optimized for maximum structural performance while minimizing material use and cost. Most of the prototypes were built indoor, and none of them had to comply with the building codes in order to be constructed. Lastly, social relevance and life-cycle costs were not provided.

At the time when the world's population is growing rapidly, there is a growing need for structural systems that are capable of advancing sustainability, survivability, mobility, and efficiency. This thesis presents and discusses the potential of sequentially erected elastic timber gridshells as promising systems that can advance structural engineering while creating a social value within the spaces in which they are built-in. The construction of the INFRAME pavilion sheds new light on the potential adaptation of elastic timber grid systems to the existing building regulations and outlines the potential of functional applications for such systems.

1.1 Motivation and goals

Motivation

The main motivation for this research is to create a design-oriented framework for cost-efficient, impressive temporary structures, which can be constructed in a rapid way by unqualified builders. The selection of an elastic gridshell structural system is motivated by its incredible economy, ease of construction and high potential of deployability. Despite the ongoing research in the area of their construction, simulation and analysis, the design workflow and potential applications remain open-ended.

Goal

The objective of this thesis is to develop a design-oriented framework with integrated form and topology optimization for the structurally-sound elastic timber gridshells. The said framework has as its main goals (1) finding feasible geometries of elastic timber gridshells with high bearing capacity, and (2) serving as a universal design workflow, which can be adopted in the realization of similar structures.

Potential contribution

The geometry is the most important aspect of any structural system. Single-layer irregular gridshells can form a developable pattern on almost any surface. Early design exploration of feasible shapes and grid configurations is of great importance and is highly determinative of the final bearing capacity of the structure. The successful proposal of an effective design methodology can not only popularize elastic timber gridshells in practice, but also can increase their efficiency and help in achieving stiffer structures with longer spans.

Thesis structure

This thesis is divided into six chapters. The *Introduction* and *Literature review* chapters consist of an extensive overview of state-of-art research, built prototypes, form-finding methods and tools for simulation and analysis of bending active structure. The early design concepts and brief of the project are developed in the *Conceptual design methodology* chapter. The structural analysis and calculations necessary for the construction permission at the MIT Campus and fabrication documentation are presented in Chapters 4 and 5, respectively. Summary of the contributions, potential impact and future work are presented in the *Conclusions* section.

1.2 Definition and classification

Definition

An elastic gridshell is a system “consisting of flexible members” (Kuijnhoven & Hoogenboom, 2012:p.31). The desired geometry is achieved through the progressive elastic bending of initially in-plane grid members (Lienhard et al., 2013). The erection process can be performed on initially plane flat grid configuration (site-sprung) or through sequential bending of single members (sequentially erected) (Figure 1.1).



Figure 1.1 – Left: Site-sprung gridshell. Source: www.karamba3d.com. Right: sequentially erected elastic timber gridshell. Source: coda-office.com.

A traditional gridshell is understood as a grid sprung on-site from an initially planar, regular configuration. Traditional (regular) elastic timber gridshells use long continuous beams and are formed from flat deployable grid mats. They achieve large spans with minimal material cost, despite the complexity of the erection method.

“Whilst timber lath gridshells are traditionally formed from a fixed topology with hinged connections” (Harding *et al.*, 2017:p.1), the sequentially erected gridshells allow alternative irregular grid configurations. Sequentially erected gridshells can be constructed from members of rotational or non-rotational cross sections. They are cost-effective and can be constructed with hand-power with a mold-less process (Soriano, 2017). Elastic timber gridshells made of laths are usually called geodesic gridshells, as the geometry of laths is restricted to follow geodesic curves (Soriano, 2017). The use of geodesic curves makes it possible to construct the elastic gridshells from initially flat elements. In comparison to site-sprung gridshells, their shape is easier to control, as the predefined surface can be treated as a constraint. However, the double curvature shapes, known to be structurally efficient, usually do not “belong into the group of developable surfaces” (Schulitz, 2017:p.3). The control of geodesic patterns is not straightforward and requires intelligent rules and interactive adjustments (Pottmann *et al.*, 2010). As a consequence, in recent case studies the process of generation of the geodesic patterns was separated from the form-finding of primary shapes (Harding *et al.*, 2014, 2017).

Categorization of timber elastic gridshells

It is particularly difficult to provide one consistent categorization of the elastic timber gridshells. Nevertheless, several categories can be distinguished based on the construction process (site-sprung and sequentially bent), the definition of the surface (arbitrary, form-found), the configuration of the grid (regular and irregular) and the number of layers (single- and multiple- layers). Table 1.1 summarizes different categories that can be encountered in the literature.

Table 1.1 - Categorization of the elastic timber gridshells.

Erection process	site-sprung	sequentially erected
Shape	predefined surface	form-found shape
Grid generation	surface as a constraint	surface as a reference
Grid configuration	regular grid	irregular grid
Number of layers	single layer	multiple layers

1.3 Research question

Due to the easiness of achieving double curvature, cost-effectiveness and rapid construction process, there is a growing interest among engineers and architects in elastic gridshells, both site-sprung and sequentially erected. However, elastic gridshells are limited in their spans due to their high susceptibility to deflection and buckling (Coar *et al.*, 2018; Yuan, Chai & Jin, 2018). Sustaining relatively high bearing ability is even more difficult for single-layer geodesic gridshells. The fact, that the same double-curved surface can be produced with different developable geodesic patterns with various load-bearing capacities makes it highly challenging to find a grid configuration, which both exhibits the desired structural performance and meets geometrical and material requirements. Due to the proneness of geodesic gridshells erected sequentially to the material failure (Adiels *et al.*, 2018) and a greatly challenging design process of structurally-sound grid configurations, such systems have been built so far as rather experimental prototypes and their functional applications have been limited.

This thesis attempts to define a methodology for designing a structurally efficient elastic timber gridshell with the aid of multi-objective optimization. The methodology should then be used to construct a temporary outdoor stage INFRAME that meets building regulations. The real-life potential reuse and functional applications of the elastic timber gridshells systems in real-life scenario will be offering the structure on social media provided they inform me of the intended use.

2. Literature review

This part provides an overview of the state-of-art of the design, analysis and construction methods for timber elastic gridshells.

2.1 Review of research on elastic timber gridshells

Over the last decade, numerous research studies have focused on the form-finding procedures, software advancements for modeling and analysis of the resulting geometries, methods for defining grid configurations, stiffening techniques and construction methods dedicated for bending-active gridshells. The latest developments in these areas are presented in **Table 2.1** - Recent developments in research on elastic gridshells. Table 2.1.

Table 2.1 - Recent developments in research on elastic gridshells.

TOPIC	KEY WORDS	CONCLUSIONS	POTENTIAL CONTRIBUTION
CONSTRUCTION PROCESS	vernacular construction (Huang & Zhou, 2018), sequential erection method (Adiels <i>et al.</i> , 2018), 3D printed joinery (Schleicher, 2018), robotic fabrication (Huang & Zhou, 2018) (Yuan, Chai & Jin, 2018)	emerging mixed construction technologies	new erection processes, advancements of existing techniques
DEPLOYABILITY	deployable gridshells (Vassallo & Malek, 2017; Veenendaal, Augustynowicz & Tang, 2017), X-shells (Panetta <i>et al.</i> , 2019)	application of X-shells in a larger scale would require geometric representation with offset distance between joined beams	development of large deployable structures
ELASTICA	planar discrete elastica (Sakai & Ohsaki, 2018) designing discrete elastica by minimizing the strain energy (Sakai & Ohsaki, 2017)	elastica cannot deform in the out-plane direction (Sakai & Ohsaki, 2018), curved beams of gridshell can be modeled as discrete elastica (Sakai & Ohsaki, 2017)	obtaining the curved surfaces with elastica as solving optimization problems
ELASTIC GRIDSHELL PATTERNS	gridshell with principal stress pattern (Huang & Zhou, 2018), translation-gridshell (Oliva-Salinas, 2018), unconventional grid weave pattern (Brancart <i>et al.</i> , 2018), effective stiffening techniques (Brancart <i>et al.</i> , 2018), Geodesic Segments (GS) grid design (Schulitz, 2017)	best behavior when combined in regular woven patterns (Kozlov, 2018), GS-method combines the advantages of a Compass Method's uniform grid density with uniaxial bending (Schulitz, 2017)	extension of the GS method to larger grids (more than 30 panels) (Schulitz, 2017), a new method for defining geodesic patterns which activate the membrane behavior of elastic members

FORM-FINDING	nonlinear form-finding (Anastasiadou, Alexandrou & Phocas, 2018), geometry-driven and topology-driven approaches (Suzuki, Slabbinck & Knippers, 2017), prestressed gridshells with force densities (Ander <i>et al.</i> , 2017), dynamic relaxation including effects of bending and torsion in the process for bending active systems (Rombouts <i>et al.</i> , 2017)	topology-driven approaches suitable for design of bending and tensile form-active components (Suzuki, Slabbinck & Knippers, 2017), the dynamic relaxation method becomes identical to the Newton-Raphson method for bending active systems (Rombouts <i>et al.</i> , 2017), 6-DoF dynamic relaxation approach is accurate, even for large displacements and the coupling of torsion, bending moments, and axial forces (Rombouts <i>et al.</i> , 2017)	form-finding through virtual and augmented realities (Suzuki, Slabbinck & Knippers, 2017), combine form-finding with the generation of geodesics – “integrated the structural and the geometrical behavior in a more natural way” (Adiels <i>et al.</i> , 2018)
HISTORY/BACK-GROUND	recent developments in bending – active structures (Lienhard & Gengnagel, 2018)	Mulithalle Mannheim is still the largest timber lattice shell (Möller & Fischer, 2018)	achievement of larger spans
HYBRID SYSTEMS	combination with RF polyhedral morphologies (Larsen <i>et al.</i> , 2018), textile hybrid (Magna <i>et al.</i> , 2018)	active-bending as a promising approach to novel hybrid building structures (Lienhard & Gengnagel, 2018)	definition of new hybrid system
SOFTWARE FOR MODELING & ANALYSIS	GOEG (1982) – geometry of translation surfaces (Oliva-Salinas, 2018), simulation with SOFiSTiK, Kangaroo, Kiwi3D (Bauer <i>et al.</i> , 2018), software comparison for bending-active systems (Magna <i>et al.</i> , 2018)	FEM analysis for active bending with SOFiSTiK, Kiwi3D	extensions for the exiting tools
STRUCTURAL BEHAVIOR	influence of the residual stress on the structural behavior of elastic structures (Lienhard, 2014; Mesnil, Ochsendorf & Douthe, 2015)	elastic gridshells susceptible to deflection and buckling, limited long spans (Coar <i>et al.</i> , 2018), limited large spans (Yuan, Chai & Jin, 2018), stress-stiffening effects are at great importance for structures with small elastic stiffness (Lienhard, 2014), initial strain reduces the bearing capacity of an elastic structure (Mesnil, Ochsendorf & Douthe, 2015)	increase in bearing ability and stabilization of elastic gridshell to achieve greater spans

Recent developments in bending-active structures are largely elaborated by Lienhard and Gengnagel (2018). An extensive state of the art research on site-sprung elastic gridshells is provided in chapter *1.4 Research works on elastic gridshells: a review* (Peloux, 2018).

2.2 Form-finding methods

When form-finding bending active structures, “like for form-active structures, the shape is dependent on the internal force equilibrium but in this case primarily from bending action rather than tension/compression” (Brandt-Olsen, 2016:p.1).

Development of form-finding approaches

Elastic timber gridshells form part of wider group of bending-active structures. Therefore, advancements in the form-finding approaches for elastic timber gridshells have been a part of developments in processes of finding forms of active-bending systems. The following approaches for the form-finding of active-bending systems can be distinguished in the chronological order:

- **BEHAVIOR BASED APPROACH (EMPIRIC)** - “the system’s geometry and structural behavior is studied empirically” (Lienhard *et al.*, 2013:p.190).
- **GEOMETRY BASED APPROACH (ANALYTICAL)** - “the system’s geometry is predefined based on analytical geometry or experimental form-finding methods, both of which are used as a controlled means to approximate the actual bending geometry” (Lienhard *et al.*, 2013:p.190).
- **INTEGRAL APPROACH (NUMERICAL)** - “the elastic bending deformation is analyzed through numerical form-finding, which enables full control of material behavior based geometry” (Lienhard *et al.*, 2013:p.190).

Form-finding naturally developed from empirical experiments through geometric analytical methods to more modern techniques based on the dynamic equilibrium. The extensive review of the existing form-finding methods was provided by Block and Veenendaal (2012) in: *An overview and comparison of structural form finding methods for general networks* and then compared by the same authors in *Comparison of form-finding methods* (Veenendaal & Block, 2014). In Table 2.2 the known form-finding methods for the design of timber gridshells are presented.

Table 2.2 - Form-finding methods applicable for timber gridshell design.

	METHOD & ELEMENT TYPE	APPLICATION
Geometric Stiffness	Force density method (FDM) 1971/1974 bar + surface (1995)	unstrained timber gridshells (Linkwitz, 2014)
	Nonlinear Force Density Method (FDM) (1974)	strained timber gridshells e.g. Multihalle in Mannheim (Grundig & Schek, 1974)
Dynamic Equilibrium	Dynamic Relaxation (DR) (1977) bar + surface (1977)	strained timber gridshells e.g. Savill Building (2006) Windsor Great Park (2006) (Adriaenssens <i>et al.</i> , 2014)
	Particle-Spring System (PS) bar (2005)	strained timber gridshells (Kuijnhoven & Hoogenboom, 2012)

Geometry-based approaches

Analytical methods outlined by Lienhard and others (2013) and geometric stiffness methods described by Block and Veenendaal (2012) seem to share the same principle: geometry is obtained in an analytical way, without accommodating material properties or the effects of bending. This material independence can be perceived as the advantage of selecting individual material for each network member. On the other hand, the omission of the bending effects and material properties in the analytical and geometric stiffness form-finding methods might result in inaccurate or even false forms found. Nevertheless, “new analytical approaches from engineers like Timoshenko in the 1950’s led to the development and general availability of nonlinear Finite Element Methods and created the basis of modern engineering mechanics, now offering a complete framework for the form-finding and analysis of bending-active structures.” (Lienhard *et al.*, 2013:p.188). Dynamic Relaxation and Particle Spring Systems are two modern procedures available for form-finding of elastic timber gridshells.

Dynamic Equilibrium approaches

- *Dynamic Relaxation (DR)*

Dynamic Relaxation (DR) “is a time discretization of the dynamical behavior of physical systems, introduced in the 1960s” (Cuvilliers *et al.*, 2018:p.76). DR has been implemented in Kangaroo 1 - a software package for Rhinoceros 3D/Grasshopper. Dynamic Relaxation can incorporate effects of bending and torsion for form-finding and analysis of bending-active structures by using either 3-DoF, 4-DoF, or 6-DoF beam elements (Rombouts *et al.*, 2017). It has been widely implemented and applied in design and simulation of elastic gridshells (Barnes, Adriaenssens & Krupka, 2013; Li & Knippers, 2013; D’Amico, Kermani & Zhang, 2014; Poulsen, 2015; Peloux, 2018). Dynamic relaxation was used to design the strained timber gridshell of Savill Building at the Windsor Great Park (2006) (Adriaenssens *et al.*, 2014).

- *Particle-Spring Systems*

Form-finding of shell structures with particle-spring systems was introduced by Killian and Ochsendorf (2005) and can be used for simulation of pretensioned grids (Bhooshan, Veenendaal & Block, 2014). In the first implementation it considered only the axial forces (Killian & Ochsendorf, 2005). Kuijvenhoven & Hoogenboom (2012) extended the Particle-Spring method to generate gridshells as close as possible to the target surfaces while not exceeding the material’s permissible stresses.

- *Projective Constraints*

The projective constraint-based solving method works as follows: “At each iteration, the solver moves closer to the equilibrium position by projecting the positions on the sets of constraints representing the relationships between them. The solution is a physical equilibrium with correct derived forces, if the constraints are physically accurate.” (Cuvilliers *et al.*, 2018:p.76). Solver based on projective constraints is implemented in Kangaroo 2.

- *Large Deformations*

Large deformation analysis in Karamba3D can be used to generate shapes of bent members. As Olsen (2016) presents (Section 2.1.3) the generated shapes are trustful in some range of the tested buckled states (accuracy decreases with the progress of buckling).

The simulation of large deflection is also implemented as a non-linear solver in SOFiSTiK, with benchmarks available at the software website.

Arbitrary surfaces

Particle Spring System and Dynamic Relaxation have been mostly applied for form-finding and analysis of site-sprung gridshells. Grid of geodesic sequentially erected gridshells can be defined on any surface - arbitrary or defined with the aid of form-finding techniques. Funicular surfaces were used for Geodesic Gridshell (Adiels *et al.*, 2018) and Timber Gridshell with Geodesic Segments (Schulitz, 2017), while UWE pavilion (Harding *et al.*, 2017) and Almond Pavilion (Soriano, 2017) were based on arbitrarily chosen shapes.

2.3 Structural analysis of active-bending systems

Active-bending structural systems are formed from initially straight members, therefore, elements “seek to spring back to their initial state” (Isaksson & Skeppstedt, 2018:p.32). Their flexibility makes them difficult to analyze as most of the finite element programs for structural analysis are based on the assumptions of the small displacements (Brandt-Olsen, 2016). The stresses in members due to initial bending are much higher than from external loads (Lafuente Hernandez, 2015). To analyze such structures the prestress due to initial bending should be incorporated into the analysis. For bending-active structures made from high-strength materials like GFRP or carbon fiber¹, the initial bending prestress might be omitted to a certain degree in the structural analysis, however for elastic timber gridshells the bending stresses cannot be ignored (Brandt-Olsen, 2016).

While using form-finding based on the FE analysis, the stresses due to initial bending are incorporated via simulation. The incorporation of initial prestress can be trickier for elastic gridshells with structural components that follow geodesic curves on a surface. In the analysis of the Ongreening pavilion the principle of superposition was applied: “the stresses in the members resulting from the applied loads were added to the stresses arising from the initial curvature of the laths” (Brandt-Olsen, 2016:p.9). This approach is suitable for defining the moment distribution and resulting utilization due to bending. However, in this method, prestress is not taken into the displacement calculations; therefore, the displacements are inaccurate. For the UWE Pavilion bending stresses were evaluated using the 3-DOF model implemented in K2Engineering and Kangaroo2, while biaxial bending stiffness was assessed with the FE model using Karamba3D (Isaksson & Skeppstedt, 2018).

¹ The allowable stress of a structure made of GFRP is 5 times higher than a similar structure made of timber (Lafuente Hernandez, 2015).

Selected software packages used for analysis of elastic structures

- *Karamba3D*

Karamba3D is a Finite Element program fully embedded in the Rhino/Grasshopper environment, which offers an easy way to combine parametric models with structural analysis and optimization (Preisinger, 2019).

- *Kangaroo and Kangaroo2*

The bending simulation in Kangaroo is based on the 3DOF model presented by Barnes, Adriaenssens and Krupka (2013). It uses discrete elements and is based on the local stiffness solver (Bauer *et al.*, 2018). Kangaroo is mostly used for the simulation and not the analysis of the bending-active structures. A brief benchmarking comparison of Kangaroo, Kiwi3d and SOFiSTiK is presented by (Bauer *et al.*, 2018) which confirms the SOFiSTiK is one of the most precise FE analysis software packages, Kiwi3d is a promising tool for isogeometric analysis and projection-based dynamic relaxation in Kangaroo2 introduces fair accuracy of simulation with high level of interactivity.

- *K2Engineering*

A plug-in extending the Kangaroo2 framework dedicated for design and analysis of form-active structures within the Rhino/Grasshopper environment. It incorporates axial and bending behavior based on the 3DOF system and provides useful visualization of geometrical and analysis data (Brandt-Olsen, 2016).

- *Kiwi3d*

The Isogeometric Analysis (IGA) is implemented in Kiwi3d – a plugin for Grasshopper. It is based on the FEM-kernel Carat++ and it performs structural analysis on continuous geometrical elements such as Non-Uniform Rational B-Splines without the need for discretization (Bauer *et al.*, 2018). Kiwi3d is based on the Euler-Bernoulli theory (Bauer *et al.*, 2018). Kiwi3d seems a suitable tool for analysis of elastic gridshell due to its capability of handling NURBS elements. However, it was found that WIP version does not allow adjustments of the local coordinate system of the beam, therefore the cross section follows the curved axis without adjustment of the local z-axis to the surface normal vectors. Consequently, the available at the time of this research version was not suitable for analysis of geodesic gridshells.

- *SOFiSTiK*

Detailed analysis including torsion and membrane behavior can be conducted with SOFiSTiK. The recently implemented Active Bending module (ACTB) automatically calculates the internal stress state from a curved beam under the assumption that it was initially straight. SOFiSTiK employs the Timoshenko beam theory (Bauer *et al.*, 2018).

2.4 Review of the built elastic timber gridshells

Despite the recent numerous research studies on methods of generating grid configurations and analysis of the resulting geometries, their long span applications are still limited. The Mannheim Multihalle, built in 1974 for the 1975 National Garden Show (Hill, 2018) remains the largest timber lattice shell (Möller & Fischer, 2018). The next in the span size was the Japanese Pavilion built for EXPO (2000) in Hannover (cardboard tubes), Savill Building (2006) and the Downland Gridshell at the Weald and Downland Open Air Museum (2002). Figure 2.1 shows the known built elastic gridshells since 1960.

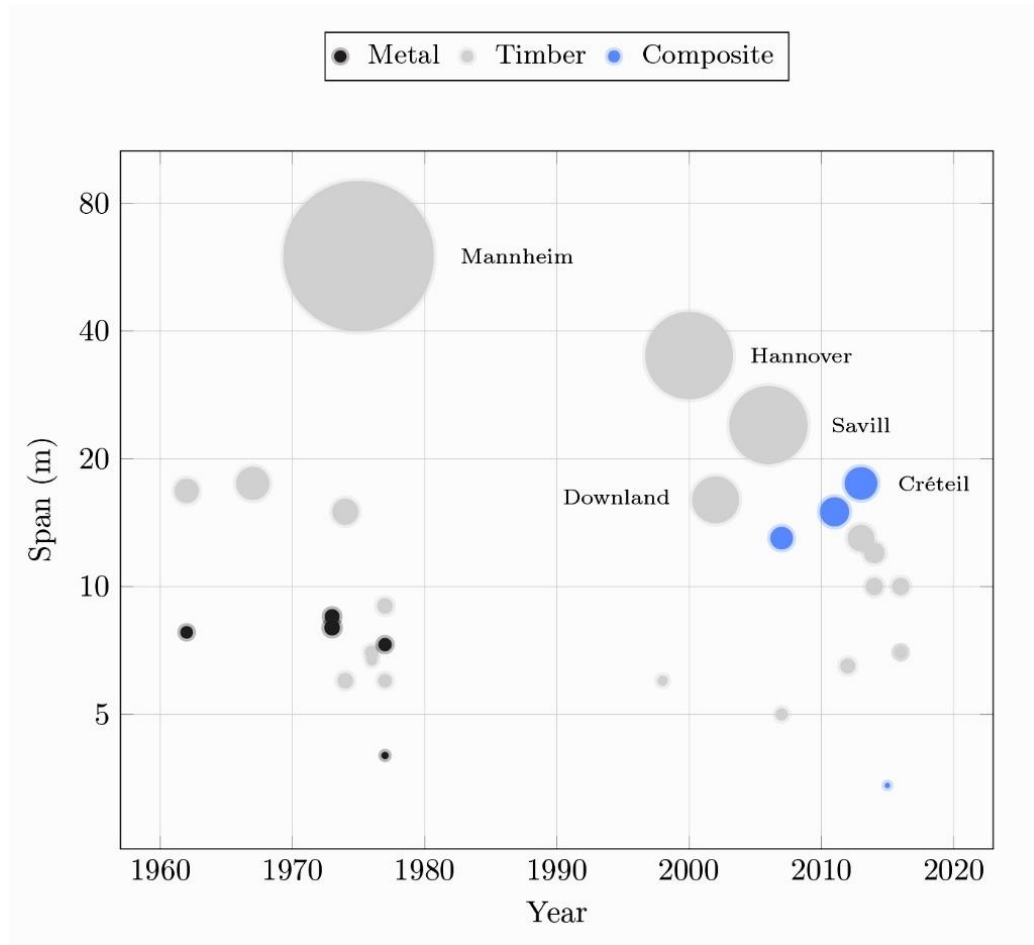


Figure 2.1 - Known built elastic gridshells (Peloux, 2018:p.13).

Traditional Timber Gridshells (regular-grid/site-sprung)

After almost a decade after the Multihalle construction, small realizations of elastic site-sprung gridshell structures started to appear after 2010 initiated by a research group gridshell.it. One of their first pavilions was built in 2010 in Lecce, followed by Toledo pavilion (2012) and Toledo 2.0 (2014), both built in Naples, Italy (Peloux, 2018). Table 2.3 presents an overview of Multihalle Mannheim and Downland Gridshell.

Table 2.3 - Review of the site-sprung gridshells - Multihalle Mannheim and Downland Gridshell.

Multihalle Mannheim (1974)

Engineer: Frei Otto
Architects: Carlfried Mutschler
and Winfried Langner
Location: Mannheim, Germany
Footprint: 60x60m
Photo source: (Möller & Fischer,
2018)



Form/Form-Finding	model-based, a hanging chain model, non-linear FDM (Grundig & Schek, 1974)
Main structure	4 layers of Hammock laths 50x50mm
Structural analysis	model tests
Stiffening	twin 6mm cables every 6th node
Construction process	site-sprung, with scaffolding
Problems	stiffening required
Conclusions	it is better to introduce multiple layers than increase the cross sections of the bent members

The Downland Gridshell at the Weald and Downland Open Air Museum (2002)

Architect: Edward Cullinan
Engineer: Buro Happold
Location: Sussex, England
Footprint: 50 m × 15.2 m
Photo credit:
@helenhookerarchitecture






Form/Form-Finding	Dynamic Relaxation
Main structure	35 mm × 50 mm solid rectangular sections Oak laths with triangular panels
Structural analysis	integrated with DR form-finding
Stiffening	panels
Construction process	site-sprung
Problems	complex assembly in wet conditions
Conclusions	it was used as a temporary entrance canopy

Ribbed (geodesic) timber gridshells (irregular grid, sequentially-erected)

Along with the development of the site-sprung timber gridshells around 2010, timber gridshells started to be built in a sequential construction manner. While *gridshell.it* has been mostly focused on building double-layer site-sprung structures, several experimental sequentially erected structures have been built since 2010 - very often as a result of a collaboration between academia and industry (BuroHappold, Ramboll or CODA). Single-layer, sequentially erected gridshell structures are very often called geodesic gridshells, as their lath configuration follows the geodesics on the predefined surfaces. As opposed to simple geodesic curves, the structural splines have width, and are called plank lines (laths). Structural members with rectangular cross sections that follow the zero-geodesic curvature on a surface can use simple pin-joint connections and can be unrolled to the initial flat state. The geodesic grid configurations have been applied in several projects such as Ongreening Pavilion (Harding *et al.*, 2014), UWE Research Pavilion (Harding *et al.*, 2017), the Almond Pavilion (Soriano, 2017), and the Geodesic pavilion at Chalmers University (Adiels *et al.*, 2018). A review of selected sequentially erected geodesic timber gridshell structures is presented in Table 2.4.

Table 2.4 - Review of the built sequentially erected elastic timber gridshell prototypes.

Ongreening Pavilion (2014) Designer: Ramboll Computational Location: EcoBuild, London Photo credit: © Ramboll	
Form/Form-Finding	doubly-curved shell, surface as a result of loft through the form-found elastica curves
Main structure	pre-stressed timber members of constant bending stiffness, primary laths based on geodesic curves
Structural analysis	Karamba3D (prestress manually included in the analysis by supersposition), non-linear analysis in SOFiSTIK
Stiffening	random nature of the secondary topological layer, refined manually
Construction process	sequential bending, Finnish Birch plywood laths, 6.5x100mm
Problems	assembly order of the laths in order to minimize any temporary supports required during construction
Conclusions	“acting similarly to a continuous monocoque” (Harding <i>et al.</i> , 2014)

UWE Pavilion (2016) Designer: Format Engineers (Structural Design) Location: University of West England, UK Dimensions: inscribed in a circle of radius 4m Photo credit: John Harding	
Form/Form-Finding	lofts through sets of splines, defined parametrically from perimeter base curves and heights (free-form)
Main structure	geodesic curves on the surface form (Harding <i>et al.</i> , 2017), Finnish Birch plywood, 6.5 x 100mm
Structural analysis	Karamba3D and later incorporating K2Engineering based on the Kangaroo 2 Physics engine
Stiffening	unidirectional lath pattern, critical buckling issues addressed by altering the gridshell topology live, the introduction of double-layer members with shear blocks at the free edges
Construction process	sequential bending - all laths bent and installed on-site
Problems	The density of the lath pattern in areas of large double-curvature, geometry required the introduction of two types of laths, buckling problems
Conclusions	resulting structure was extremely stiff due to its high double curvature and a monocoque grid pattern (Harding <i>et al.</i> , 2017)
Geodesic gridshell workshop (2017) Responsible teachers: Emil Adiels, Isak Näslund Location: Chalmers University of Technology in Gothenburg Sweden Dimensions: 11x11 m Photo credit: Emil Adiels	
Form/Form-Finding	gravity-driven funicular shape
Main structure	combination of laths mostly forming arches, 6 mm thick Birch plywood, cross section 6x50mm
Structural analysis	a structural analysis plugin for Grasshopper 3d named Emu (Poulsen, 2015) by using its' built-in time-stepping based non-linear solver, a basic bending stress check was performed
Stiffening	n/a
Construction process	sequential erection method to avoid material failure during erection and in its final position
Problems	two laths did break, one during erection and one when built, the first had a knot in the middle layer and the second broke near a connection in the finger joints of the plywood
Conclusions	material cost less than 1000EUR, "less stiff connection in combination with a curvature driven segmentation could have avoided the [material] second failure [...] other improvements could have been to combine form-finding with the generation of geodesics." (Adiels <i>et al.</i> , 2018:p.8)

Timber Gridshell Exploration using Geodesic Segments (2017)

Designer: Mark Schulits
Location: California, USA
Dimensions: 6m x 6m x 3m
Photo credit: N.Lopez



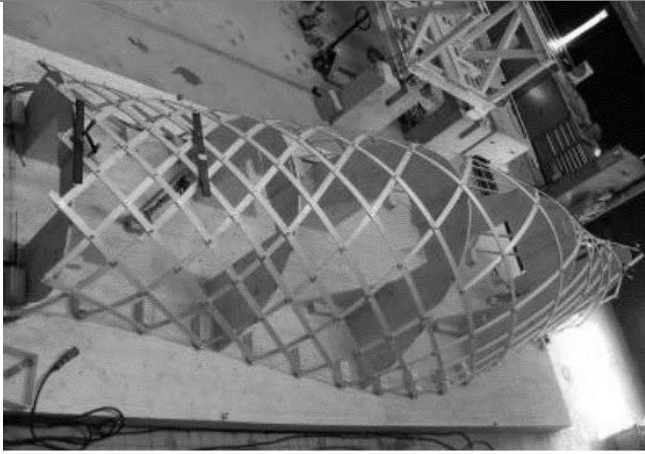
Form/Form-Finding	funicular shell, “Kangaroo’s dynamic relaxation - funicular models by inversion of uniformly loaded equidistant nets, which also served as the Compass Method starting grid” (Schulitz, 2017:p.5)
Main structure	Geodesic Segments (GS) – relies solely on the axial forces, geodesic curves, Southern pine 6.35mm x 89mm
Structural analysis	n/a
Stiffening	“each x-direction segment’s end points are connected to the mid points of two segments (running in the y-direction and vice versa (just like Zollinger/Lamella)” (Schulitz, 2017:p.1)
Construction process	on-site, “first the base was laid out to provide a uniform nailing surface for the foundation blocks” (Schulitz, 2017:p.9)
Problems	the available computational power limited the exploration to grids not larger than 30 panels in the x- and y-directions and to fifty iterations
Conclusions	grid mapping methods emphasizes the GS-methods design potentials and grid properties due to uniaxial bending

Almond Pavilion (2013)

Designers: Enrique Soriano, Pep Tornabell, Gerard Bertomeu, Miriam Cabanas, Xavi Santodomingo, Ramon Sastre
Location: Spain
Dimensions: not provided
Photo credit: Andres Flajszer



Form/Form-Finding	a free-form surface created by lofting three curves, “the surface was designed in order to reduce curvature in the boundaries” (Soriano, 2017:p.36)
Main structure	the network of UV lines transformed in to a geodesic network, 1,5 m3 of pinus halepensis
Structural analysis	n/a
Stiffening	no stiffening, but network density “controlled by n evenly spaced starting points on boundary curves and the grid angle aspect is controlled by the shift of corresponding points in the next curve” (Soriano, 2017:p.33)
Construction process	on-site, mold-less, “sequential bending of coupled planks without scaffolding” (Soriano, 2017:p.36)

Problems	a custom algorithm locates the splicing joint avoiding the overlap with the node joint has to be developed
Conclusions	an elastic bending shell transforms after drying into a rigid shell
Prototype “Geodesic Lines on Free-Form Surfaces” of (2006) Design: Swiss Federal Institute of Technology in Lausanne (EPFL) Location: Lausanne, Switzerland Dimensions: 8m x 3m x 2.06m Photo source: (Pirazzi & Weinand, 2006)	
	
Form/Form-Finding	a free-form surface defined “by manipulating control points of cubic Bézier-polynomials” (Pirazzi & Weinand, 2006)
Main structure	software GEOS, “the iterative calculation of the geodesic lines is based on an L-BFGS-B algorithm”(Pirazzi & Weinand, 2006), rectangular cross section: 12/60 mm, Swiss spruce wood (Picea abies)
Structural analysis	load tests
Stiffening	n/a
Construction process	sequential bending
Problems	resulting geodesic grids are “not always compatible to structural and architectural demands like the regularity of the grid or the minimum radius of curvature of a single board.” (Pirazzi & Weinand, 2006)
Conclusions	the scaffolds were not necessary – used just for the precision

2.5 Research gap

All of the built prototypes were of experimental character, often not structurally analyzed e.g. prototypes presented by Soriano (2017) and Schultz (2017). For the reviewed precedencies, the grid exploration was limited (UWE Pavilion) or omitted. The structural grid optimization was limited to local interventions. Most of the prototypes were built indoor, and none of them had to comply with the building codes. The functional applications of structures remained unexplored. This thesis provides a comprehensive design workflow, with incorporated grid configuration optimization. It then lead to the construction of the structurally-sound elastic timber gridshell – INFRAME. The potential future functional roles were explored through the social media post.

3. Conceptual design methodology

“For all ... structures, efficiency and economy are absolutes, something all engineers must strive for, but elegance is the bulls-eye, if you hit elegance, and efficiency, and economy then you have reached a level called Structural Art.”

-M. Garlock

The idea of an artistic intervention that activates the public space between buildings E15 and E25 was awarded a CAMIT grant 2019 from the Council for the Arts at MIT. A temporary structure was proposed as an outdoor stage for experimental music and video performances to take place over a weekend timeframe. The structure should endeavor to embody the principles of structural art and provide space for art in and around it.

3.1 Project overview

The goal of this project was to design an elastic timber gridshell which can serve as a temporary performance pavilion in the Richard Fleischer Lower Courtyard, between buildings E14, E15, and E23 at the MIT campus. The pavilion should provide enough space for the various artistic performances, including audio-visual projections and live music acts during a planned festival. The pavilion should sustain at least 2 times its self-weight and wind-load, be low-cost and produce minimal waste. The permission for the construction was contingent upon the final design drawings stamped by a licensed structural engineer in Massachusetts and the construction schedule reviewed by the Office of Environment, Health & Safety (EHS), and the Department of Facilities (permission process and required documents in Appendix B). The project explores state-of-art design aids e.g. shape and grid configurations optimization, while keeping a focus on constructability and meeting the code requirements.

3.2 Initial concepts

Early concepts – location Lower Courtyard

Development of the early concepts (Figure 3.1) involved trying out different locations at the Richard Fleischer Lower Courtyard and consultation of them with the owner of the grounds and the EHS office. The locations in the area of the grass (Figure 3.1: top, middle) created a risk of destroying the lawn which was a part of the artwork, while the location on the hard ground middle stripe was blocking the fire route (Figure 3.1: bottom). The final location was approved on the pavement over the staircase (Figure 3.2).

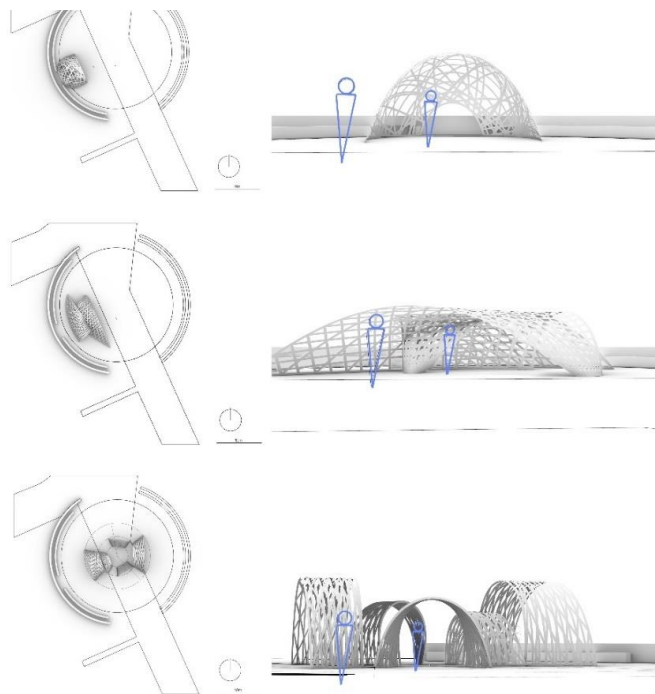


Figure 3.1 - Early design concepts for INFRAME.

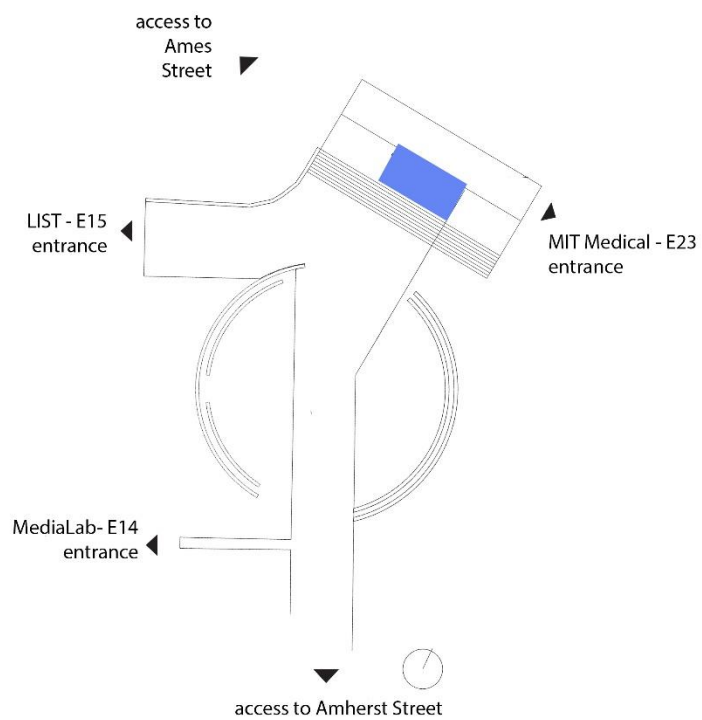


Figure 3.2 – The approved location for the temporary stage.

3.3 Design workflow

The early concept phase allowed on the specification of the new location of the pavilion over the staircase and development of the design workflow (Figure 3.3), which was utilized to propose more detailed concepts for the approved location.

Surface

Sequentially erected elastic timber gridshell can be constructed both on the form-found and arbitrary chosen surfaces. In the proposed workflow a semi-form-found surface is suggested - a shape resulting through lofting through form-found elastica curves. Double-curvature is desired to counteract buckling. To introduce an iterative adaptation of the shape it is desirable that the shape is controlled by parameters.

Curvature check (optional)

In order to inspect the surface for allowable curvature without specifying the grid configuration, the principal curvatures should be evaluated. For the principal curvatures in the matrix form, the Ky Fan norm for the maximum curvature of the surfaces can be computed. The surface should satisfy the condition that at any point on a surface:

$$k_{max} < ||k_1 * k_2||^{1/2}$$

where k_1 and k_2 are the principal curvatures of the surface, and k_{max} is the maximum allowable curvature for the considered material. In other words, at any point on the surface the absolute value of either of the principal curvatures should not exceed the maximum allowable curvature k_{max} .

Primary grid²

When the surface is form-found, the primary grid could be set as the geodesic curves approximating initial elastica curves resulting from the form-finding. The gridshell is formed by the first layer of such defined laths and the secondary complementary laths. Alternatively, the primary grid can be defined by the designer, but with the constructability in mind.

Secondary grid

The role of the secondary grid is to provide maximum stiffness. “The same curved shell surface can be reproduced by various developable grid configurations” (Lafuente *et al.*, 2011:p.1), therefore grid arrangement influences the gridshell load-bearing capacity. For the elastic gridshells with a non-rotational cross section like those made from timber, the grid configurations are restricted to follow zero geodesic curvature on surfaces. The primary and secondary grid form together a multi-direction single layer grid configuration.

Minimum radius check

In order to specify the desired curvature (activating self-stiffening effects) and minimum allowable radius of the bent timber laths, a series of physical tests should be conducted. The allowable radius can be also specified analytically.

² In the proposed workflow, grid design is separated into the primary and secondary grid definition, however the multi-directional final grid configuration can be defined in one step, as well.

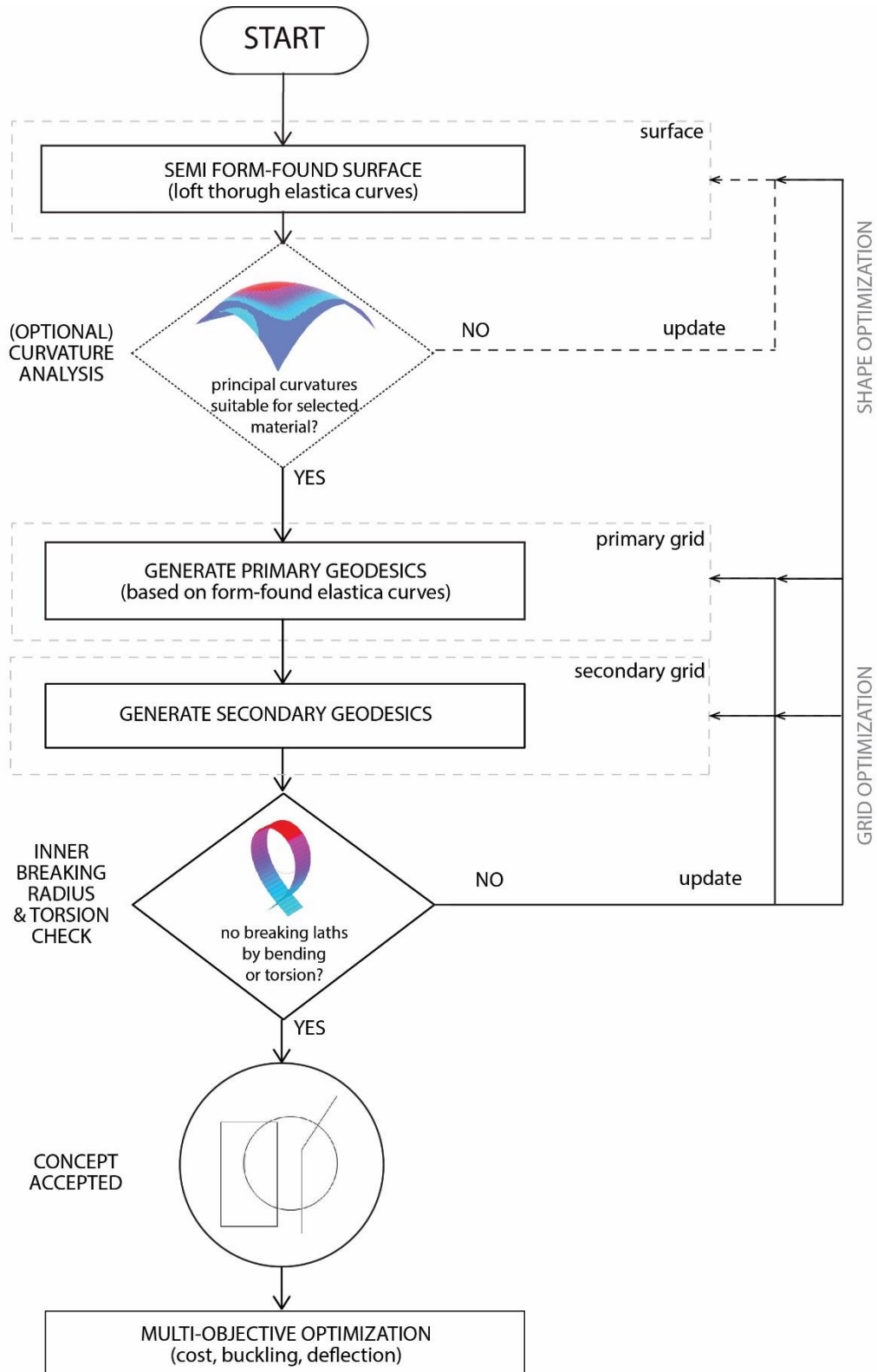


Figure 3.3 - Developed design workflow for conceptual design.

3.4 Design concepts

A few concepts were developed using the proposed workflow (Figure 3.5 and Figure 3.6). In the initial considerations, the structure was meant to be covered with a membrane. In order to avoid the requirement for a building permit, all the concepts were below 12ft height and the covered area below 120ft². The approximate cost was estimated using a custom-made cost estimator. The price was estimated based on the length of the perimeter beam, number of support points, total length of members, and number of joints. All the design proposals met the requirement of the minimum bending radius for Baltic Birch plywood defined in Section 4.3. The proposed concepts were evaluated in four categories: users, performance, structure and research (Table 3.1). The visibility of performers and the possibility to walk through the structure are visualized in Figure 3.4. Based on the proposed evaluation criteria, proposal 4 was selected for further development.

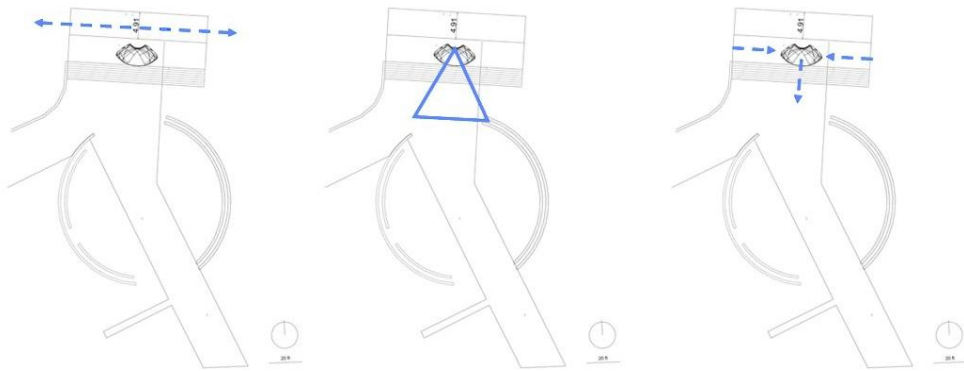


Figure 3.4 – Selected features of the selected proposal 4, from the left: access to the neighboring buildings, stage visibility, the possibility to walk through the structure, when the stage is not used.

Table 3.1 – Evaluation of the concepts for the approved location.

		OPTION 1	OPTION 2	OPTION 3	OPTION 4
		TUNNEL	DOME-LIKE	FOLDING	DD
USERS	walk through?	1	0	1	1
	dj visibility	1	1	0	1
PERFORMANCE	enough rain coverage	1	1	1	0
	space for speakers	1	1	1	1
STRUCTURE	size of the membrane	1	0	1	1
	span	0	0	1	1
	foundation difficulty	-1	1	1	1
RESEARCH	topology opt. applies	1	1	1	1
	shape opt. applies	1	1	1	1
TOTAL		6	6	8	8

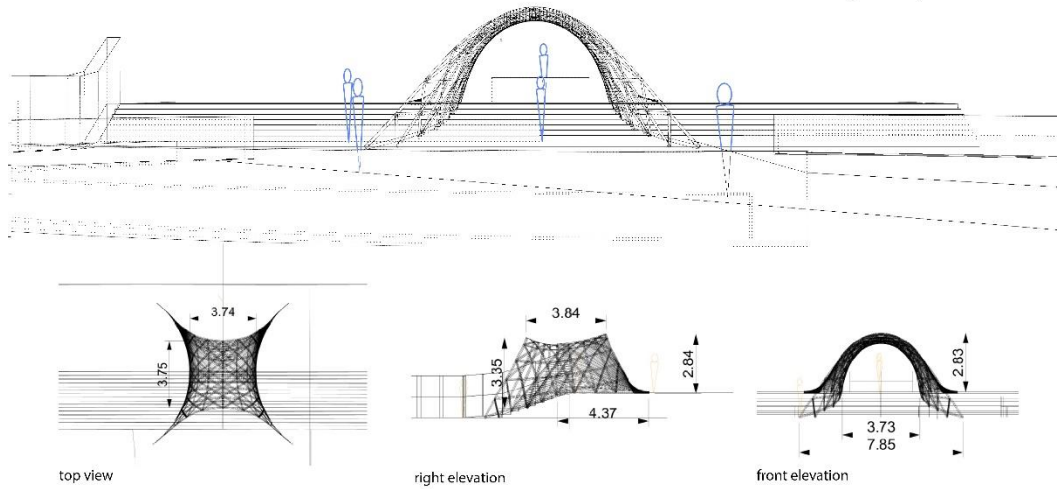
Proposal 1

approximate total cost:

2880 USD

covered area:

11.32 m² (120 ft²)



Proposal 2

approximate total cost:

2781 USD

covered area:

11.1 m² (<120 ft²)

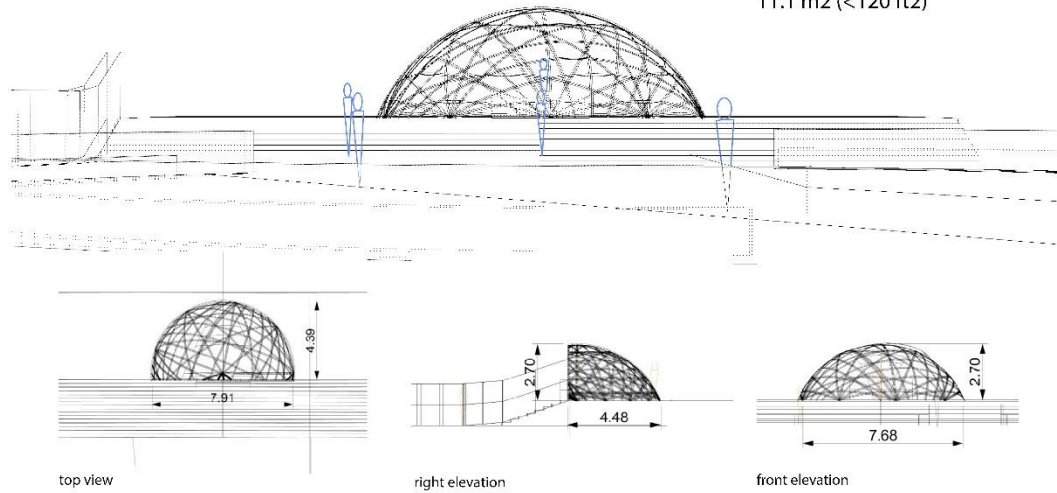


Figure 3.5 - Concept development at the approved location – proposal 1 and 2.

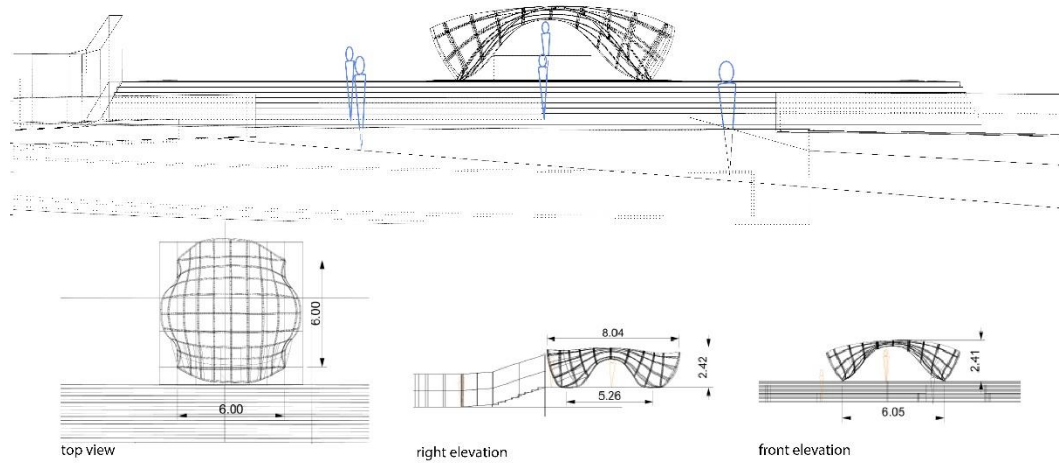
Proposal 3

approximate total cost:

2223 USD

covered area:

11.6 m² (120 ft²)



Proposal 4

approximate total cost:

2503 USD

covered area:

11.6 m² (~120 ft²)

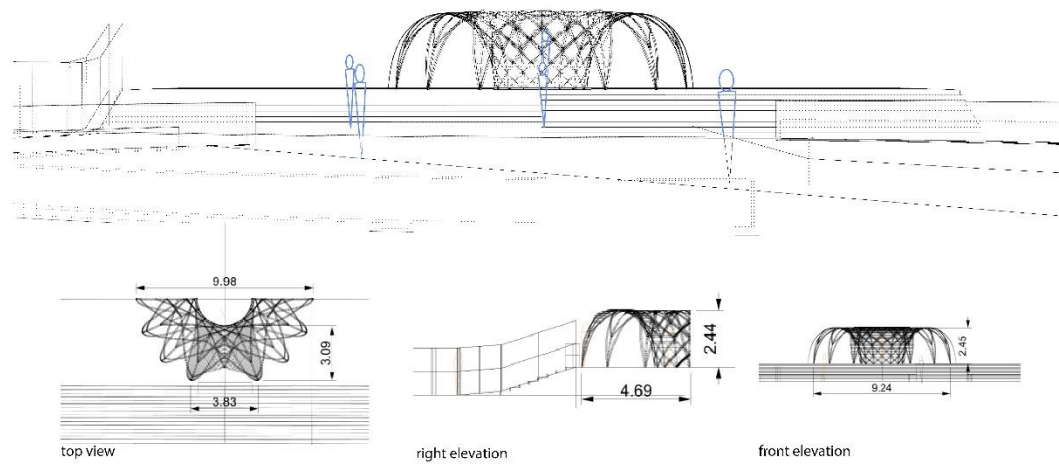


Figure 3.6 - Concept development at the approved location– proposal 3 and 4.

3.5 Multi-objective optimization

To specify a grid configuration with maximum load-bearing capacity, a parametric model was defined. The models were optimized towards three objectives: minimization of the cost and deflection, and maximization of the buckling factor (Figure 3.7, Figure 3.8). The cost was estimated using a custom-made cost function, while the deflection and buckling factor were evaluated with Karamba3D under factorized dead load (1.3D).

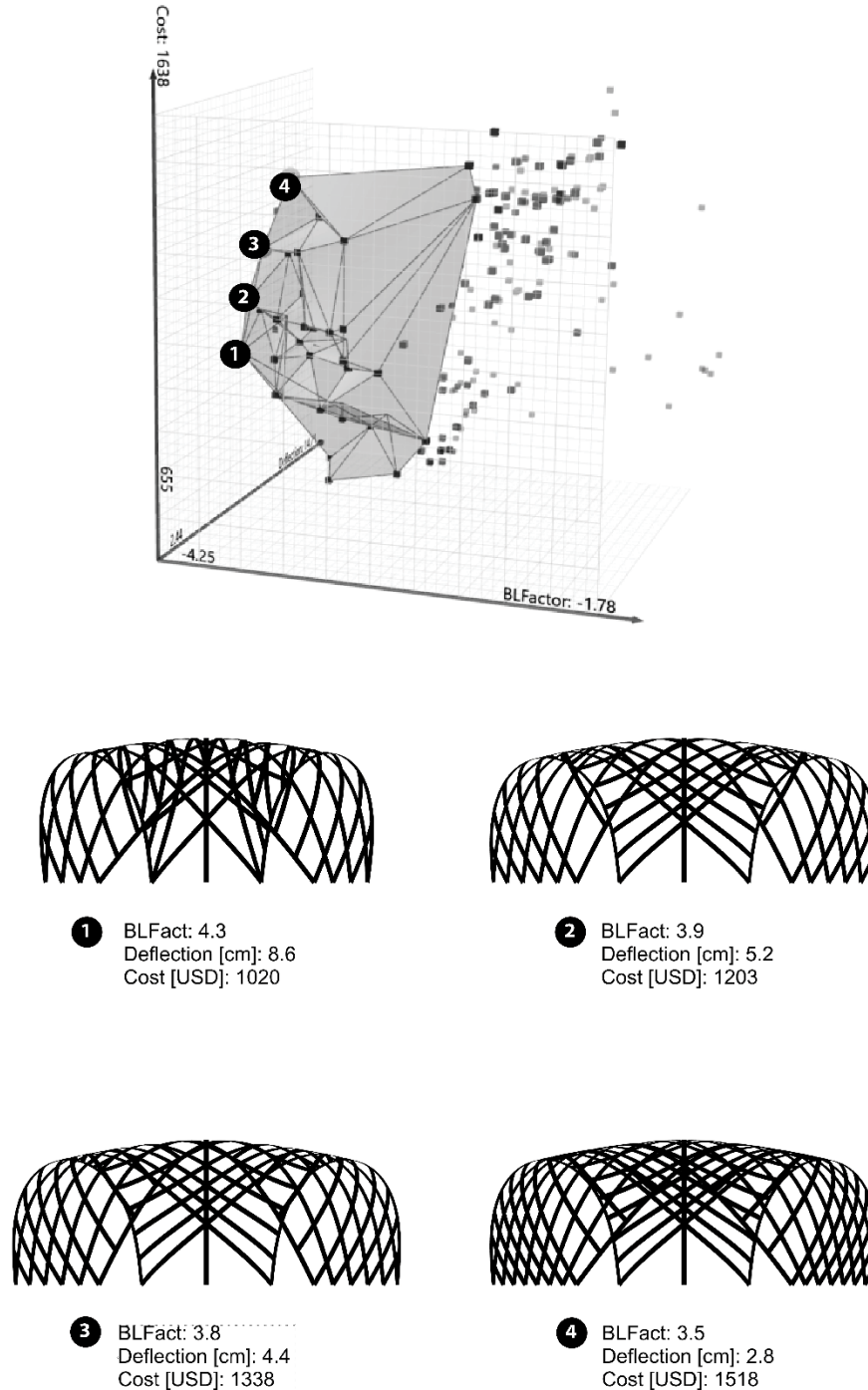


Figure 3.7 - Multi-objective optimization of grid configuration.

The parameters controlled the overall size and grid's density. In the first run the size of the front opening could have been modified as well. In Figure 3.7 a lot of pareto-front solutions have a small frontal opening, which obviously helps in achieving better structural performance, but is impractical (visibility of the performers). The second run of the multi-objective optimization was conducted on the refined model which introduced additional ribs (Figure 3.8). As a trade-off between cost (and related construction time) and the structural performance, the solution no 2 was selected (Figure 3.8) for further analysis.

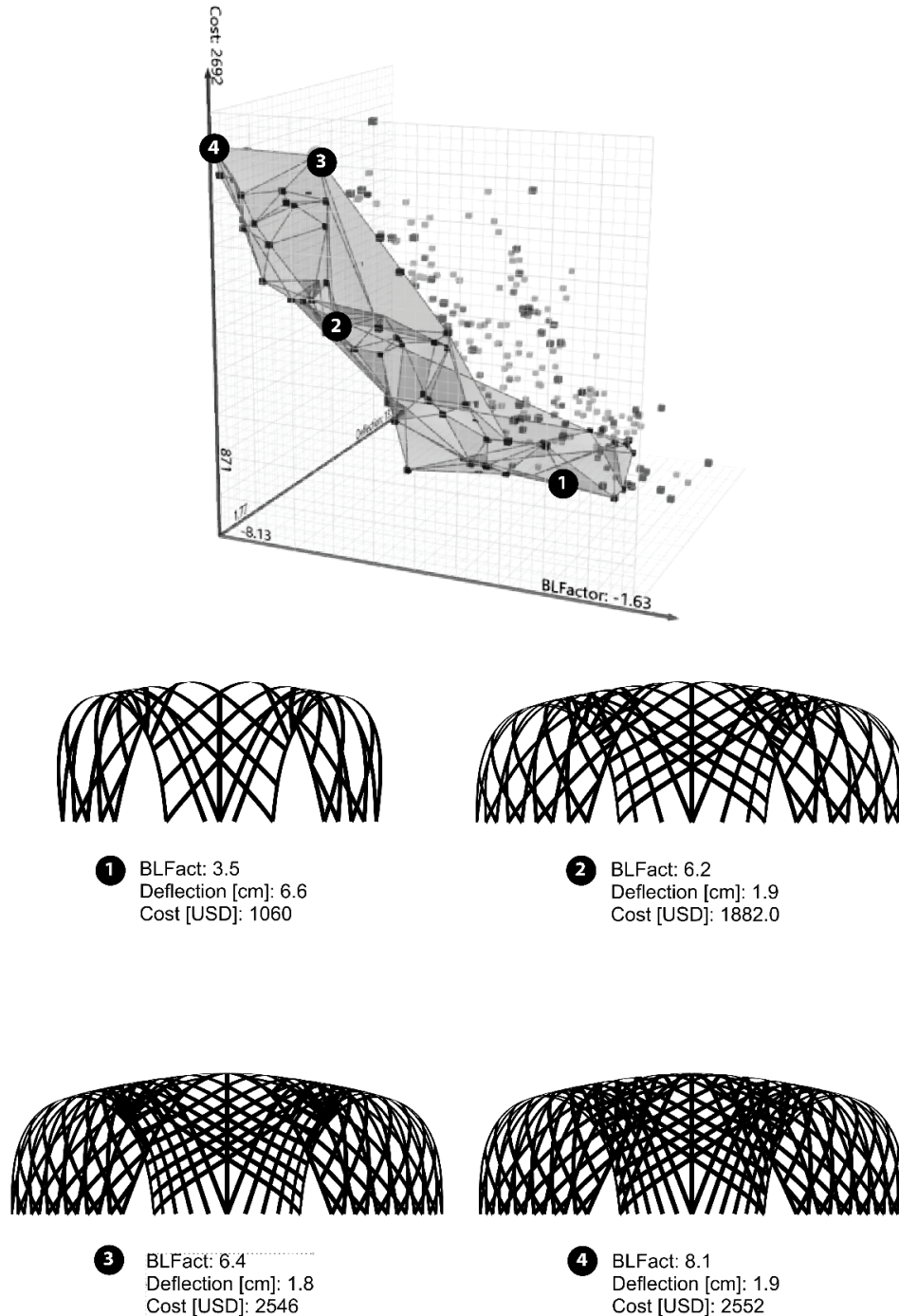


Figure 3.8 - Multi-objective optimization of grid configuration with additional bracing.

4. Engineering calculations and codes

4.1 Conceptual overview

The temporary performance pavilion was designed to be constructed in the courtyard of the MIT List Visual Arts Center for the open-air electronic music event in mid-September 2019. The pavilion should provide space for audio-visual and musical performances, be constructible in a rapid way and at a minimum cost. The project shall conform to the Massachusetts State Building Code (CMR 780), 9th Edition, which is an amended version of the 2015 International Building Code (IBC). The construction permission was contingent upon the final structural drawings being stamped by a licensed structural engineer as well as the construction schedule and a safety plan being reviewed by the MIT Health, Environment and Safety Office (Appendix B). The following design assumptions were made:

Assumptions for design:

1. Minimum cost
 - a. Fabrication and erection (constructability)
 - b. In-service maintenance (sustainability)
2. Minimum weight
3. Minimum construction time
4. Minimum labor
5. Ease of renewal and reuse of materials (recyclability)
6. Innovative use of materials
7. Reuse, deployability of the structure

The structure was designed with reference to the following codes and manuals:

Reference codes and manuals:

- Commonwealth of Massachusetts State Building Code, CMR 780, 9th Edition
- Minimum Design Loads and Associated Criteria for Buildings and Other Structures (ASCE/SEI 7-16)
- Design of Wood Structures-ASD/LRFD. 7th ed. (2015)
- NDS Supplement: Design Values for Wood Construction, 2018 Edition, American Wood Council

Planning and conceptualizing:

Functions:	a temporary structure on the MIT campus, between buildings E15, MIT Medical
Optimality Criteria:	a safe design conforming to the ASCE 7
Design Philosophy:	Ultimate Strength Design LRFD, serviceability limits: max. stress, conservative approach
Materials:	Okoume plywood or Baltic Birch plywood

Engineering calculations were performed in two stages: conceptual design and structural design (Figure 4.1). Firstly, in the conceptual design phase the allowable radius of curvature and design bending stress were defined based on the material properties and physical testing of the selected materials (Appendix A). These values were necessary to inform the feasibility of the considered conceptual designs. The conceptual design phase involved multi-objective optimization with linear structural analysis under factorized self-weight (1.3D) to give an overview of the structural performance of the developed versions of the selected concept. Secondly, the structural analysis with the defined in ASCE load cases was performed on the best performing conceptual design to determine; if the combined axial and bending stresses are acceptable. In this stage, Okoume 9mm material was selected, and the second layer of members was introduced.

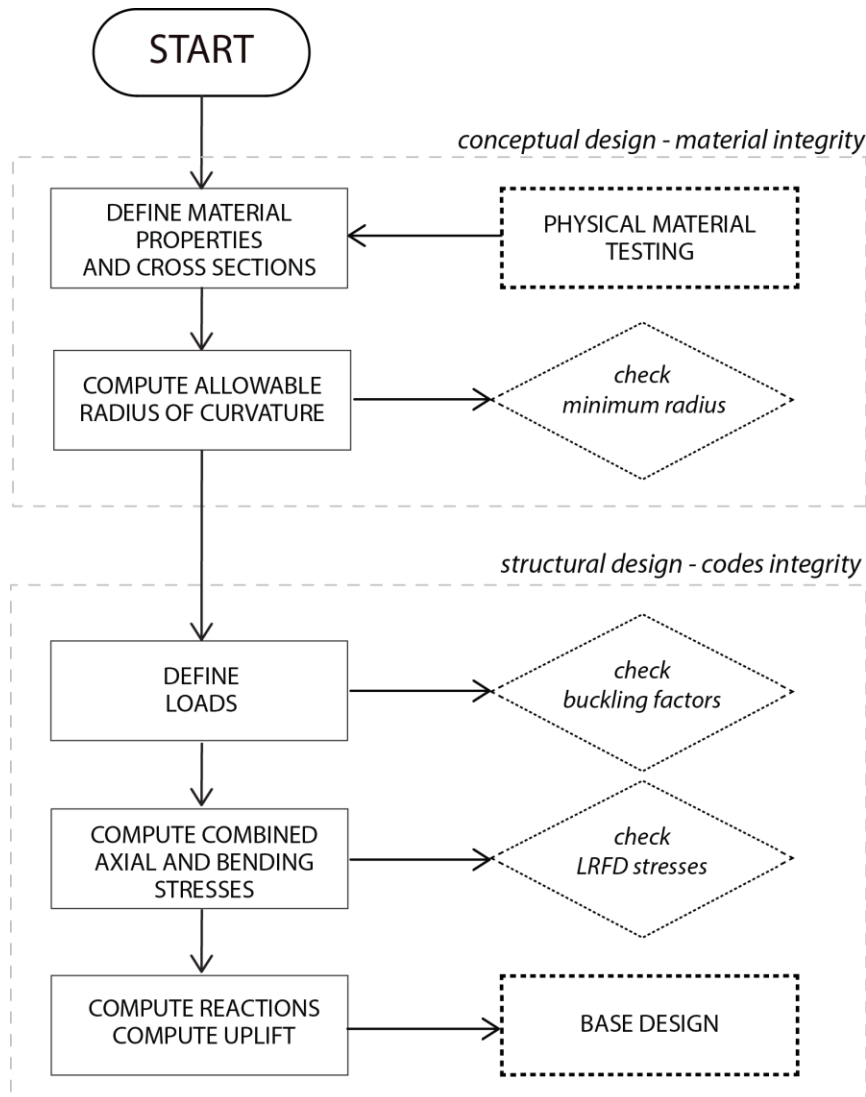


Figure 4.1 - Diagram for engineering calculations.

4.2 Material properties

Plywood was selected as a design material as it is cost-effective, lightweight and recyclable. The tested plywood was purchased at Boulter Plywood Boston: Okoume A/B BS1088 Lloyds Approved (thicknesses: 6mm, 9mm and 12mm) and Baltic Birch B/BB (thicknesses: 6mm). Birch plywood has been commonly used for previously built prototypes e.g. UWE Pavilion (Harding *et al.*, 2017). Okoume is a marine plywood that is lighter and more flexible than Baltic Birch. Laminations of Okoume boards are bonded with water and boil proof glue (WBP); therefore, this material is more appropriate for the exposure to the weather conditions. Selected material properties for Okoume plywood are described in Table 4.1.

Table 4.1 - Selected material properties of Okoume plywood. Source: producent information and (MatWeb, 2019).

Material Properties	Okoume		Symbol
	[SI]	[imperial]	
Elasticity Modulus parallel to grain	9100 MPa	1320 ksi	E
Shear Modulus. in-plane (rolling shear)	3600 MPa	522 ksi	G
Shear Modulus transversal (edgewise shear)	3600 MPa	522 ksi	G
Bending Strength parallel to grain	71Mpa	10.3 ksi	f_{r,0}
Compressive Strength parallel to grain	38 MPa	5510 psi	f_{c,0}
Compressive Strength perpendicular to grain	5.30 MPa	769 psi	f_{c,90}
Tensile Strength, parallel to grain	57.0 MPa	8270 psi	f_{t,0}
Tensile Strength, perpendicular to grain	1.8MPa	261 psi	f_{t,90}
Poisson ratio	0.3	0.3	v
Density	450 kg/m ³	28.09 lb/ft ³	ρ

4.3 Bending stress and radius of curvature

For the purpose of this thesis, we have assumed that “plywood” comes under glued laminated soft timber category. Glulam beams are usually loaded in bending around the strong axis; however, examples of bending around the minor axis are also present (e.g. bridge decks) (Breyer *et al.*, 2015). It needs to be highlighted that the x- and y-axis for glulam beams do not refer to the weak and strong axis but they are related to the orientation of the laminations (Breyer *et al.*, 2015). Where depth is less than the width and the x-axis is parallel to the lamination, it is an unusual case, and the x-axis is not the strong axis (Figure 4.2).

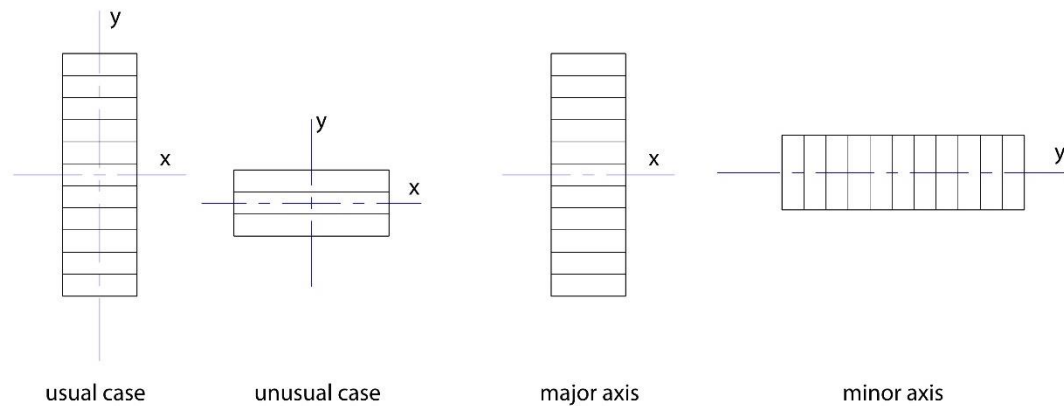


Figure 4.2 - The orientation of the x and y axes for glulam beam is related to the orientation of the laminations, and not to strong and weak axes (Breyer *et al.*, 2015).

Figure 4.3 below provides clarification on the referred local coordinate systems. The calculations performed in this chapter are based on the local coordinate system common for structural analysis software (Figure 4.3: left). Reference design values and integration formulas are originally formulated in the coordinate system presented in the right illustration (Figure 4.3: right).

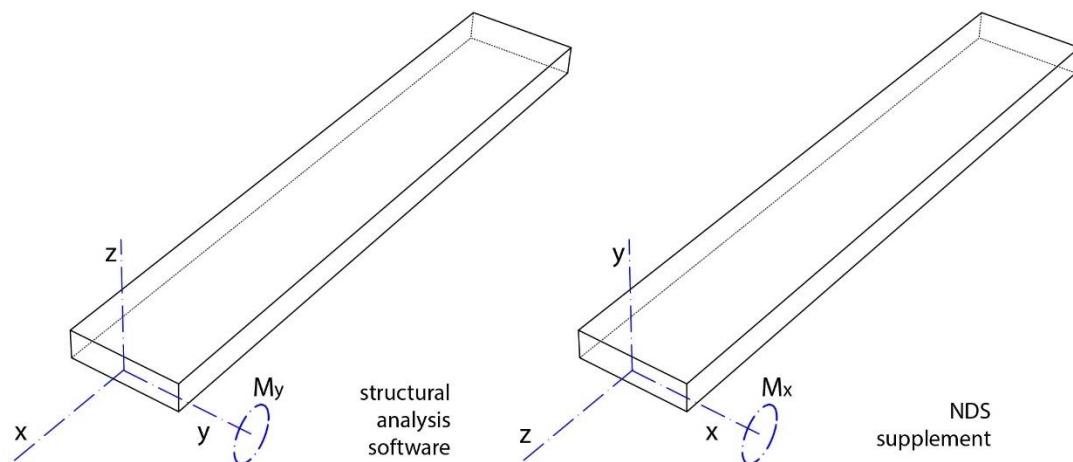


Figure 4.3 - Orientation of the local axes in analysis software and the NDS supplement.

Cracking stress and cracking radii

Bending results in couple tension and compression stresses on either side of the cross-sectional neutral axis. Wooden beams subjected to bending may fail as a result of:

- direct compression at the concave compression surface
- tension on the convex tension surface.

A slender beam subjected to pure bending from Euler-Bernoulli Beam Theory:

a) Bending Moment:

$$M_y = \frac{EI_y}{r} \quad (4.1)$$

From the elastic theory the bending stress is calculated as:

b) Bending stress

$$\sigma_x = \frac{M_y z}{I_y} \quad (4.2)$$

where

z – a distance from the neutral axis to the considered fiber.

E – flexural modulus of elasticity

I_y – moment of inertia of the section

r – radius of curvature

The maximum bending stress:

$$\sigma_{x,max} = \frac{M_{cr} z_{max}}{I_y} = \sigma_{cr} \quad (4.3)$$

Therefore, the cracking moment is when the maximum bending stress reaches the modulus of rupture:

$$M_{cr} = \frac{\sigma_{x,max} I_y}{z_{max}} = \frac{f_r I_y}{z_{max}} \quad (4.4)$$

Consequently, the cracking radius can be defined using the material bending strength:

c) Cracking radius

$$r_{cr} = \frac{EI_y}{M_{cr}} = \frac{E z_{max}}{f_r} \quad (4.5)$$

While the cracking stress can be evaluated based on the measured minimum radius of the bent material before cracks are observed:

d) Cracking stress

$$\sigma_{cr} = \frac{E z_{max}}{r_{cr}} \quad (4.6)$$

Design stress and allowable radii

In order to define design stress and the allowable radius of curvature, the specified by material properties bending strength is verified with the physical testing of the considered materials. In the physical tests the minimum radius of curvature is defined based on the first observed cracks. The analytical and experimental bending strength values are presented in Table 4.2 and the comprehensive testing results in Appendix A.

Table 4.2 - Analytical and experimental bending strength.

Material	Radius of curvature, when first cracks occurred r_{cr}	Bending strength Physical Testing $\sigma_{cr} = \frac{Ez_{max}}{r_{cr}}$	Bending strength Material Properties f_r
Birch 6mm	0.49m	53.6MPa	50.9 MPa
Okoume 6mm	0.29m	94.1MPa	71 MPa
Okoume 9mm	0.44m	93.1MPa	
Okoume 12mm	0.72m*	75.8MPa	

*material failure without prior cracking behavior observed

Design stress

Modulus of rupture in bending defines the stress in a material just before it yields, while cracks can appear in the plastic limit phase. Following a conservative approach, the cracking stress is assumed to be equal to the modulus of rupture. A safety factor of 0.6 was used to define the reference design bending stress value based on the recommendations of Jonathan Roynon (BuroHappold Engineering) provided in April 2019. In order to assure proper stress reserves in the pre-stressed structure, the design stress is defined as:

$$\sigma_d = 0.6f_r$$

$$\text{for Birch: } \sigma_d = 0.6 \times 50.9 \text{ MPa} = 30.54 \text{ MPa}$$

$$\text{for Okoume: } \sigma_d = 0.6 \times 71.0 \text{ MPa} = 42.6 \text{ MPa}$$

Based on the defined reference design bending stress the allowable radii of curvature were defined for the considered materials as:

Allowable radius

$$r_{all} = \frac{E}{\sigma_d} z_{max}$$

$$\text{for Birch 6mm: } r_{all} = 8750 \text{ MPa} \times 0.0030\text{m} / 30.54\text{MPa} = 0.859\text{m} \approx 0.86\text{m}$$

$$\text{for Okoume 6mm: } r_{all} = 9100 \text{ MPa} \times 0.0030\text{m} / 42.60\text{MPa} = 0.641\text{m} \approx 0.64\text{m}$$

$$\text{for Okoume 9mm: } r_{all} = 9100 \text{ MPa} \times 0.0045\text{m} / 42.60\text{MPa} = 0.961\text{m} \approx 0.96\text{m}$$

$$\text{for Okoume 12mm: } r_{all} = 9100 \text{ MPa} \times 0.0060\text{m} / 42.60\text{MPa} = 1.282\text{m} \approx 1.28\text{m}$$

Allowable radius of curvature is used for the feasibility evaluation of the concept designs.

4.4 Load Cases

The types of loads considered for design are defined in the American Society of Civil Engineers (ASCE) Standard 7-10, *Minimum Design Loads for Buildings and Other Structures*.

Determination of the anticipated loads

The following load combinations with safety factors for Ultimate Strength Design are selected (ASCE, 2.3.2):

LC0: 1.4D
LC1: 0.9D + 1.0W
LC2: 1.2D + 1.6LL1
LC3: 1.2D + 1.6LL2

- *Live Loads*

LL1 – A person hanging from the structure = $90\text{kg} \times 9.81\text{m/s}^2 = 0.89\text{ kN}$

LL2 – A person pushing the structure = 0.89 kN (ASCE 4.5.1 - All handrail and guardrail systems shall be designed to resist a single concentrated load of 200 lb (0.89 kN))

- *Dead Loads*

Dead Load is calculated as a total mass of plywood for the main structure of the gridshell without the base.

- *Wind Loads*

To determine wind loads the risk category, basic wind speed and wind load parameters are required. The necessary values are obtained in the following steps:

Step 1: Determine risk category, see Table 1.5-1

- Use Risk Category I - Buildings and other structures that represent a low risk to human life in the event of failure.

Step 2: Determine wind load parameters:

Wind directionality factor K_d , see Section 26.6 and Table 26.6.1

- Use $K_d = 0.85$

➤ Exposure category B, C or D, see Section 26.7

Exposure Category B (ASCE 7 - 26.7.3) - For buildings with a mean roof height of less than or equal to 30 ft (9.1 m) on Surface Roughness B: Urban and suburban areas.

- Use Exposure Category B

➤ *Topographic factor K_{zt} , see Section 26.8 and Figure 26.8-1*

If site conditions and locations of structures do not meet all the conditions specified in Section 26.8.1 then $K_{zt} = 1.0$.

➤ Use $K_{zt} = 1.0$

Step 3: *Determine the basic wind speed, V , for applicable risk category*

The basic wind values are specified in 780 CMR: Massachusetts amendments to the International Building Code 2015. Basic wind speed for Risk Category I in Boston is equal to 118mph.

➤ Use Basic Speed Wind 118 mph

Wind speeds for the design of permanent structures correspond to approximately a 3% probability of exceedance in 50 years (Annual Exceedance Probability = 0.000588, MRI = 700 Years). These wind speeds are specified with exposure period 50 years with the assumed mean recurrence interval of the wind greater than the lifespan of the structure. Boggs and Peterka (1992) proposed a method of calculation of the reduced speed winds by “specifying the design recurrence interval for a temporary structure such that the probability of failure is the same as in traditional design of permanent structures” (Boggs & Peterka, 1992:p.1). The reduced wind speed is calculated based on several parameters including the wind speed probability distribution, factor of safety, mean recurrence interval of the design wind speed, and the exposure period. Using the Boggs and Peterka’s approach, the reduced basic wind speed is defined as 65.2 mph (7.62psf).

➤ Use Reduced Basic Wind Speed: $V = 65.2\text{mph}$ (104.9 km/h)

➤ Use Reduced Design Wind Pressure: $p = 7.62\text{psf}$ (0.365 kN/m²)

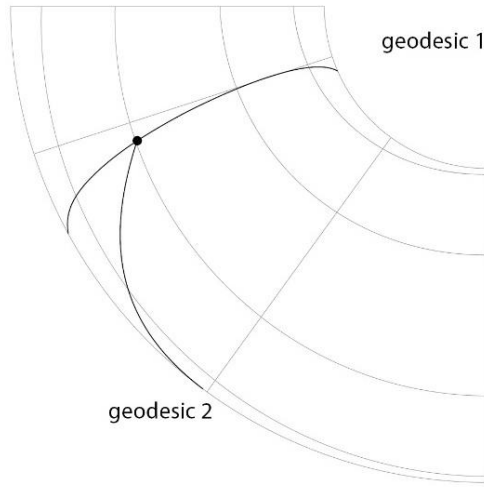
4.5 Structural model

This section describes the preparation of the geometry for the structural analysis. As described in the software analysis section the analysis of curved beams without the prior discretization would be possible only with Kiwi3d. The limitations of the WIP version available at that time [May-July 2019] was not suitable for analysis of geodesic gridshells (Section 2.3). Consequently, the curved beams had to be discretized into linear segments for the analysis with Karamba3D and SOFiSiK.

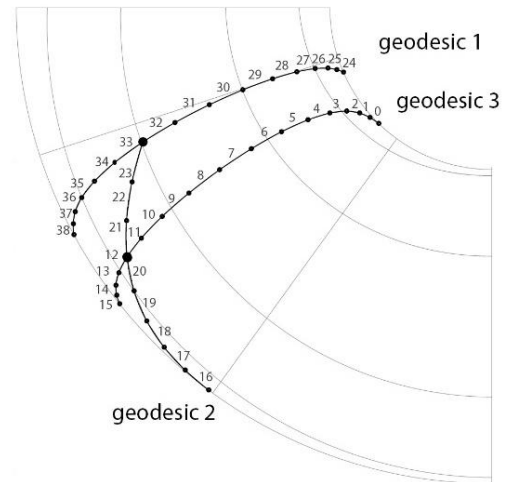
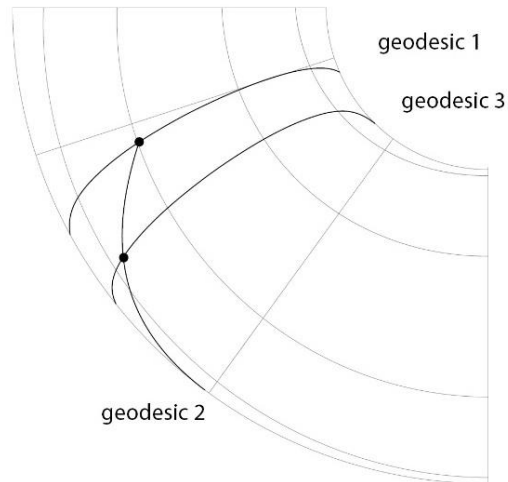
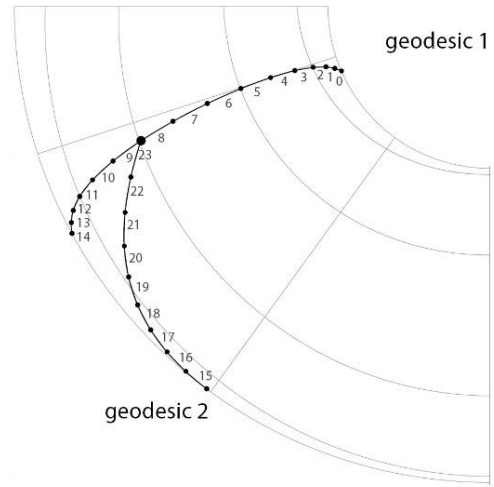
Discretization

Preparation of the model for structural analysis involved custom discretization of the geodesic curves (source code in Appendix C). The procedure splits firsts the geodesic curves at intersection points into curved segments and then subdivide these segments into linear elements of desired length (Figure 4.4). Linear elements are grouped in reference to the original curves.

A - curve splitting



B - discretization



- geodesic intersection node
- discretization node

Figure 4.4 - Shattering and discretization of geodesic curves with approximate linear length of 0.4m (procedure source code in Appendix C).

Joints and supports

In the structure there are 41 support points and around 300 intersection points (Figure 4.5).

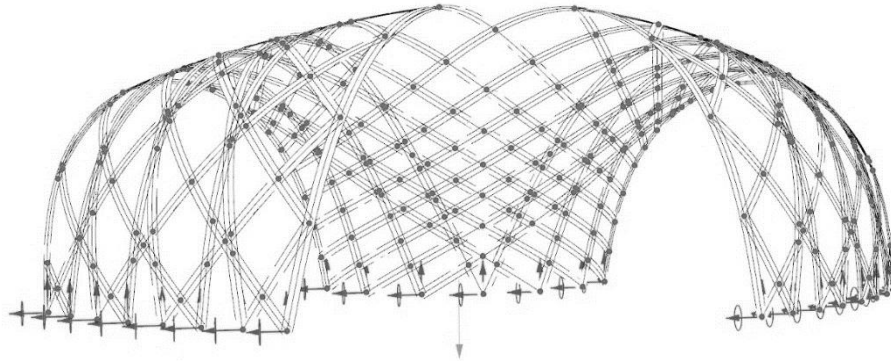


Figure 4.5 - Rotational joints and pin supports in the model.

Laths are connected to the floor plate (perimeter beam) with metal hinge connections. To model a simple rotational joint connection with a single bolt, the vertical and lateral movements of the joints between laths are restrained, however, in-plane rotation is allowed. The laths are intersecting multiple times with each other and the rotation about the z-axis is limited, while the rotation about the local x and y axis is restrained by the width of the lath. In general moment connections in timber are very rare (Breyer *et al.*, 2015), and it is a conservative approach to assume pin connections. For analysis in SOFiSTiK, the structure is modeled as a frame structure with pin supports.

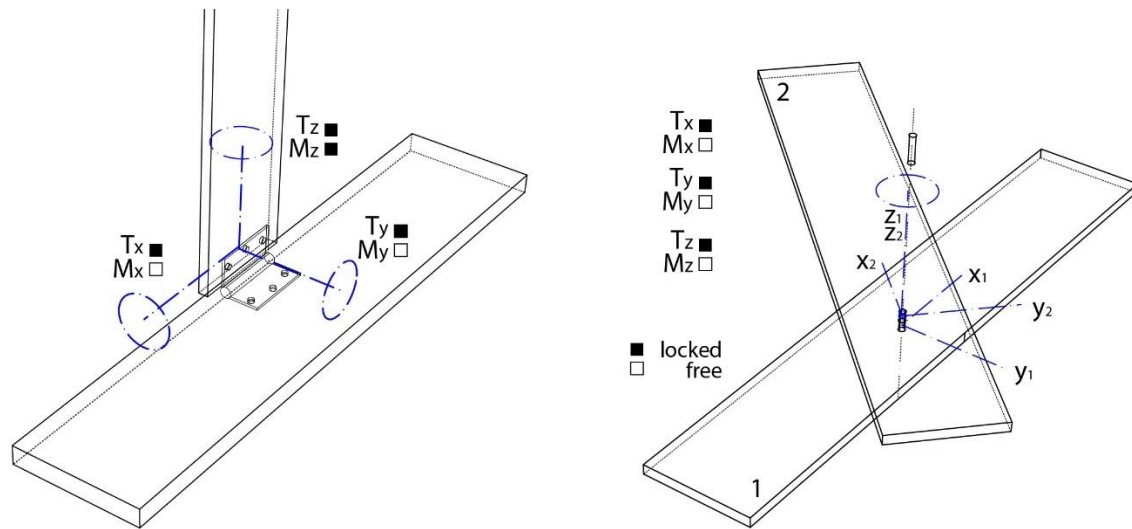


Figure 4.6 - Support conditions at the floor plate and rotational joint between laths.

4.6 Analysis of the final structural configuration.

Figure 4.7 below provides a summary of the considered loads. The structure was analyzed under factored self-weight, reduced wind speed and accidental live loads.

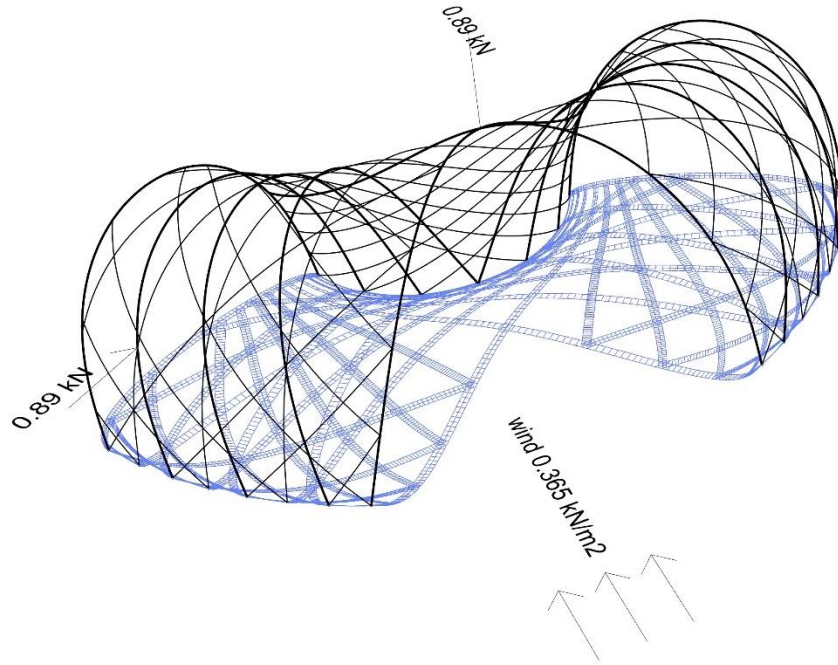


Figure 4.7 - Summary of the loads, division of laths for single- and double-layer members (thick curves) and the projected area of the laths considered for the uplift calculation.

The parametric model of grid configuration of geodesic members was defined in Rhino/Grasshopper. The final structural configuration was found in a multi-objective search among different possible grid configurations measuring the approximate cost, buckling factor and maximum deflection (Section 3.5). The structural analysis for the concept development and optimization assumed the use of 6mm thick Baltic Birch plywood. The selected promising concept went through several iterations of changing cross sections size and material. Surprisingly not the accidental live loads such as a person hanging or pushing the structure, but wind load was governing. The final iteration using 9mm Okoume plywood with double layer members over the main ribs met the expectations of the maximum deflection and minimum buckling factor for LC0 and LC1. The final structural configuration (Figure 4.7) was composed of 46 single-layer laths and 10 laths for the double-layer. Members with numbers 1,2,3,4,9,24,25,26,27,32 were designed as double-layer members with shear blocks. For the software analysis the double-layer laths were modeled as single members with a double thickness (18mm).

4.6.1 Nodal Displacements

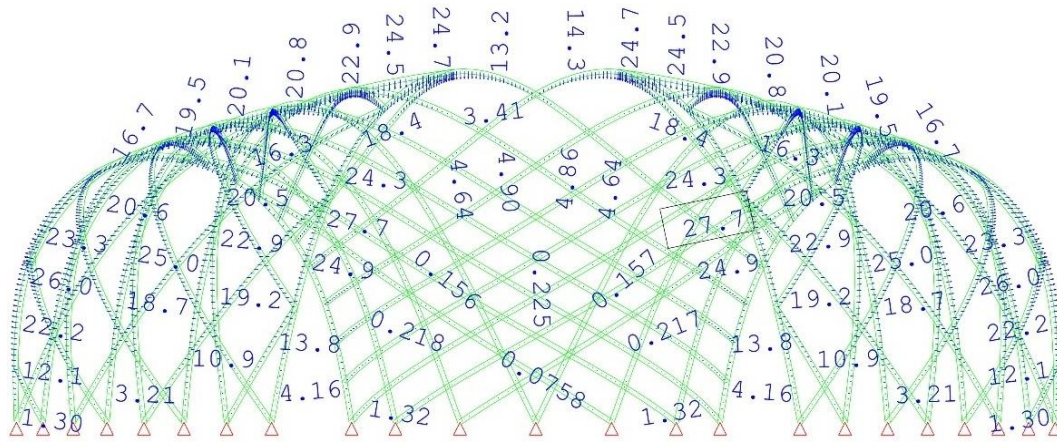


Figure 4.8 - Nodal displacements calculated with SOFiSTiK for 1.4D.

Maximum nodal displacements from linear analysis disregarding the prestress effects with Karamba3D are shown in Table 4.3. The structural analysis in SOFiSTiK (SYST prob line) was computed for all the considered load cases with the ACTB (Active-Bending Module) (Table 4.4). Buckling Factor is calculated using Buckling Modes Method and provided as a range for 6 eigenvalues. Figure 4.8 visually presents the deflections under the factorized dead load 1.4D.

Table 4.3 - Structural analysis results for final structural configuration (Karamba3D).

Load case	Combination	Max. Displacement [cm]				
		Linear 1-st order	Linear 2-nd order	Non-Linear Newton Raphson	<1.5in ³ <3.81 cm	BL Factor
LC0 Dead Load	1.4D	0.31	0.31	0.31	yes	17.64
LC1 Wind Load	1.0W+0.9D	3.61	3.98	3.76	yes	3.72
LC2 Person Hanging	1.2D +1.6LL1	5.68	6.02	6.66	no	6.28
LC3 Person Pushing	1.2D +1.6LL2	4.59	5.58	4.22	no	2.04

Table 4.4- Structural analysis results for final structural configuration (SOFiSTiK).

Load case	Combination	Max. Displacement [cm]		
		Linear SYST prob line	<1.5in <3.81 cm	BL Factor Range
LC0 Dead Load	1.4D	2.7	yes	2.03-2.53
LC1 Wind Load	1.0W+0.9D	2.8	yes	2.99-4.55
LC2 Person Hanging	1.2D +1.6LL1	6.6	no	1.71-2.05
LC3 Person Pushing	1.2D +1.6LL2	3.1	yes	2.52-3.23

³ Requirement discussed in personal communication with Paul Richardson from BuroHappold Engineering in Boston.

4.6.2 Bending and axial stresses

The structure faces bending stresses from the bending of the initially flat laths and additional bending and axial stresses from the externally applied forces. As both compression and tension is present in different parts of the members and bending causes tensile stresses on one side and compression on the other side, there is four potential combinations of stresses (Axial Compression + Bending Tension, Axial Compression + Bending Compression, Axial Tension + Bending Tension, Axial Tension + Bending Compression). As bending tension reduces axial compression and bending compression reduces axial tension, and as shown (Figure 4.9) the parts of the laths could be under axial tension or compression depending on the considered load case, a conservative approach is to check all the members:

- For combined Axial Compression + Bending Compression
- For combined Axial Tension + Bending Tension

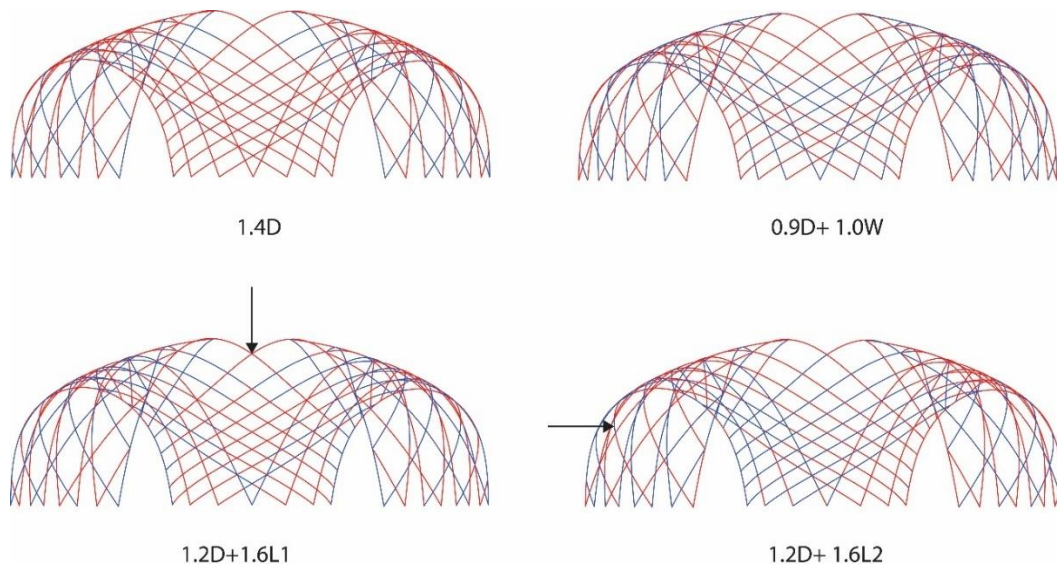


Figure 4.9 - Compression and tension parts under considered load cases.

Assumptions

The relevant regulations provided in *ASD/LRFD Manual National Design Specification for Wood Construction* are designed for wood-frame buildings; therefore, they are not perfectly suitable for bending-active timber structures. Okoume plywood is not considered as structural glued laminated softwood timber and it is not included the NDS Supplement.

Reference design values for structural glued laminated timber materials are defined in accordance with American Institute of Timber Construction (AITC) and APA – The Engineered Wood Association. The design reference values are based on the tests conducted by the accredited testing agencies and defined in accordance “with principles originally established by the U.S. Forest Products Laboratory in the early 1950s”. (American Wood Council, 2018:p.iii). To account for safety, the standard reductions are applied to the strength properties. The magnitude of reductions is based on factors such as size of member, number of laminations, density or slope of grain (American Wood Council, 2018). The mechanical properties of glued laminated timber materials should be established by method given in ASTM D3737 (Moody & Hernandez, 2015).

As the selected material is not accredited, for a conservative approach a strength adjustment factor of 0.9 is applied to the strength values provided by the producent (Table 4.1) The following reference design values are used in the stress calculations:

$$\begin{aligned} F_c &= 0.9 \times 38 \text{ MPa} = 34.2 \text{ MPa} \\ F_{bx} &= 0.9 \times 71 \text{ MPa} = 63.9 \text{ MPa} \\ E_{x \min} &= 0.9 \times 9100 \text{ MPa} = 8190 \text{ MPa} \\ F_t &= 0.9 \times 57 \text{ MPa} = 51.3 \text{ MPa} \end{aligned}$$

The adjustment and conversion factors are presented in Table 4.5.

Table 4.5 - Resistance, conversion and adjustment factors.

Symbol	Description	Value	Reference
K_F Compression	Format conversion factor for compression parallel to the grain F_c	2.4	(Breyer <i>et al.</i> , 2015:p.216)
K_F Tension	Format conversion factor for tension	2.7	
K_F Bending	Format conversion factor for bending	2.54	
K_F Stability	Format conversion factor for stability E_{\min}	1.76	
ϕ_c	Resistance factor for compression(both parallel and perpendicular to grain) (LFRD)	0.9	(Breyer <i>et al.</i> , 2015:p.215)
ϕ_b	Resistance factor for bending (LFRD)	0.85	
ϕ_t	Resistance factor for tension (LFRD)	0.8	
ϕ_s	Resistance factor for stability E_{\min}	0.85	
λ	Time effect factor (LFRD only)	1.4D = 0.6 1.2D + 1.6L = 0.8 0.9D + 1.0 W = 1.0	(Breyer <i>et al.</i> , 2015:p.211)
C_t	Temperature factor	1.0 (normal temperature conditions) ⁴	(Breyer <i>et al.</i> , 2015:p.214)
C_F	Size factor	For glulams replaced with C_V	(Breyer <i>et al.</i> , 2015:p.212)
C_V	Volume factor	$(21/L)^{1/x} (12/d)^{1/x} (5.125/b)^{1/x} \leq 1.0$	Table 5A (American Wood Council, 2018:p.62)
C_M	Wet service factor When structural glued laminated timber is used where moisture content will be 16% or greater	1.0 – dry service conditions For F_b , 0.8 For F_t , 0.8 For F_c , 0.73 (parallel) For F_c , 0.53 (perpendicular)	(Breyer <i>et al.</i> , 2015:p.384)
c	buckling and crushing interaction factor for columns	0.9 for glulam	
C_P	Column stability factor	1.0 for fully supported columns that are prevented from buckling	(Breyer <i>et al.</i> , 2015)

⁴ The first temperature range that requires reduction of C_t is 100°F(37.8 °C) < T < 125 °F (51.77 °C)

Combined Axial Tension and Bending Tension (LRFD):

Interaction equations can be used to define the allowable stress for combined axial tension and bending in members:

$$\frac{f_{tu}}{F'_{tn}} + \frac{f_{bu}}{F^*_{bn}} \leq 1.0 \quad (4.7)$$

f_{tu} – factored (LRFD) tensile stress parallel to grain
 $= T_u / A$

F'_{tn} – adjusted LRFD tension design value
 $= F_{tn} (\varphi_t)(\lambda)(C_M)(C_t)$ for glulam

f_{bu} – factored (LRFD) bending stress
 $= M_u / S$

F^*_{bn} – adjusted LRFD bending design value without the adjustment for lateral stability
 $= F_{bn} (\varphi_b)(\lambda)(C_M)(C_t)(C_V)$ for glulam

Plywood is assumed to be used in wet conditions when the moisture content will be 16% or greater and with $C_M = 0.8$ for bending and $C_M = 0.8$ for tension capacity. Structure is for normal temperature conditions (below 37.8 °C). The format conversion factors: for tension $K_F = 2.7$, for bending $K_F = 2.54$. The following reference design values are used:

$$F_{tn} = F_t(K_F) \\ = 51.3 \text{MPa} (2.7) = 138.51 \text{MPa}$$

$$F_{bn} = F_b(K_F) \\ = 63.9 \text{MPa} (2.54) = 153.36 \text{MPa}$$

Tension capacity:

For 1.4D:

$$F'_{tn} = F_{tn} (\varphi_t)(\lambda)(C_M)(C_t) \\ = 138.51 \text{MPa} (0.8)(0.6)(0.8)(1.0) = 53.19 \text{MPa}$$

For 0.9D + 1.0W:

$$F'_{tn} = F_{tn} (\varphi_t)(\lambda)(C_M)(C_t) \\ = 138.51 \text{MPa} (0.8)(1.0)(0.8)(1.0) = 88.65 \text{MPa}$$

For 1.2D + 1.6L:

$$F'_{tn} = F_{tn} (\varphi_t)(\lambda)(C_M)(C_t) \\ = 138.51 \text{MPa} (0.8)(0.8)(0.8)(1.0) = 70.92 \text{MPa}$$

Bending capacity:

Volume Factor can be calculated using equation below (American Wood Council, 2018 Table 5A):

$$C_v = (21/L)^{1/x} (12/d)^{1/x} (5.125/b)^{1/x} \leq 1.0 \quad (4.8)$$

L – length of bending member between points of zero moment, ft

d – depth of bending member, in.

b – width (breadth) of bending member, in. For multiple piece width, b = width of widest piece in the layup. Thus $b \leq 10.75$ ".

x – 20 for Southern Pine

x – 10 for all other species

Average length of the laths from support to support equals 7.06m = 23.16ft, depth for single layer members: 9mm = 3/8in, for double layer: 18mm = 6/8in and width for all 10cm = 3.94in. Thus, for single layer members the volume factor:

$$C_v = (21/23.16\text{ft})^{1/10} (12/(3/8"))^{1/10} (5.125/3.94")^{1/10} \\ = 0.9903 \times 1.4142 \times 1.0266 = 1.4377 > 1.0$$

Consequently, for double layer members the volume factor:

$$C_v = (21/23.16\text{ft})^{1/10} (12/(6/8"))^{1/10} (5.125/3.94")^{1/10} \\ = 0.9903 \times 1.3195 \times 1.0266 = 1.3414 > 1.0$$

➤ Use $C_v = 1$ for all members

For 1.4D:

$$F_{bn}^* = F_{bn}(\varphi_b)(\lambda)(C_M)(C_t)(C_v) \\ = 153.36\text{MPa} (0.85)(0.6)(0.8)(1.0)(1.0) = 62.57 \text{ MPa}$$

For 0.9D + 1.0 W:

$$F_{bn}^* = F_{bn}(\varphi_b)(\lambda)(C_M)(C_t)(C_v) \\ = 153.36\text{MPa} (0.85)(1.0)(0.8)(1.0)(1.0) = 104.28 \text{ MPa}$$

For 1.2D + 1.6L:

$$F_{bn}^* = F_{bn}(\varphi_b)(\lambda)(C_M)(C_t)(C_v) \\ = 153.36 \text{ MPa} (0.85)(0.8)(0.8)(1.0)(1.0) = 83.43 \text{ MPa}$$

Table 4.6 - Summary of the adjusted LRFD bending and tension design values.

Load Case	1.4D	0.9D + 1.0 W	1.2D + 1.6L
$F_{tn}' = F_{tn}(\varphi_t)(\lambda)(C_M)(C_t)$	53.19 MPa	88.65 MPa	70.92 MPa
$F_{bn}^* = F_{bn}(\varphi_b)(\lambda)(C_M)(C_t)(C_v)$	62.57 MPa	104.28 MPa	83.43 MPa

Combined Bending and Compression

Structural members that are stressed simultaneously in bending and in compression are known as beam-columns. The general interaction formula for the axial compressive force combined with a bending moment:

$$\left(\frac{f_{cu}}{F_{cn}'}\right)^2 + \left(\frac{1}{1 - f_{cu}/F_{cExn}}\right) \frac{f_{bxu}}{F_{bxn}'} \leq 1.0 \text{ (LRFD)} \quad (4.9)$$

f_{cu} - factored (LRFD) compressive stress = P_u/A

F_{cn}' - adjusted LRFD compressive value as given by Ylinen formula:

$$F_{cn}' = F_{cn}(\varphi_c)(\lambda)(C_M)(C_t)(C_F)(C_P)(C_i)$$

f_{cu} - factored (LRFD) compressive stress = P_u/A

F_{cExn} - Euler-based elastic buckling stress, based on slenderness ratio for the x axis for LRFD:

$$F_{cExn} = \frac{0.822E'_{x \min n}}{[(l_e/d)_x]^2} \quad (4.10)$$

l_e/d - slenderness ratio for rectangular columns defined as ratio between the effective unbraced length of the column divided by the least dimension of the cross section

$E'_{x \min_n}$ - adjusted LRFD modulus of elasticity for column buckling

$$= E_{x \min_n}(\varphi_s)(C_M)(C_t) = E_{x \min}(K_F)(\varphi_s)(C_M)(C_t) \text{ (Breyer } et al., 2015)$$

f_{bxu} - factored (LRFD) bending stress about x axis = M_{xu}/S_x

F'_{bxn} - adjusted LRFD bending value about x axis considering effects of lateral torsional buckling = $F_{bxn}(\varphi_b)(\lambda)(C_M)(C_t)(C_V)$ for glulam

F_{bxn} - nominal LRFD bending design value about x-axis = $F_{bn} K_F$

φ_c - resistance factor for compression (LRFD) = 0.9

φ_b - resistance factor for bending (LRFD) = 0.85

Lath capacity for compression and bending is checked for the cross section 100x9mm and 100x18mm. Plywood is assumed to be used in wet conditions when the moisture content will be 16% or greater and with $C_M = 0.8$ for bending and $C_M = 0.73$ for compression capacity. For compression $K_F = 2.4$, $K_F = 1.76$ for stability and $K_F = 2.54$ for bending.

$$\begin{aligned} F_{cn} &= F_c(K_F) \\ &= 34.2 \text{ MPa} (2.4) = 82.08 \text{ MPa} \\ E_{x \min_n} &= E_{x \min}(K_F) \\ &= 8190 \text{ MPa} (1.76) = 14414.40 \text{ MPa} \end{aligned}$$

Reference design value for bending is defined based on the material properties and physical testing:

$$\begin{aligned} F_{bxn} &= F_{bx}(K_F) \\ &= 63.9 \text{ MPa} (2.54) = 162.31 \text{ MPa} \end{aligned}$$

Buckling stress based on the slenderness ratio

Glulam has different material properties for x and y axes. Evaluation of the column stability is given for x-axis. For pinned-end column effective length factor $K_e = 1.0$, (although the connections might have some moment resisting capacity it is a conservative approach to take effective length equal to the unbraced length). The average unbraced length of 0.37m is used for the calculation of slenderness ratios.

$$\begin{aligned} E'_{x \min_n} &= E_{x \min_n}(\varphi_s)(C_M)(C_t) \\ &= 14414.40 \text{ MPa} (0.85)(0.8)(1.0) = 9801.79 \text{ MPa} \end{aligned}$$

For single layer:

$$\begin{aligned} (l_e/d)_x &= (lK_e/d)_x = 0.37 \times 1/0.009 = 41.11 \\ F_{cExn} &= 0.822 \times 9801.79 \text{ MPa} / 41.11^2 = 4.77 \text{ MPa} \end{aligned}$$

For double layer:

$$\begin{aligned} (l_e/d)_x &= (lK_e/d)_x = 0.37 \times 1/0.018 = 20.56 \\ F_{cExn} &= 0.822 \times 9801.79 \text{ MPa} / 20.56^2 = 19.07 \text{ MPa} \end{aligned}$$

Compression capacity:

To evaluate compression capacity of member, firstly column stability factor for LRFD has to be defined (computed values in Table 4.7):

$$C_p = \frac{1 + F_{cEn}/F_{cn}^*}{2c} - \sqrt{\left(\frac{1 + F_{cEn}/F_{cn}^*}{2c}\right)^2 - \frac{F_{cEn}/F_{cn}^*}{c}} \quad (4.11)$$

F_{cEn} - nominal Euler critical buckling stress for columns LRFD:

$$F_{cEn} = \frac{0.822E'_{min_n}}{[l_e/d]^2}$$

F_{cn}^* = nominal LRFD compressive design value parallel to grain multiplied by all LRFD adjustment factors except C_p

$$= F_{cn}(\varphi_c)(\lambda)(C_M)(C_t)$$

c = buckling and crushing interaction factor for columns
= 0.9 for glulam

For 1.4D:

$$\begin{aligned} F_{cn}^* &= F_{cn}(\varphi_c)(\lambda)(C_M)(C_t) \\ &= 82.08 \text{ MPa} (0.9)(0.6)(0.73)(1.0) = 32.35 \text{ MPa} \end{aligned}$$

For 0.9D + 1.0 W:

$$\begin{aligned} F_{cn}^* &= F_{cn}(\varphi_c)(\lambda)(C_M)(C_t) \\ &= 82.08 \text{ MPa} (0.9)(1.0)(0.73)(1.0) = 53.93 \text{ MPa} \end{aligned}$$

For 1.2D + 1.6L:

$$\begin{aligned} F_{cn}^* &= F_{cn}(\varphi_c)(\lambda)(C_M)(C_t) \\ &= 82.08 \text{ MPa} (0.9)(0.8)(0.73)(1.0) = 43.14 \text{ MPa} \end{aligned}$$

Bending capacity:

For 1.4D:

$$\begin{aligned} F'_{bxn} &= F_{bxn}(\varphi_b)(\lambda)(C_M)(C_t)(C_V) \\ &= 153.36 \text{ MPa} (0.85)(0.6)(0.8)(1.0)(1.0) = 66.22 \text{ MPa} \end{aligned}$$

For 0.9D + 1.0 W:

$$\begin{aligned} F'_{bxn} &= F_{bxn}(\varphi_b)(\lambda)(C_M)(C_t)(C_V) \\ &= 153.36 \text{ MPa} (0.85)(1.0)(0.8)(1.0)(1.0) = 110.37 \text{ MPa} \end{aligned}$$

For 1.2D + 1.6L:

$$\begin{aligned} F'_{bxn} &= F_{bxn}(\varphi_b)(\lambda)(C_M)(C_t)(C_V) \\ &= 153.36 \text{ MPa} (0.85)(0.8)(0.8)(1.0)(1.0) = 88.29 \text{ MPa} \end{aligned}$$

Table 4.7 - Summary of adjusted LRFD compression design values.

Load Case	1.4D		0.9D + 1.0 W		1.2D + 1.6L	
	single	double	single	double	single	double
(C_p)	0.13	0.50	0.08	0.31	0.1	0.39
F_{cn}^* $= F_{cn}(\varphi_c)(\lambda)(C_M)(C_t)$	35.35 MPa		53.93 MPa		43.14 MPa	
F'_{cn} $= F_{cn}(\varphi_c)(\lambda)(C_M)(C_t)(C_p)$	4.69 MPa	17.14 MPa	4.72 MPa	18.15 MPa	4.71 MPa	17.82 MPa
F'_{bxn} $= F_{bxn}(\varphi_b)(\lambda)(C_M)(C_t)(C_V)$	66.22 MPa		110.37 MPa		88.29 MPa	

Table 4.8 - Summary of the LRDF stresses (double-layer members in bold).

Lath No.	Combined Tension and Bending				Combined Compression and Bending			
	1.4D	0.9D + 1.0W	1.2D + 1.6L1	1.2D + 1.6L2	1.4D	0.9D + 1.0W	1.2D + 1.6L1	1.2D + 1.6L2
1	0.47	0.28	0.36	0.37	0.71	0.34	0.39	0.44
2	0.46	0.28	0.38	0.35	0.71	0.31	0.40	0.71
3	0.45	0.28	0.35	0.34	0.69	0.29	0.38	0.40
4	0.44	0.27	0.37	0.34	0.68	0.30	0.40	0.37
5	0.14	0.12	0.12	0.26	0.33	0.44	0.40	0.34
6	0.24	0.19	0.19	0.23	0.32	0.48	0.33	0.34
7	0.29	0.23	0.25	0.25	0.33	0.29	1.41	0.29
8	0.33	0.23	0.26	0.25	0.22	0.56	0.33	0.16
9	0.35	0.23	0.27	0.26	0.71	0.31	0.40	0.36
10	0.13	0.13	0.13	0.10	0.73	0.36	0.46	0.40
11	0.19	0.12	0.15	0.16	0.70	0.36	0.55	0.40
12	0.19	0.13	0.15	0.16	0.37	0.21	0.33	0.18
13	0.21	0.14	0.17	0.19	0.33	0.26	0.45	0.18
14	0.33	0.20	0.26	0.27	0.34	0.48	0.31	0.16
15	0.32	0.24	0.25	0.27	0.23	0.24	1.34	0.24
16	0.32	0.20	0.25	0.25	0.45	0.32	0.49	0.42
17	0.33	0.20	0.27	0.26	0.58	0.41	0.32	0.83
18	0.31	0.19	0.25	0.25	0.51	0.99	0.28	0.51
19	0.38	0.23	0.29	0.30	0.50	0.28	0.39	0.41
20	0.41	0.25	0.31	0.31	0.37	0.60	0.26	0.40
21	0.40	0.25	0.31	0.31	0.23	0.27	0.14	1.50
22	0.39	0.25	0.31	0.30	0.62	0.31	0.45	0.40
23	0.38	0.23	0.29	0.29	0.49	0.25	0.34	0.29
24	0.47	0.28	0.35	0.36	0.48	0.20	0.25	0.27
25	0.46	0.28	0.35	0.36	0.50	0.21	0.26	0.31
26	0.45	0.28	0.34	0.35	0.53	0.22	0.27	0.28
27	0.44	0.29	0.34	0.34	0.47	0.20	0.25	0.25
28	0.14	0.11	0.14	0.11	0.60	0.27	0.41	0.35
29	0.23	0.15	0.18	0.18	0.60	0.25	0.34	0.32
30	0.29	0.18	0.24	0.22	0.62	0.29	0.49	0.37
31	0.33	0.20	0.26	0.24	0.23	0.23	0.16	0.13
32	0.35	0.23	0.27	0.26	0.62	0.29	0.33	0.31
33	0.13	0.08	0.09	0.09	0.38	0.22	0.29	0.18
34	0.20	0.12	0.17	0.15	0.61	0.49	0.36	0.30
35	0.19	0.12	0.15	0.14	0.62	0.80	0.37	0.31
36	0.21	0.13	0.17	0.16	0.59	0.46	0.38	0.30
37	0.32	0.20	0.24	0.24	0.54	0.28	0.30	0.27
38	0.32	0.20	0.25	0.24	0.47	0.21	0.29	0.24
39	0.32	0.20	0.25	0.24	0.50	0.21	0.37	0.26
40	0.33	0.20	0.25	0.25	0.49	0.25	0.35	0.26
41	0.31	0.19	0.23	0.23	0.49	0.22	0.34	0.25
42	0.38	0.24	0.29	0.29	0.47	0.21	0.30	0.24
43	0.41	0.25	0.31	0.31	0.51	0.28	0.35	0.29
44	0.40	0.26	0.31	0.31	0.60	0.29	0.40	0.31
45	0.39	0.28	0.31	0.30	0.46	0.24	0.34	0.24
46	0.38	0.24	0.31	0.33	0.74	0.77	0.59	0.38
maximum	0.47	0.29	0.38	0.37	0.74	0.99	1.41	1.50

It should be taken into account that for each member the maximum axial and bending stress was combined. In long laths the maximum compression stress usually is observed at the bottom of the structure while maximum bending stress at the top. For factorized dead and wind load the LFRD stresses are under 1.0 (Table 4.8).

4.6.3 Reaction Forces

The summary of the reaction forces for all load cases is provided in Table 4.9 and the visualization of horizontal and vertical components for deadload in Figure 4.11 and Figure 4.10. The horizontal reactions are equilibrated by the tension ties in the base. There is another load case considering uplift, which is discussed in the next section.

Table 4.9 - Summary of the reaction forces for all the load cases.

LC: 100-101,110,120, Loadcase

LC	LC-title	RZ [kN]	RX [kN]	RY [kN]
100	1.4D	17.3	0.0	0.0
101	0.9D+1.0W	11.1	-3.1	0.0
110	1.2D+1.6LL1	16.2	0.0	0.0
120	1.2D+1.6LL2	14.8	-0.8	1.2

LC load case number
 LC-title Load case description
 RZ sum of support PZ
 RX sum of support PX
 RY sum of support PY

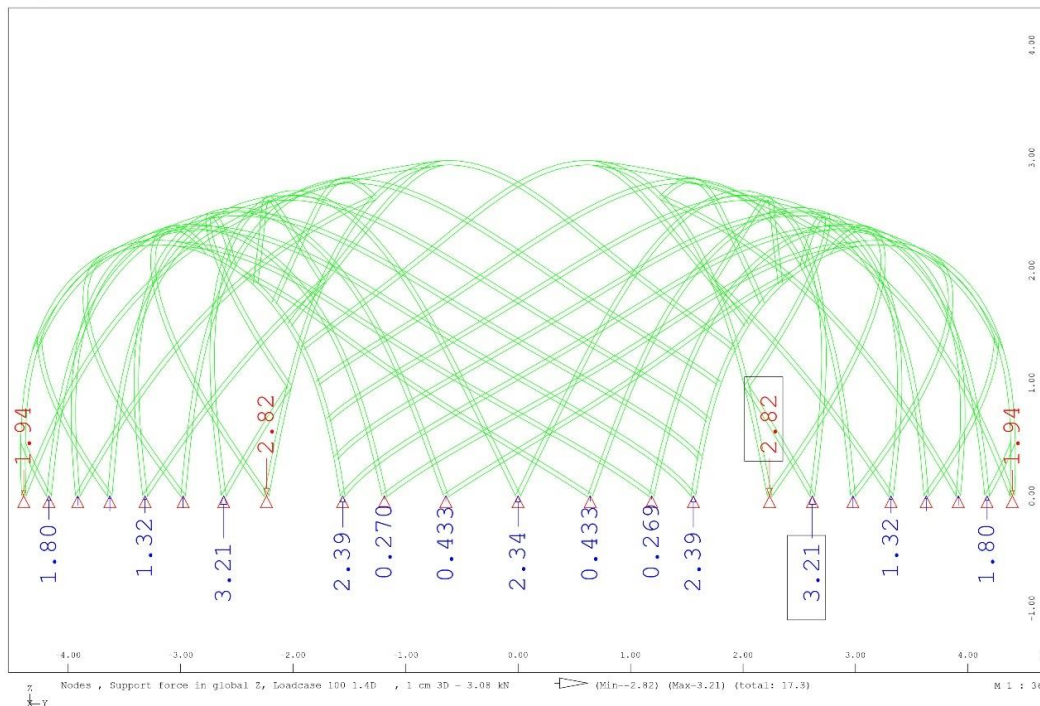


Figure 4.10 - Vertical components of the reaction forces under 1.4D.

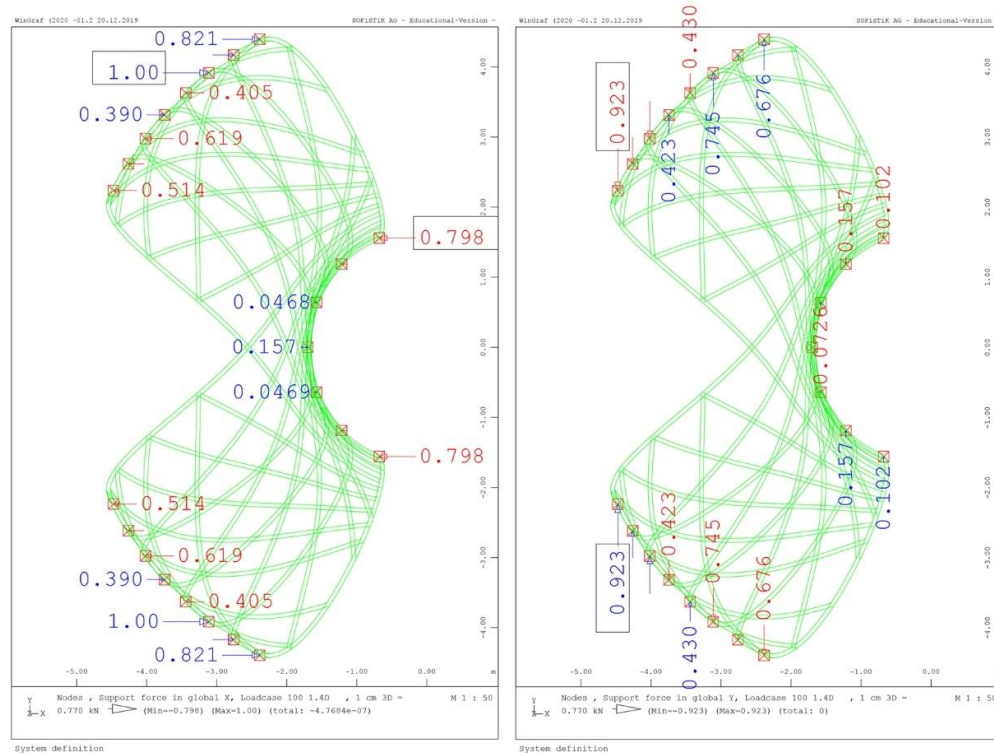


Figure 4.11 - Horizontal x and y components of the reaction forces under 1.4D.

4.6.4 Vertical Forces – Uplift

The vertical forces from possible uplift wind are going to be balanced by additional weight. For the uplift wind of 20psf (0.96 kN/m²), the projected on the x-y plane area of laths equals 11.27m² (Figure 4.7):

- Resultant Vertical Force from 20psf uplift wind: 10.82kN

In order to sustain 20psf uplift: $10.27\text{kN} / 9,81\text{m/s}^2 = 1103.35\text{ kg}$ of weight is necessary. Additional weight can be calculated as difference between resultant vertical force and the non-factorized dead load of the structure.

Table 4.10 - Non-factorized dead load of the final design.

	Density[kg/m ³]	Volume [m ³]	Weight [kg]
Base	590	0.246748	145.58
Laths	450	0.275804	124.11
		Total weight	269.69

Deadload including the base is calculated in Table 4.10. Additional mass necessary: $1103.35 - 269.69\text{ kg} = 833.66\text{kg}$

- Use 834 kg of additional mass for the uplift wind of 20psf.

The concrete blocks were used to add the required ballast.

4.7 Final structural notes

The final structural drawings are presented in Appendix B. Based on the engineering calculations provided in this chapter, and the following notes were made:

General notes:

1. The project is intended to be a temporary structure, to be erected for maximum of 5 days. The structure has been designed for a 3-year storm with a reduced wind speed of 64.2 mph due to the structure meeting ASCE requirements for a temporary structure installed for less than 1 year.
2. Do not use scaled dimensions, use only written dimensions. Where no dimension is provided, consult the architect for clarifications before proceeding with work.
3. Structural elements shall be centered about gridlines or dimension lines, unless otherwise noted.
4. Dimensions and details of existing construction given in structural drawings are approximate and are based on limited information. The contractor shall verify all information pertaining to existing conditions by actual measurement and observation at the site.
5. The contractor shall be solely responsible for the conditions of the job site including safety of persons and property and the means and methods of construction.
6. All forces indicated in the structural drawings are ultimate factored (LRFD) loads as defined by ASCE 7, unless noted otherwise. The structure has been designed for the in-service live loads described in the design loads notes and plans.
7. The contractor is responsible for the stability of the structure until the construction of the structure reaches its final condition. The structure is stable only in its completed form. Laths should be installed sequentially in order presented in the drawings.
8. The contractor shall protect existing facilities, structures, and utilities from all damage.

Foundation:

1. The foundation base shall rest on pavement of 1000psf minimum bearing capacity. Adequacy of bearing capacity should be verified.
2. Plywood at the base should be a hard plywood red oak with minimum properties as follows: modulus of rupture: 14,380 psi (99.2 MPa), elastic modulus: 1,761,000 psi (12.14 GPa), crushing strength: 6,780 psi (46.8 MPa).

Plywood Framing:

1. All installed laths should be Okoume plywood with minimum properties as follows: modulus of rupture: 10,300 psi (71.0 MPa), elastic modulus: 1,320,000 psi (9.10 GPa), crushing strength: 5,500 psi (38 MPa).

Metal Fasteners:

1. All installed metal joints and hinge connections should be made of 304 stainless steel or stronger with minimum properties as follows: tensile yield strength: 31,200 psi (215 MPa), elastic modulus: 28,000 ksi (193 GPa).

The structure is designed for the following loads:

1. Wind Load

Basic Speed Wind	V = 118 mph
Reduced Speed Wind	V = 64.2 mph
a) Building Risk Category	I
b) Wind Exposure Category	B
c) Mean Roof Height	H = 10ft
d) Directionality Factor, K _d	0.85
e) Topographic Factor, K _z t	1.00

2. In the event that wind speeds expected to exceed 64.2mph, the structure shall be disassembled.
3. Climbing or hanging from the structure is prohibited.

5. Fabrication and construction

The pavilion was designed with ease of construction in mind, meaning that it has a rapid assembly and that it can be put together without the need for sophisticated tools. The current chapter describes the fabrication and construction steps that were followed for its deployment. The main structural components were fabricated as follows: Firstly, the base pieces were cut on a large CNC router using 1" Red Oak plywood boards. Next, Okoume plywood boards, with dimensions of 4×8 ft, were cut into stripes at a local wood workshop. Lastly, plywood stripes with a length of 8 ft were measured, drilled and assembled in longer laths, on the site of construction, by a group of volunteering students. It is relevant to outline that the symmetry of the structural system accelerated manufacturing times, as it allowed for manually fabricated laths to be connected together and drilled simultaneously.

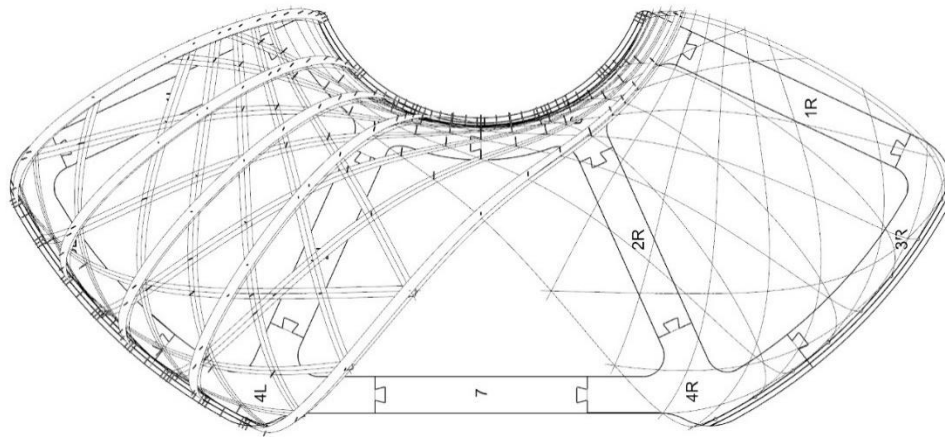


Figure 5.1 – Half of the laths of the pavilion – geometry for fabrication.

In order to maintain an organized assembly arrangement, laths were numbered in a pre-defined sequence and divided into symmetrical groups (Figure 5.2, Figure 5.3). This sequence and division allowed the building activity, on-site, to be split into groups and enabled simultaneous production of identical laths, making the construction of the structure more efficient. Volunteers responsible for the production of laths received the member template (Figure 5.4) and the following list of instructions:

1. Write the number of the lath on each piece.
2. Draw cross marks and write “start”, “end”.
3. On each piece draw an arrow pointing to “start”.
4. Tape together the same pieces.
5. Mark cuts and holes.
6. Drill holes.
7. Cut endings.
8. Assemble plywood stripes into laths following the marked arrows.

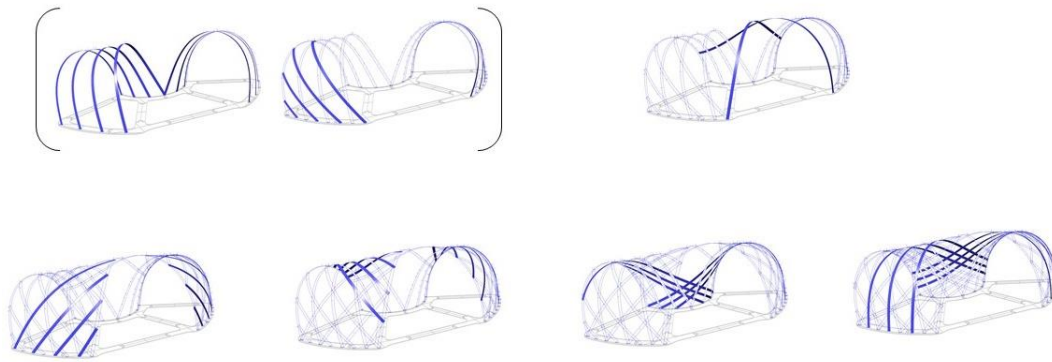


Figure 5.2 - Planned sequence of assembly– laths divided into symmetrical groups.

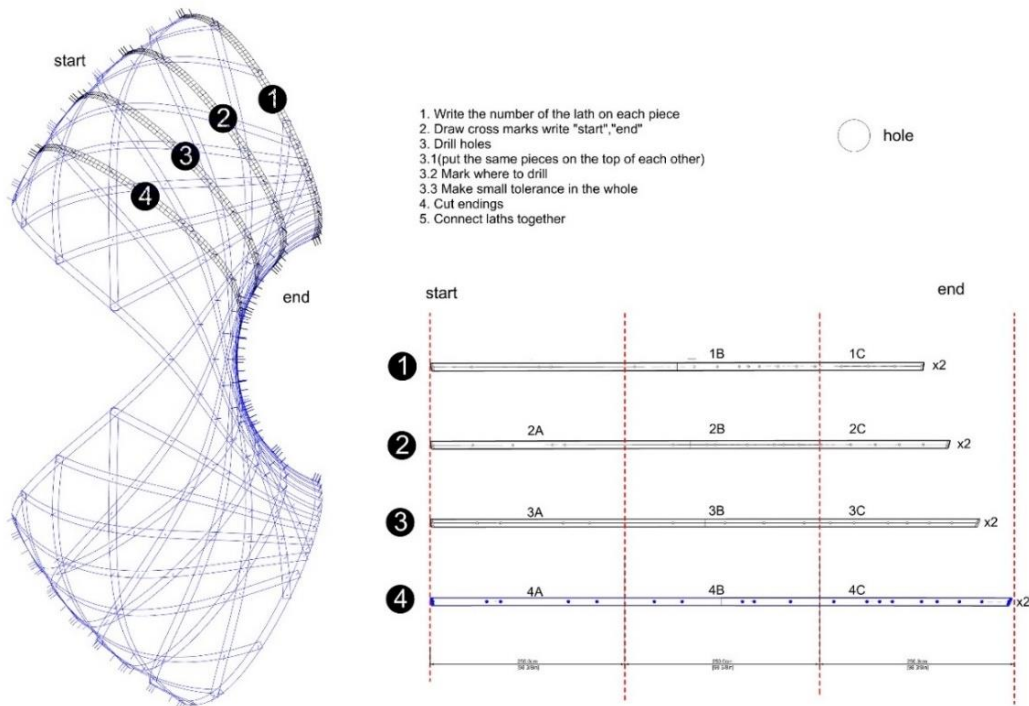


Figure 5.3 - First group of laths, instructions for the on-site fabrication.

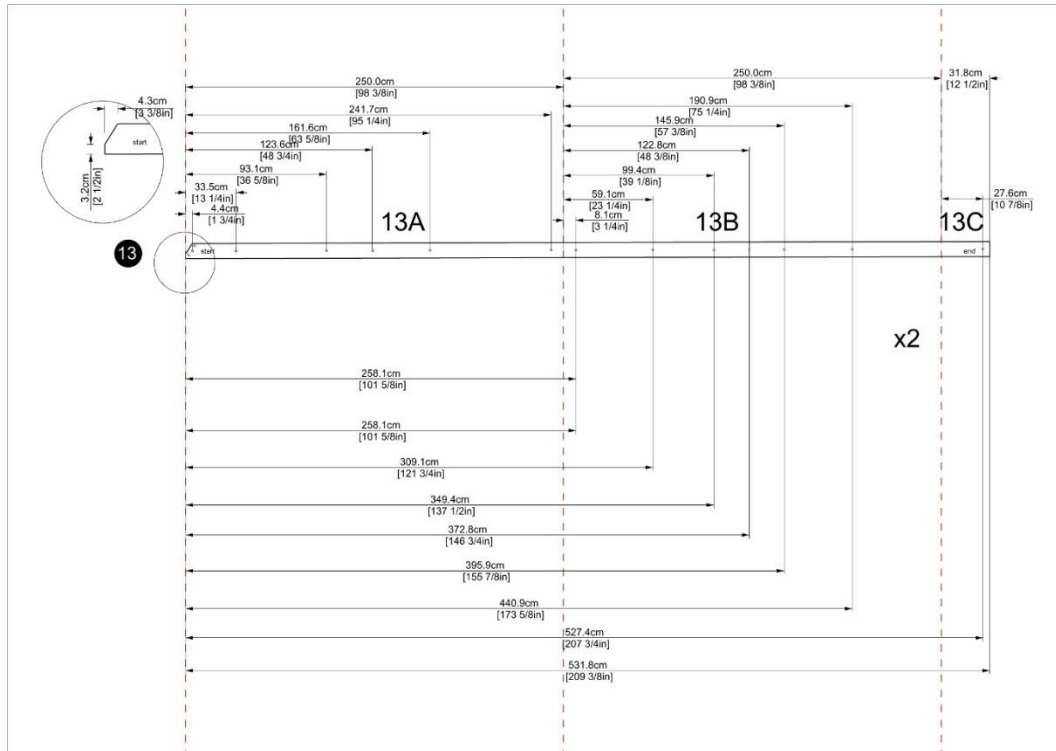


Figure 5.4 - The drilling and cutting template for the on-site production of laths.

5.1 Base Design

Base elements were prepared for CNC machining by fitting 4x8 ft boards with CAM files prepared in Fusion 360. The boards had to be mounted to the machine's bed to prevent unwanted movements during fabrication, therefore, each board was prepared with a safety margin marked with a dashed line (Figure 5.5) to guarantee a 1-in wide stripe around for a firm attachment. All parts were milled using the Amana Tool 46429 SC Spiral Plunge 1/2 D x 2 CH x 1/2 SHK x 4-Inch-Long 2 Flute Down-Cut Router Bit. The pieces were first milled around the outer edges in order to leave blocks that helped prevent any kind of movement. The blocks were removed with the use of a manual tool after being cut. The tool size and working principles of the CNC router do not allow for the fabrication of sharp corners, therefore, to preserve the precision needed for fitting pieces together, all corners of the base' connections had to be filleted. The tolerance of 0.5mm guaranteed tight dove-tail connection for the 1in thick elements. Note that some of the dove tail joints were not perfectly symmetrical (Figure 5.5). The connection of 3L-4L and 3R-4R are moved toward the center on purpose, leaving the lines for hinges not interrupted. The connections of 2L and 2R are slightly asymmetrical to fit bigger pieces connected to them into the 4 x 8ft boards.

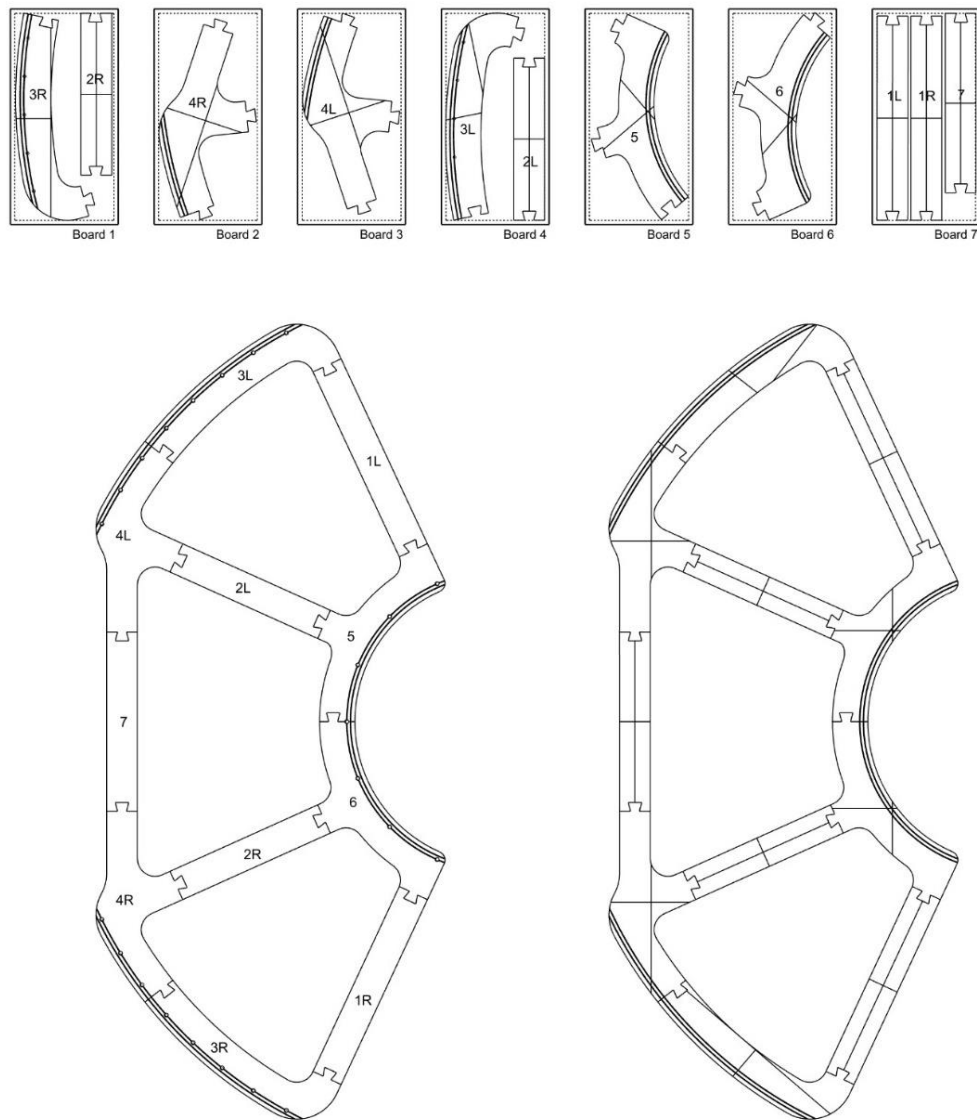


Figure 5.5 - Base plan and the boards for the CNC fabrication.

5.2 Details

The present section outlines and explains the quantities and types of joints used in the layout. A single layer design requires only 5 types of connections: 2-lath joint, 3-lath joint, lath-lath connection, hinge to 2 laths and hinge to base. The introduction of the second layer members increases the number of types of connections. Figure 5.6 presents the types and quantities of the connections used. A detailed description of each type of joint is given in the following paragraphs.

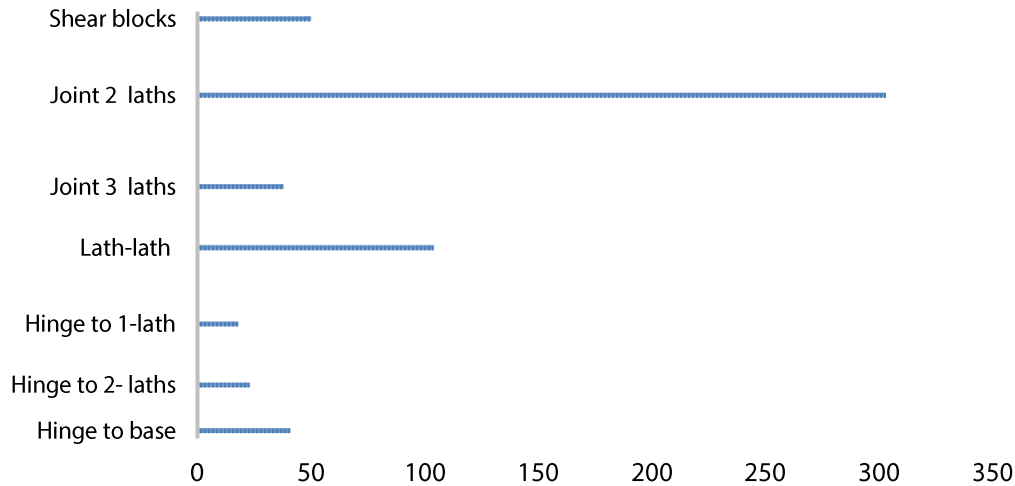


Figure 5.6 - Diagram with types and amounts of connections.

Base-Lath Connection

The base-lath connection was designed to mount each layer of the laths on separate hinges. The distance between two hinges (Figure 5.7) was designed to keep proper space reserve for the screws and to fit 1in thick 10x10cm shear blocks, which were cut out from the leftover material from the base fabrication. The base was designed to rest on the thin rubber protecting the pavement and preventing sliding of the structure.

Lath-Lath Connection

The laths were connected using a common bolt connection with the wood member between two steel plates. The metal plates have holes prepunched and the holes in the laths were drilled on site. During the assembly of these connections a practical field problem occurred. It was difficult to drill the holes through the still plates to perfectly align both laths and plate from the other side. The plates were firstly connected to one lath and then the second lath was aligned and drilled through metal plates. The bent properties of the connection were tested in 1:1 scale in the workshop in the process of progressive bending.

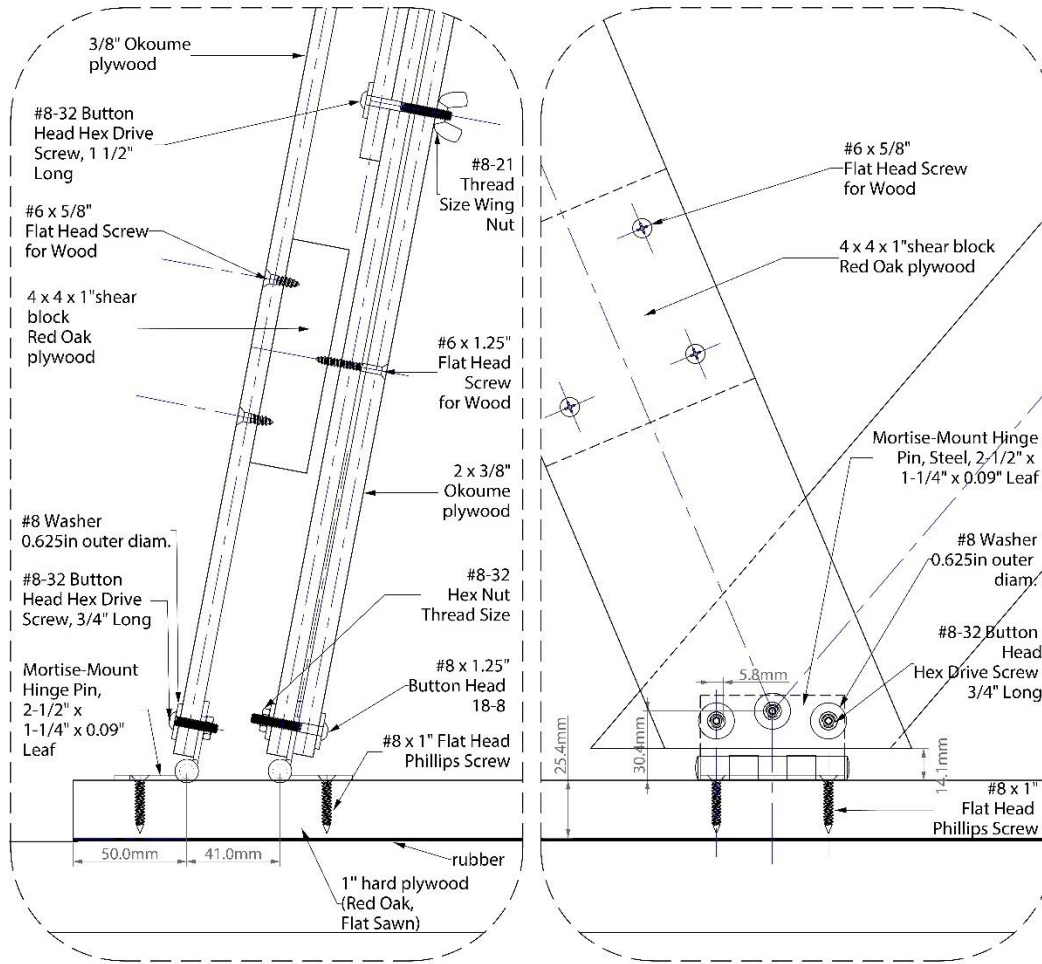


Figure 5.7 - Base-lath connection detail.

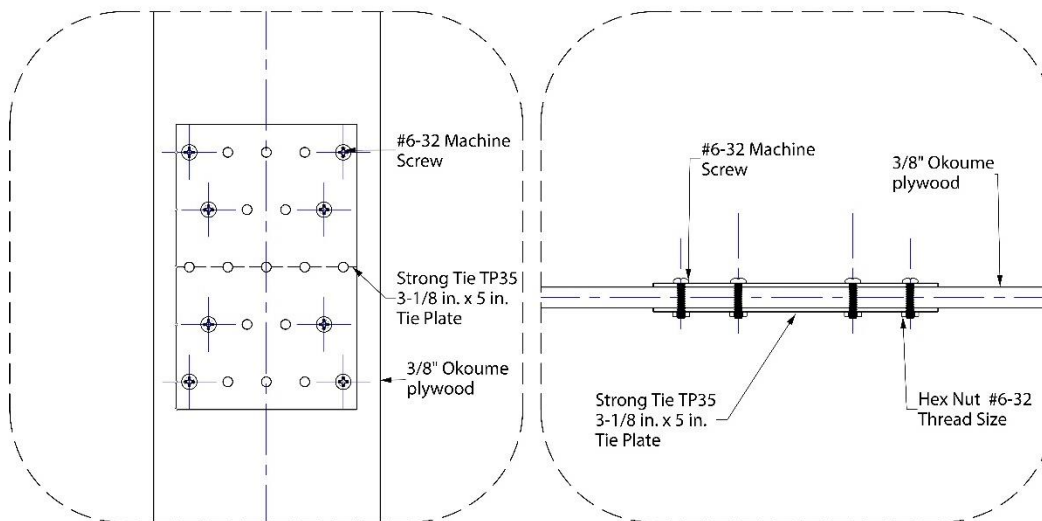


Figure 5.8 - Lath-lath connection detail.

2-Lath Joint

The simple rotational joint was used to connect two intersecting laths (Figure 5.9 and Figure 5.10). Wing nuts helped in the fast assembly of the joints on site. The NDS (Ref.7.2) requires that the hole diameter should be larger than the bolt diameter and be in range 1/32 to 1/16.

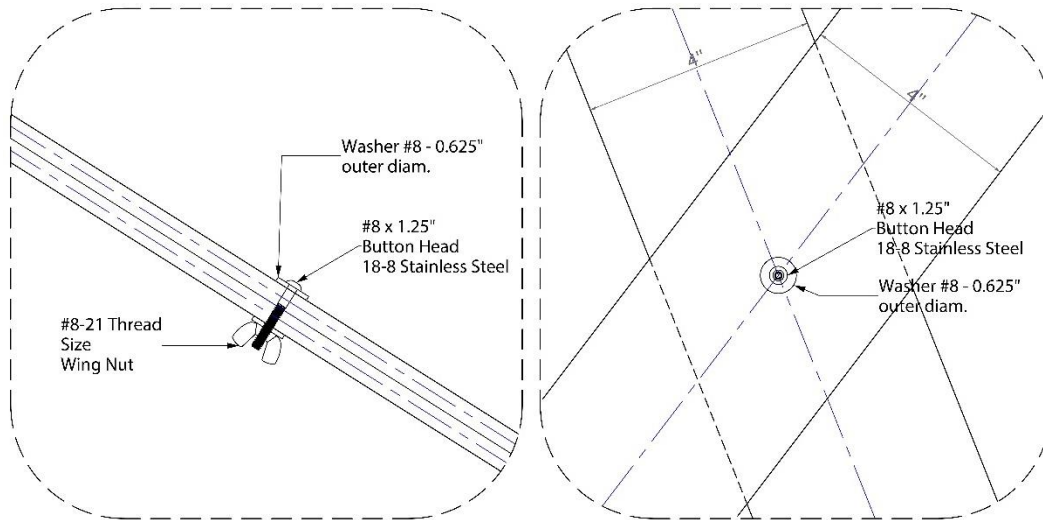


Figure 5.9 - Rotational joint connecting 2 laths.



Figure 5.10 - Rotational joint connecting 2 laths. Photo credit: Heidi Erickson.

5.3 Photos

The structure was designed to be a temporal exposition for a short period of time. Due to its short-time character and a two-day delay (forced by unexpected weather conditions) in the construction process, the second layer of members could not be assembled. Nevertheless, the single-layer structure members were successfully bent into the desired shape and correctly assembled without any of them breaking. The finished single-layer structure is presented in Figure 5.11, Figure 5.12, Figure 5.13 and in Figure 5.14.

The structure had to be marked with “no-climbing” signages (Figure 5.13). The base of the pavilion was rested on the pavement and separated with protective material. The completed structure served as a stage for the electronic music performance (Figure 5.15, Figure 5.16) and as a canvas for a video-mapping night show (Figure 5.17, Figure 5.18).



Figure 5.11 - The assembled INFRAME pavilion – front view. Photo credit: Judyta Cichocka.

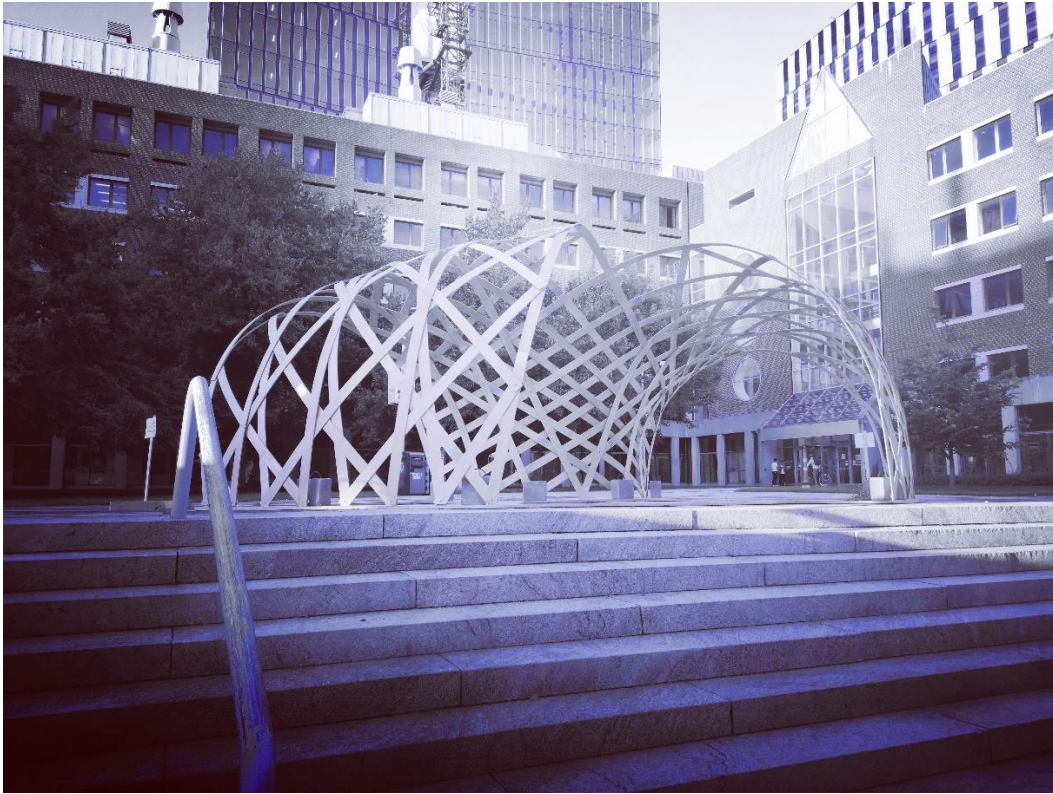


Figure 5.12 - The assembled INFRAME pavilion – a perspective view. Photo credit: Judyta Cichocka.



Figure 5.13 - The assembled INFRAME pavilion – back view. Photo credit: Judyta Cichocka.

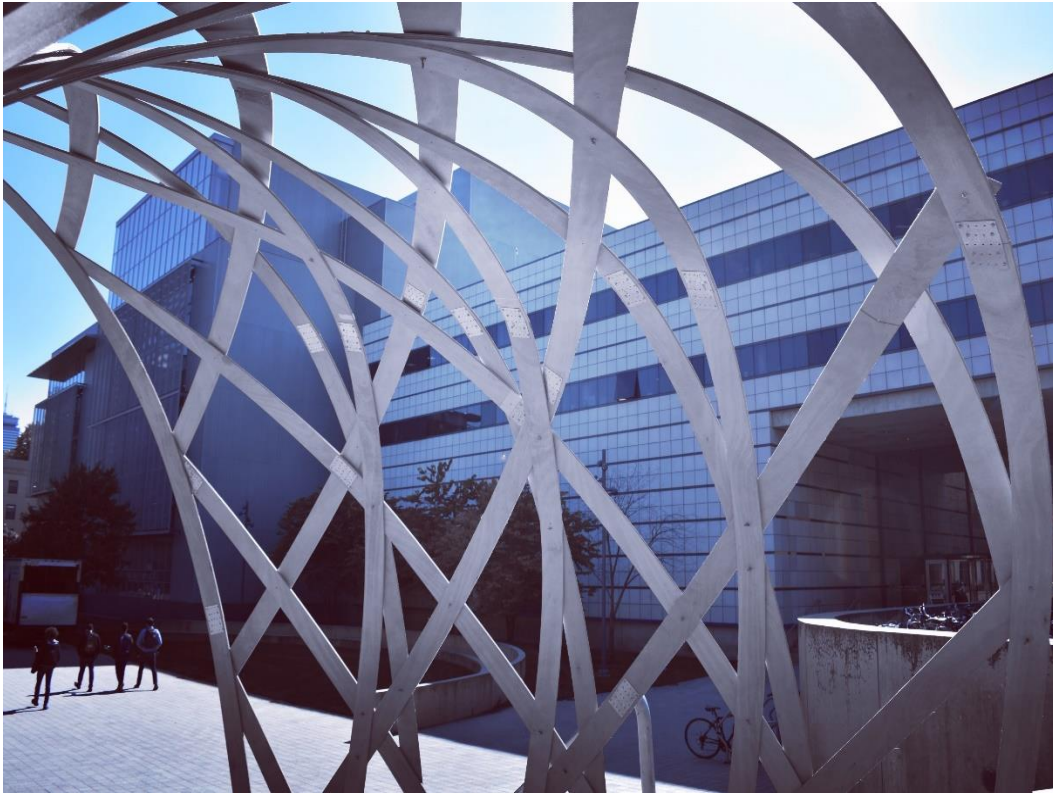


Figure 5.14 - View from the inside of the structure. Photo credit: Heidi Erickson.



Figure 5.15 - The opening event – a view from the MIT Media Lab. Photo credit: Gabriela Bila Advincula.



Figure 5.16 – Daniela Hensel performing in INFRAME. Photo credit: Judyta Cichocka.



Figure 5.17 - Theresa Silver in preparation of a video-mapping performance. Photo credit: Judyta Cichocka.



Figure 5.18 - A video-mapping performance by Theresa Silver. Photo credit: Judyta Cichocka.

5.4 Relocation, disassembly and transport

On 20th September 2019, at 8.30AM the disassembly phase was planned by the MIT Department of Facilities, involving a contractor to assist in disassembling the structure and the MIT Recycling to take the material away. At 8.00AM the structure was gone from the LIST courtyard, but it was not taken by the MIT facilities. It would appear to be a student prank and the pavilion was relocated over night to the East Campus (Figure 5.19). It is unknown who exactly and how relocated the pavilion, nevertheless the structure was found in the East Campus in a perfect condition (Figure 5.20). The elements of the base were connected with additional screwed elements, suggesting that the structure was relocated in one piece.



Figure 5.19 - The structure after the relocation “prank” in the MIT East Campus. Photo credit: Judyta Cichocka.



Figure 5.20 - The relocated structure. Photo credit: Judyta Cichocka.

The unexpected relocation extended the intended life-span of the structure for two additional days. Volunteers for disassembly were scouted via social media with a post containing an image of the structure. The post encouraged potential new owners of INFRAME to express their intended future use of the structure. Within one day, the offer was viewed 2,554 times and had more than 70 responses showing interest. The structure was imagined in completely new roles, ranging from an add-on to an outdoor training dog facility, to a structure for climbing roses for the New England Rose Society. A few responses are quoted below:

“I am the [professional role] of the New England Rose Society and I am thinking that beautiful climbing roses along the sides would compliment it and make an incredible area of respite!” Anonym.

“I can pick it up tomorrow for free, it would look beautiful in my yard. We run an upscale dog training facility and this piece would be admired by many in our training yard.” Anonym.

“It is a beautiful structure. [...]. One of the yearly projects that I am involved in is creating an enchanted forest walk through the woods. Audiences make their way along a path that runs through the woods. There they encounter our mysterious dwellers, witness small spectacles, hear stories, and engage in different forms of interactive play with our performers. We have a number of installations that help create the atmosphere. We are a collaborative and do not have large budget. Most of us are simply committed to creating the magic for the kids and adults who enjoy it.” Anonym.

The author of the last quote offered help with dismounting the pavilion and taking a structure for the stage for the magical event described above. He mentioned that he would like to engage a group of teenagers in the reassembly. He believed that the construction of the pavilion would be a valuable learning experience. The structure was disassembled within a few hours and all elements fitted to the back of a van (Figure 5.21).



Figure 5.21 - Left: The disassembled structured prepared for transportation. Photo credit: Loai Namaani, Right: The assembled structure. Photo credit: Heidi Erickson.

6. Conclusions

6.1 Summary of contributions

The design process in the presented research outlines the development and verification of a design-oriented workflow, through the realization of a structurally sound elastic timber gridshell, INFRAME (Figure 6.1). The structure was constructed from the marine plywood, Okoume, usually used to make kayaks, and was composed of 46 actively bent laths⁵ of a joint length of 234.1m. The structure was designed for ultimate factored (LRFD) loads as defined by ASCE. Most of the design assumptions presented in Section 4.1 were successfully met. The structure was low cost (3335 USD for all the materials including hardware), lightweight (96kg without the base), and constructible, within a two-day time frame, by a group of five unqualified builders. The structure was successfully deployed and will be repurposed for future installations and activities.

The construction of the INFRAME pavilion as a temporary outdoor stage led to the following conclusions:

- It was difficult to provide sufficient stability of the elastic structure for an outdoor use with the use of only one layer. Similarly, as the UWE Pavilion, double-layer members had to be introduced in the design on the critical ribs of the structure.
- Although the structure was not covered, wind load was of much importance to the implementation.
- A multi-objective search of topology can aid the design of the geodesic gridshells.
- Introduction of plywood and timber materials of high elastic properties to the NDS supplements would be a significant step towards the adaptation of the bending-active systems by the building codes.
- The unplanned relocation of the pavilion has demonstrated its resilience to material failure and its potential to be transported without disassembly.
- The potential of the structure to be adapted to other uses has been examined by analyzing responses gathered through the social media post containing images of the structure (Section 5.4).
- The deployability and ease of transportation of the structure has been proven (Figure 5.21).

6.2 Potential impact

This thesis serves as a brief introduction and proof of how a temporary bending-active structure can be adopted to the building codes. The construction of the pavilion has proven that the presented methodology might lead to the design of structurally sound geodesic timber gridshells. The proposed design process, with integrated grid-exploration, can, in practice, popularize elastic timber gridshells, help to increase their efficiency and achieve larger spans.

⁵ The numbers are provided for the constructed single-layer. The intended second layer would add 10 additional members of the joint length of 70m.

6.3 Future work

Future work will aim to solve the challenge of defining structurally-sound geodesic grid configuration by the adaptation of the topology optimization for elastic structures. The stiff geodesic grid configuration can be selected from a dense ground geodesic curves arrangement by solving a minimum compliance problem. The applications of topology optimization in the design of elastic gridshells were presented at the IASS 2019:

Cichocka, J.M., Carstensen, J.V. and Mueller C.T. (2019). Topology optimization of elastic geodesic gridshells. *IASS Annual Symposium 2019 – Structural Membranes 2019* Form and Force, 7 – 10 October 2019, Barcelona, Spain

A forthcoming publication is in preparation by the same authors.

6.4 Concluding remarks

This thesis advocates for structural systems that are augmented by technology. The mix of low-cost materials and state-of-art design tools can result in the design of a structure buildable without sophisticated tools within a few-day time frame. For comparison a 3D printed pavilion of similar a footprint needed 181.3 days of combined printing time to be manufactured⁶. The ease of construction creates an opportunity for structural systems that not only are cost-effective but can also be built by communities. Excellence in structural engineering is not solely enough to maintain the social importance of structures. Although automation in construction allows production in a faster and more precise manner, there is something special about building structures with a group of people and with your own hands. The feeling of shared creation produces a special connection between builders and the structure. Building an emotional relationship between structures and people makes them naturally sustainable. Once structures are loved, they never die too early and they will actively support the sustainable development of cities and communities.



Figure 6.1 - The final structure realized with logotypes of the project supporters. Photo credit: Daniel Seats.

⁶ Based on the information about TRABECULAE PAVILION (ACTLAB, 2019)

7. References

- ACTLAB (2019) *TRABECULAE PAVILION*. [Online]. 2019. Available from: www.actlab.polimi.it.
- Adiels, E., Bencini, N., Brandt-Olsen, C., Fisher, A., et al. (2018) Design , fabrication and assembly of a geodesic gridshell in a student workshop. *Proceedings of the IASS Annual Symposium 2018*.
- Adriaenssens, S., Barnes, M., Harris, R. & Williams, C. (2014) Dynamic Relaxation. In: Sigrid Adriaenssens, Philippe Block, Diederik Veenendaal, & Chris Williams (eds.). *Shell Structures for Architecture: Form Finding and Optimization*. Routledge. pp. 89–101.
- American Wood Council (2018) *NDS Supplement National Design Specification Design Values for Wood Construction*. [Online]. Available from: [doi:10.1017/CBO9781107415324.004](https://doi.org/10.1017/CBO9781107415324.004).
- Anastasiadou, I., Alexandrou, K. & Phocas, M.C. (2018) Deformation Control of Hybrid Bending-active Structures by Multiple Cables. *Proceedings of the IASS Annual Symposium 2018*.
- Ander, M., Sehlstrom, A., Shepherd, P. & Williams, C.J.K. (2017) Prestressed gridshell structures. *Proceedings of the IASS Annual Symposium 2017*.
- Baek, C., Sageman-Furnas, A.O., Jawed, M.K. & Reis, P.M. (2018) Form finding in elastic gridshells. *Proceedings of the National Academy of Sciences*. [Online] 115 (1), 75–80. Available from: [doi:10.1073/PNAS.1713841115](https://doi.org/10.1073/PNAS.1713841115) [Accessed: 22 March 2019].
- Barnes, M.R., Adriaenssens, S. & Krupka, M. (2013) A novel torsion/bending element for dynamic relaxation modeling. *Computers and Structures*. [Online] 119, 60–67. Available from: [doi:10.1016/j.compstruc.2012.12.027](https://doi.org/10.1016/j.compstruc.2012.12.027).
- Bauer, A.M., Längst, P., La Magna, R., Lienhard, J., et al. (2018) Exploring Software Approaches for the Design and Simulation of Bending Active Systems. *Proceedings of the IASS Symposium 2018*.
- Bhooshan, S., Veenendaal, D. & Block, P. (2014) Particle-spring systems. In: *Shell Structures for Architecture: Form Finding and Optimization*. pp. 103–113.
- Boggs, D. & Peterka, J. (1992) G : J G : J. In: *Structures Congress '92 Compact Papers, ASCE, 1992*. 1992 p.
- Brancart, S., Popovic Larsen, O., Laet, L.D.E. & Temmerman, N.D.E. (2018) Bending-active reciprocal structures : geometric parameters and their stiffening effect. *Proceedings of the IASS Annual Symposium 2018*.
- Brandt-Olsen, C.S. (2016) *Calibrated Modelling of Form-active Structures*. (June), 1–133.
- Breyer, D.E., Cobeen, K.E., Fridley, K.J. & Pollock, D.G. (2015) *Design of Wood Structures-ASD/LRFD*. 7th ed.
- Brütting, J., Körner, A., Sonntag, D. & Knippers, J. (2017) Bending-Active Segmented Shells. *Interfaces: architecture.engineering.science [Proceedings of the IASS Annual Symposium 2017]*. (Brütting 2014), 1–10.
- Coar, L., Cha, Y.-J., Jiang, Z., Piper, J., et al. (2018) The design and testing of post-tensioned bending active spatial assemblies. *Proceedings of the IASS Annual Symposium 2018*.
- Coenders, J. & Bosia, D. (2006) Computational tools for design and engineering of complex geometrical structures: from a theoretical and a practical point of view. In: K Oosterhuis & L Feireiss (eds.). *The architecture co-laboratory: game, set and match II on computer games, advanced geometries, and digital technologies*. pp. 271–279.
- Cuvilliers, P., Yang, J.R., Coar, L. & Mueller, C. (2018) A comparison of two algorithms for the simulation of bending-active structures. *International Journal of Space Structures*. [Online] Available from: [doi:10.1177/0266351118779979](https://doi.org/10.1177/0266351118779979).
- D’Amico, B., Kermani, A. & Zhang, H. (2014) Form finding and structural analysis of actively bent timber grid shells. *Engineering Structures*. [Online] 81 (0), 195–207. Available from: [doi:10.1016/j.engstruct.2014.09.043](https://doi.org/10.1016/j.engstruct.2014.09.043).
- Grundig, L. & Schek, H.-J. (1974) Analytical form finding and analysis of prestressed cable networks. In: *Machine Learning*. 1974 pp. 195–225.
- Harding, J., Pearson, W., Lewis, H. & Melville, S. (2014) The Ongreening Pavilion. *Advances in Architectural Geometry 2014*. [Online] 295–308. Available from: <https://www.springer.com/la/book/9783319114170>.
- Harding, J.E., Hills, S., Brandt-olsen, C. & Melville, S. (2017) The UWE Research Pavilion 2016. *Proceedings of the IASS Annual Symposium 2017*.
- Hill, J. (2018) *Mannheim’s ‘Sleeping Beauty’ - Biennale Architettura 2018*. [Online]. 2018. Available from: <https://www.world-architects.com/en/architecture-news/found/mannheim-s-sleeping-beauty> [Accessed: 17 December 2018].
- Huang, J.M. & Zhou, Y. (2018) Computational Bamboo Grid-Shell : an exploration of digital design with traditional craftsmanship. *Proceedings of the IASS Annual Symposium 2018*.
- Isaksson, J. & Skeppstedt, M. (2018) *Stressing Timber - An exploration of the use of prestressing in timber*

- structures through the design of a lecture pavilion. Chalmers University of Technology.
- Kensek, K., Leuppi, J. & Noble, D. (2000) Plank lines of ribbed timber shell structures. In: *ACADIA 2000: Eternity, Infinity and Virtuality*. [Online]. 2000 p. Available from: doi:f197.
- Kilian, A. & Ochsendorf, J. (2005) Particle Spring Systems for Structural Form Finding. *Theory, Technique, Valuation Maintenance: Proceedings of the IASS Symposium 2005*. Vol. 46 (148), 77–84.
- Kozlov, D. (2018) Bionic Type Structures Based Upon Resilient Cyclic Knots. *Proceedings of the IASS Annual Symposium 2018*.
- Kuijnenhoven, M. & Hoogenboom, P.C.J. (2012) Journal of the international association for shell and spatial structures. *Particle-Spring Method for Form Finding Grid Shell Structures Consisting of Flexible Members*. 53, 31–38.
- Lafuente, E., Gengnagel, C., Sechelmann, S. & Rörig, T. (2011) On the Materiality and Structural Behaviour of Highly-Elastic Gridshell Structures. *Computational Design Modelling*. [Online] (1975), 123–135. Available from: doi:10.1007/978-3-642-23435-4_15.
- Lafuente Hernandez, E. (2015) *Design and Optimisation of Elastic Gridshells*. Universität der Künste Berlin 2015.
- Larsen, O.P., Brancart, S., Temmerman, N.D.E., Laet, L.D.E., et al. (2018) ReciPlyDome and ReciPlySkin bending-active transformable lightweight shelters. *Proceedings of the IASS Annual Symposium 2018*.
- Leung, N. (2018) *The Nature of Gridshell Form Finding*. [Online]. 2018. Available from: <https://wewanttolearn.wordpress.com/2018/03/13/the-nature-of-gridshell-form-finding/> [Accessed: 4 November 2018].
- Li, J.M. & Knippers, J. (2013) *Designing Regular and Irregular Elastic Grid Shells by 6 DOF Dynamic Relaxation*. (January 2017).
- Lienhard, J. (2014) *Bending-active structures form-finding strategies using elastic deformation in static and kinetic systems and the structural potentials therein*. [Online] Available from: <https://elib.uni-stuttgart.de/handle/11682/124>.
- Lienhard, J., Alpermann, H., Gengnagel, C. & Knippers, J. (2013) Active Bending, a Review on Structures where Bending is Used as a Self-Formation Process. *International Journal of Space Structures*. [Online] 28 (3–4), 187–196. Available from: doi:10.1260/0266-3511.28.3-4.187.
- Lienhard, J. & Gengnagel, C. (2018) Recent developments in bending-active structures. In: *Proceedings of the IASS Annual Symposium 2018*. 2018 p.
- Linkwitz, K. (2014) Force density method. In: Sigrid Adriaenssens, Philippe Block, Diederik Veenendaal, & Chris Williams (eds.). *Shell Structures for Architecture: Form Finding and Optimization*. Routledge. pp. 59–69.
- Magna, R.L.A., Fragkia, V., Längst, P., Lienhard, J., et al. (2018) Isoropia : an Encompassing Approach for the Design , Analysis and Form-Finding of Bending-Active Textile Hybrids. *Proceedings of the IASS Annual Symposium 2018*.
- MatWeb (2019) *MatWeb Material Property Data*. [Online]. 2019. Available from: <http://www.matweb.com/search/datasheet.aspx?matguid=53cc39384ece4da49785af1fcd4e17f.%0A%0A>.
- Mesnil, R., Ochsendorf, J. & Douthe, C. (2015) Stability of Pseudo-Funicular Elastic Grid Shells. *International Journal of Space Structures*. [Online] 30 (1), 27–36. Available from: doi:10.1260/0266-3511.30.1.27 [Accessed: 7 February 2019].
- Möller, E. & Fischer, J. (2018) Multihalle Mannheim - maintenance ideas between creativity and extermination. In: *Proceedings of the IASS Annual Symposium 2018*. 2018 p.
- Moody, R.C. & Hernandez, R. (2015) *Glued-Laminated Timber Advantages of Glued-Laminated Timber*.
- Oliva-Salinas, J.G. (2018) Creativity and Sustainability in Translation Grid Shells. *Proceedings of the IASS Annual Symposium 2018*.
- Panetta, J., Konaković-Luković, M., Isvoranu, F., Bouleau, E., et al. (2019) X-Shells. *ACM Transactions on Graphics*. [Online] 38 (4), 1–15. Available from: doi:10.1145/3306346.3323040.
- Peloux, L. Du (2018) *Modeling of bending-torsion couplings in active-bending structures. Application to the design of elastic gridshells*.
- Pirazzi, C. & Weinand, Y. (2006) Geodesic lines on free-form surfaces: optimized grids for timber rib shells. *9th World Conference on Timber Engineering*. 72–79.
- Pottmann, H., Deng, B., Schiftner, A., Kilian, M., et al. (2010) *Geodesic Patterns*. [Online] 1 (212), 1–10. Available from: doi:10.1145/1778765.1778780.
- Poulsen, E. (2015) *Structural design and analysis of elastically bent gridshells - The development of a numerical simulation tool*. Chalmers University of Technology.
- Preisinger, C. (2019) *Karamba 1.3.2 user manual*.
- Richardson, J.N., Adriaenssens, S., Filomeno Coelho, R. & Bouillard, P. (2013) Coupled form-finding and grid optimization approach for single layer grid shells. *Engineering Structures*. [Online] 52 (February 2018), 230–239. Available from: doi:10.1016/j.engstruct.2013.02.017.
- Rombouts, J., Lombaert, G., de Laet, L. & Schevenels, M. (2017) On the equivalence of dynamic relaxation

- and the Newton-Raphson method : application to the design and analysis of bending-active structures. *Proceedings of the IASS Annual Symposium 2017*.
- Sakai, Y. & Ohsaki, M. (2018) Approximate shape design of gridshells using spatial discrete elastica. *Proceedings of the IASS Annual Symposium 2018*.
- Sakai, Y. & Ohsaki, M. (2017) Discrete elastica model for shape design of grid shells. *Proceedings of the IASS Annual Symposium 2017*.
- Schleicher, S. (2018) Potential of 3D Printed Joinery for Bending-active Structures. *Proceedings of the IASS Annual Symposium 2018*.
- Schulitz, M. (2017) Timber Gridshell Exploration using Geodesic Segments. *Proceedings of the IASS Annual Symposium 2017*.
- Soriano, E. (2017) Low-Tech Geodesic Gridshell: Almond Pavilion. *archiDoct*. 4(2) (February), 29–40.
- Struik, J. (1988) *Lectures on classical differential geometry*. 2nd ed.
- Suzuki, S., Slabbinck, E.L.M. & Knippers, J. (2017) A comparative overview of generative approaches for computational form-finding of bending-active tensile structures. *Proceedings of the IASS Annual Symposium 2017*.
- Vassallo, M. & Malek, S. (2017) Design and Structural Analysis for a Deployable Gridshell Shelter. *Proceedings of the IASS Annual Symposium 2017*.
- Veenendaal, D., Augustynowicz, E. & Tang, G. (2017) Magnolia : a glass-fibre reinforced polymer gridshell with a novel pattern and deployment concept. *Proceedings of the IASS Annual Symposium 2017*.
- Veenendaal, D. & Block, P. (2012) An overview and comparison of structural form finding methods for general networks. *International Journal of Solids and Structures*. [Online] 49 (26), 3741–3753. Available from: doi:10.1016/j.ijsolstr.2012.08.008 [Accessed: 28 October 2018].
- Veenendaal, D. & Block, P. (2014) Comparison of form-finding methods. In: *Shell Structures for Architecture: Form Finding and Optimization2*. Routledge. pp. 115–129.
- Yuan, P.F., Chai, H. & Jin, J. (2018) DigitalFUTURE 2017 Gridshell - Digital Design and Fabrication of Complex Strained Gridshell Structure. *Proceedings of the IASS Annual Symposium 2018*.

Appendix A

Material testing results

Observation:

Cracking – a moment at which first cracks were observed during testing

Failure – a state when the lath broke

Radius of curvature:

r_{all} – allowable radius calculated based on design bending stress (Section 4.3)

r_m – radius of curvature just before material yields

r_{cr} – radius of curvature when material cracking occurred

r_f – radius of curvature when material failure occurred

Table A.0.1 - Results from the physical tests for Baltic Birch plywood 6mm.

Observation	Elastica Width [cm]	r_{min} [m] at the top of elastica		Max. Curvature $\frac{1}{r_{min}}$	Bending Moment [Nm]	Bending Stress [MPa]
					$M_y = \frac{EI_y}{r}$	$\sigma_x = \frac{M_{yz}}{I_y}$
	220	1.22		0.82	12.910	21.5
	200	0.88		1.14	17.898	29.8
	198	0.86	r_{all}	1.16	18.324	30.5
	180	0.72		1.39	21.875	36.5
	160	0.62		1.61	25.403	42.3
	140	0.54		1.85	29.167	48.6
	125	0.52	r_m	1.92	30.288	50.9
cracking	120	0.49	r_{cr}	2.04	32.143	53.6
	100	0.44		2.27	35.795	59.7
	80	0.40		2.50	39.375	65.6
	60	0.37		2.70	42.568	70.9
	40	0.34		2.94	46.324	77.2
	20	0.31		3.23	50.806	84.7
failure	0	0.29	r_f	3.45	54.310	90.5

Table A.0.2- Results from the physical tests for Okoume plywood 6mm.

Observation	Elastica Width [cm]	r_{min} [m] at the top of elastica		Max. Curvature $\frac{1}{r_{min}}$	Bending Moment [Nm]	Bending Stress [MPa]
					$M_y = \frac{EI_y}{r}$	$\sigma_x = \frac{M_{yz}}{I_y}$
	220	1.22		0.82	13.426	22.4
	200	0.88		1.14	18.614	31.0
	180	0.72		1.39	22.750	37.9
	166	0.64	r_{all}	1.56	25.594	42.6
	160	0.62		1.61	26.419	44.0
	140	0.54		1.85	30.333	50.6
	120	0.49		2.04	33.429	55.7
	100	0.44		2.27	37.227	62.0
	80	0.40		2.50	40.950	68.3
	68	0.38	r_m	2.60	42.601	71.0
	60	0.37		2.70	44.270	73.8
	20	0.31		3.23	52.839	88.1
cracking	0	0.29	r_{cr}	3.45	56.483	94.1

Table A.0.3- Results from the physical tests for Okoume plywood 9mm.

Observation	Elastica Width [cm]	r_{min} [m] at the top of elastica		Max. Curvature $\frac{1}{r_{min}}$	Bending Moment [Nm]	Bending Stress [MPa]
					$M_y = \frac{EI_y}{r}$	$\sigma_x = \frac{M_y z}{I_y}$
	220	1.22		0.82	45.314	33.6
	206	0.96	r_{all}	1.04	57.586	42.6
	200	0.88		1.14	62.821	46.5
	180	0.72		1.39	76.781	56.9
	160	0.62		1.61	89.165	66.0
	152	0.58	r_m	1.73	95.850	71
	140	0.54		1.85	102.375	75.8
	120	0.49		2.04	112.821	83.6
cracking	100	0.44	r_{cr}	2.27	125.642	93.1
	80	0.40		2.50	138.206	102.4
	60	0.37		2.70	149.412	110.7
failure	50	0.36	r_f	2.82	155.725	115.4

Table A.0.4- Results from the physical tests for Okoume plywood 12mm.

Observation	Elastica Width [cm]	r_{min} [m] at the top of elastica		Max. Curvature $\frac{1}{r_{min}}$	Bending Moment [Nm]	Bending Stress [MPa]
					$M_y = \frac{EI_y}{r}$	$\sigma_x = \frac{M_y z}{I_y}$
	222	1.28	r_{all}	0.78	102.375	42.6
	220	1.22		0.82	107.410	44.8
	200	0.88		1.14	148.909	62.0
	188	0.77	r_m	1.30	170.400	71.0
failure	180	0.72	r_f	1.39	182.000	75.8

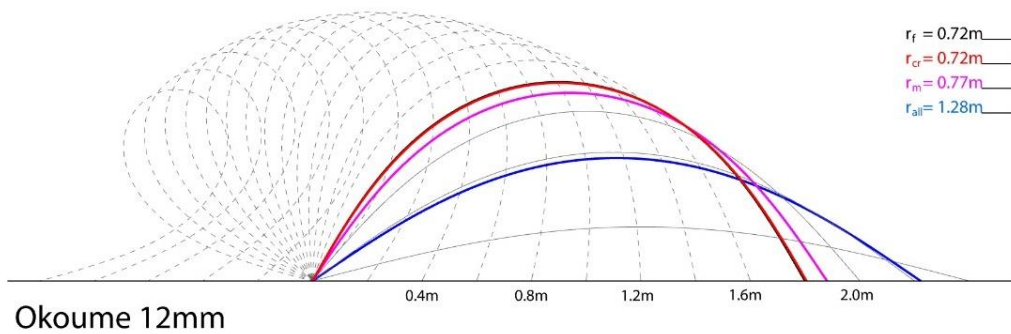
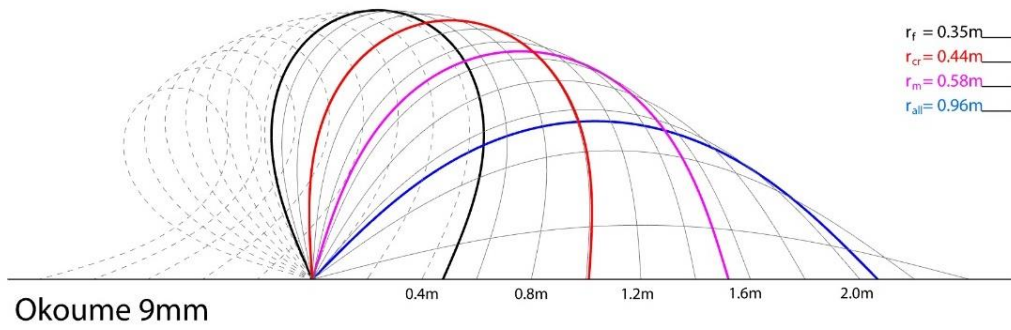
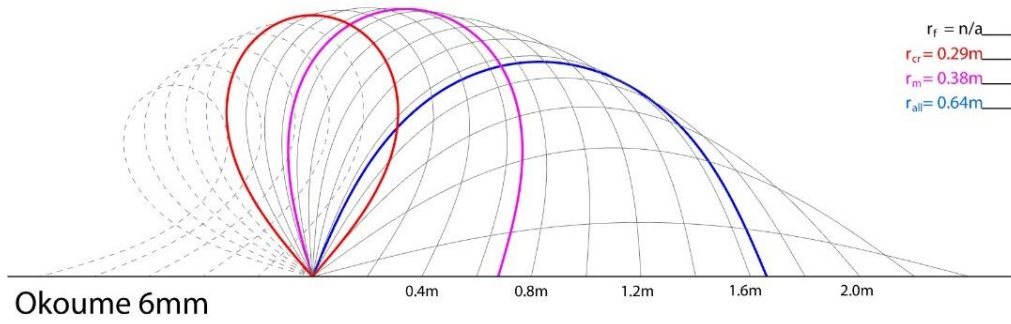
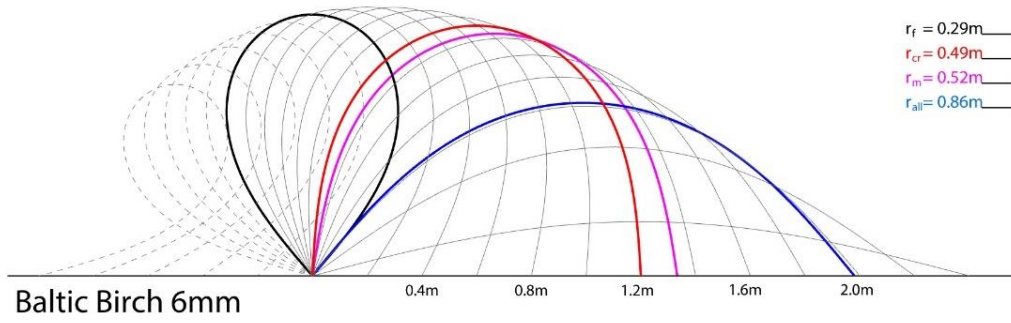


Figure A.0.1 – Shapes of the bent laths.

Appendix B

Construction approval procedures, project budget

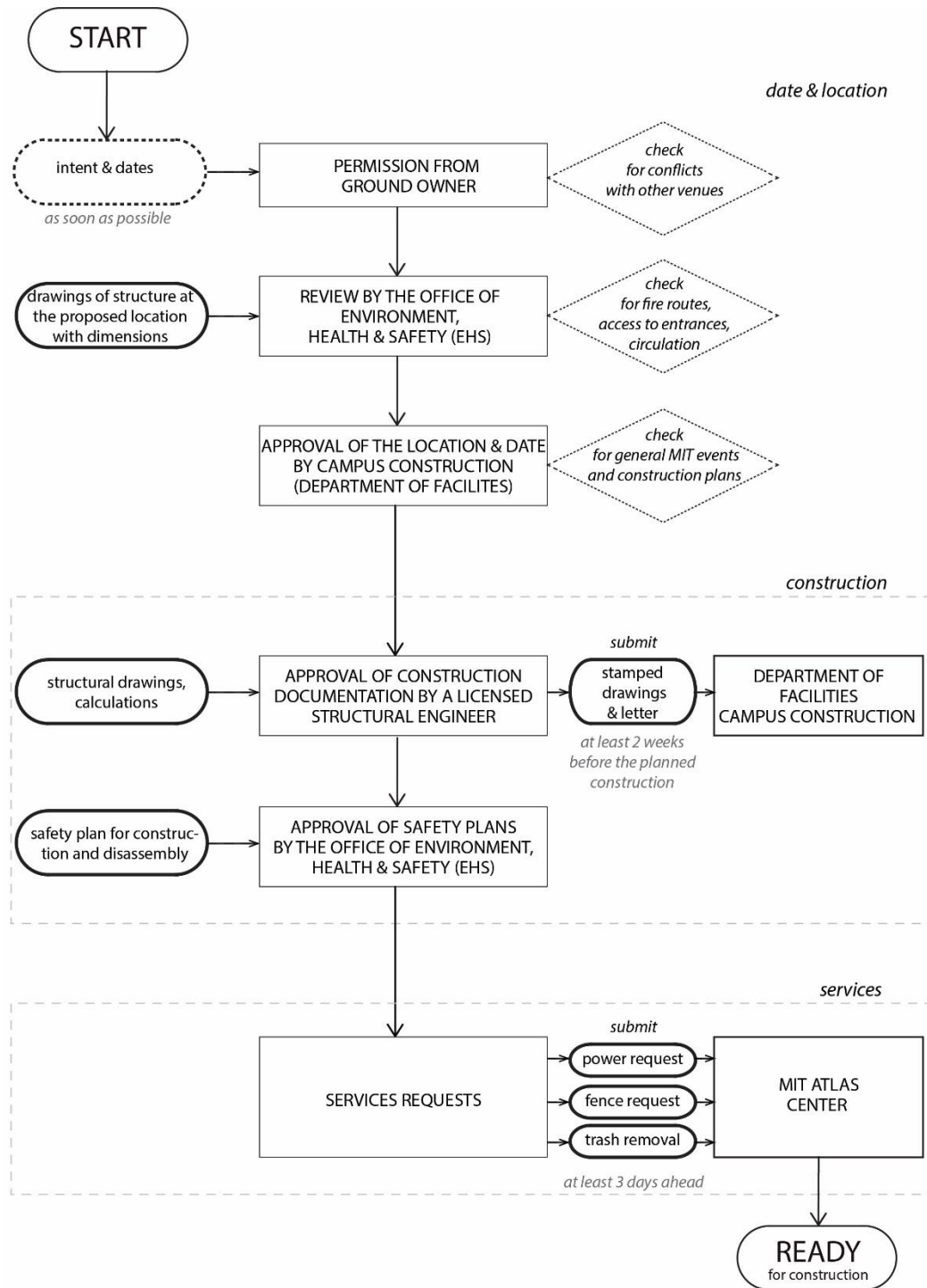
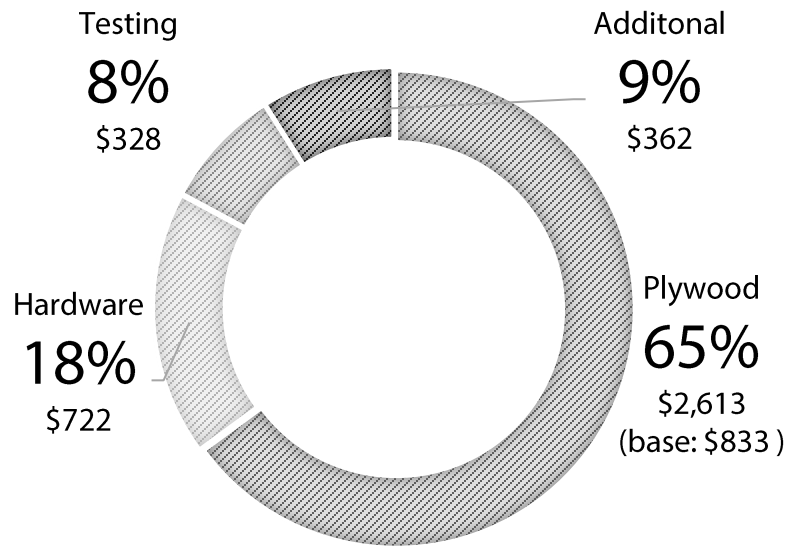


Figure B.0.1 – Flowchart - permission process for the construction at the MIT Campus.

Project budget**Figure B.0.2** - The INFRAME budget.**Table A.0.1** – Number and type of connections with hardware.

CNX type	No.	Item	Size/ dimensions	No. of items per CNX	Total No.
Hinge to base	41	Mortise-Mount Hinge	3.5" x 1.75" Leaf	1	41
		Phillips Flat Head Screws	# 8 Size, 1" Long	3	123
Hinge to 2-laths	23	Button Head Hex Drive Screw	8-32 Thread Size, 1-1/4" Long	3	69
		Hex Nut	8-32 Thread Size	3	69
		316 Stainless Steel Washer	#8 Screw Size, 0.172" ID, 0.625" OD	6	138
Hinge to 1-lath	18	Button Head Hex Drive Screw	8-32 Thread Size, 3/4" Long	3	54
		Hex Nut	8-32 Thread Size	3	54
		316 Stainless Steel Washer	#8 Screw Size, 0.172" ID, 0.625" OD	3	54
Lath-lath	104	Steel Tie Plates	TP35 3-1/8 in. x 5 in.	2	208
		Pan Head Phillips Screws	6-32 Thread, 5/8" Long	8	832
		Steel Hex Nut	6-32 Thread Size	8	832
Joint 3-laths	38	Button Head Hex Drive Screw	8-32 Thread Size, 1-1/2" Long	1	8
		Button Head Hex Drive Screw	8-32 Thread Size, 2" Long	1	30
		Hex Nut (edge)	8-32 Thread Size	1	8
		Steel Wing Nut (space)	8-32 Thread Size, 13/32" Base Diam.	1	30
		316 Stainless Steel Washer	#8 Screw Size, 0.172" ID, 0.625" OD	2	76
Joint 2-laths	303	Button Head Hex Drive Screw	8-32 Thread Size, 1-1/4" Long	1	303
		Steel Wing Nut	8-32 Thread Size, 13/32" Base Diam.	1	303
		316 Stainless Steel Washer	#8 Screw Size, 0.172" ID, 0.625" OD	2	606
Shear blocks	50	Flat Head Screws (block-1lath)	# 8 Size, 5/8" Long	4	200
		Flat Head Screws (block-2lath)	# 6 Size, 1-1/4" Long	4	200

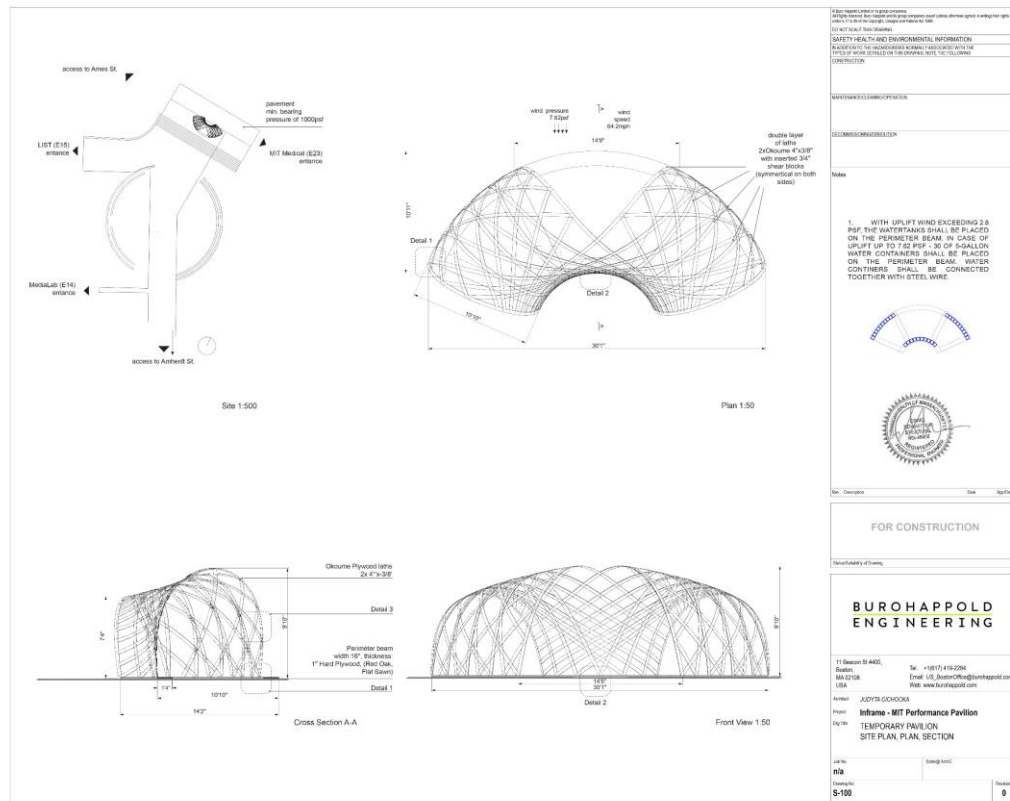


Figure B.0.4 - Drawings for construction – structural configurations and details.

Appendix C

Custom discretization of curves - Python source code

A custom component written in Python programming language was created in the Rhino/Grasshopper environment.

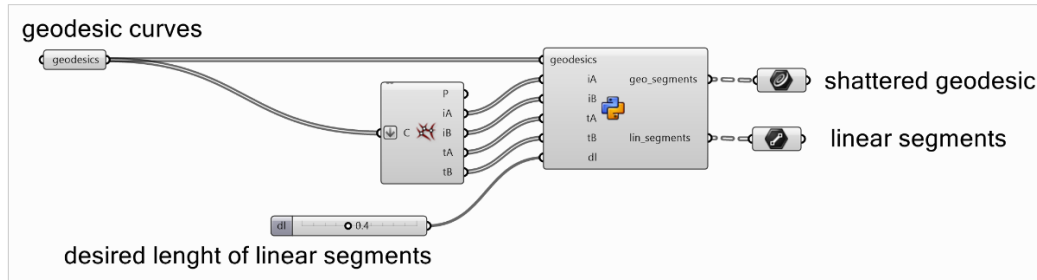


Figure C.0.1 – Custom discretization and grouping component in Python on the Grasshopper canvas.

Python source code of the component is provided below:

```
import rhinoscriptsyntax as rs
from Grasshopper.Kernel.Data import GH_Path
from Grasshopper import DataTree

def nestedListToDataTree(nestedlist):
    dataTree = DataTree[object]()
    for i,item_list in enumerate (nestedlist):
        path = GH_Path(i)
        dataTree.AddRange(item_list,path)
    return dataTree

numGeo = len(geodesics)

#create empty dictionaries of parameters t and segments for each geodesic curve
dict_t= {}
for i in range(numGeo):
    dict_t[i]=[]

#create a dictionary of parameters t
for i in range (len(IA)):
    for k in dict_t.keys():
        if IA[i] == k:
            if tA[i] != 0 and tA[i] !=1:
                dict_t[k].append(tA[i])

for i in range (len(IB)):
    for k in dict_t.keys():
        if IB[i] == k:
            if tB[i] != 0 and tB[i] !=1:
                dict_t[k].append(tB[i])
```



```
#split geodesics into segments
s_list = []
for i in range(len(geodesics)):
    segments = rs.SplitCurve(geodesics[i],dict_t[i])
    s_list.append(segments)

#create tree of geodesic segments
geo_segments = nestedListToDataTree(s_list)

# create dictionary of discrete lines
lines = {}
for i in range(len(s_list)):
    lines[i]=[]

for i in range(len(s_list)):
    for j in s_list[i]:
        num = rs.CurveLength(j)/dl
        if num <1:
            num ==1
        points = rs.DivideCurve(j,num)

        if points != None:
            if len(points) == 2:
                line = rs.AddLine(rs.CurveStartPoint(j),rs.CurveEndPoint(j))
                lines[i].append(line)
            else:
                polyline = rs.AddPolyline(points)
                psegments = rs.ExplodeCurves(polyline)
                for p in psegments:
                    lines[i].append(p)
        else:
            line = rs.AddLine(rs.CurveStartPoint(j),rs.CurveEndPoint(j))
            lines[i].append(line)

#create tree of linear segments
l_list = []
for k in lines.keys():
    l_list.append(lines[k])
lin_segments = nestedListToDataTree(l_list)
```